LA-UR-17-22962
Approved for public release; distribution is unlimited.

Title: Interim Report on Mixing During the Casting of LEU-10Mo Plates in the Triple Plate Molds

Author(s): Aikin, Robert M. Jr.

Intended for: Report

Issued: 2017-04-12

LA-UR-17-
April 10, 2017

Interim Report on Mixing During the Casting of LEU-10Mo Plates in the Triple Plate Molds

Robert M. Aikin Jr.
Sigma Division
Los Alamos National Laboratory
P.O. Box 1663, Los Alamos, NM 87545

Abstract

LEU-10%Mo castings are commonly produced by down blending unalloyed HEU with a DU-12.7%Mo master-alloy. This work uses process modeling to provide insight into the mixing of the unalloyed uranium and U-Mo master alloy during melting and mold filling of a triple plate casting. Two different sets of situations are considered: (1) mixing during mold filling from a compositionally stratified crucible and (2) convective mixing of a compositionally stratified crucible during mold heating. The mold filling simulations are performed on the original Y-12 triple plate mold and the horizontal triple plate mold.

Table of Contents

1. Introduction

The United States government is committed to further strengthening nuclear security and nonproliferation in order to reduce the threat of terrorists acquiring nuclear material. To meet this important mission, the U.S. Department of Energy/National Nuclear Security Agency's Administration's Office of Material Management and Minimization (M3) Reactor Conversion Program (CONVERT) minimizes the use of highly enriched uranium (HEU) in civilian applications by working with governments and facilities around the world to convert research reactors to the use of non-weapons-usable low-enriched uranium (LEU) fuels. Each reactor converted not only eliminates the need for HEU at civilian sites, but also reduces the amount of HEU being manufactured, stored, and transported, where it is at its most vulnerable. In instances where suitable LEU fuels do not exist for particular reactors to convert, the M3 Reactor Conversion Program contributes to the development of new LEU fuels.

Currently, the CONVERT M3 Reactor Conversion Program is developing a high-density, monolithic U-Mo fuel for the research reactor conversion, while at the same time establishing efficient and economic fabrication and manufacturing capabilities. These U-Mo fuel foils will be clad in 6061 aluminum. In order to prevent interaction between the fuel meat and the cladding, a zirconium metal diffusion barrier will be applied to the fuel prior to cladding.

The LEU-Mo fuel starts as a cast plate. Castings are produced by melting a combination of unalloyed HEU and a master-alloy composed of depleted uranium (DU) with molybdenum in a process called down blending. During this initial down blending, approximately 21 weight percent HEU is combined with 79 weight percent U-12.7wt%Mo master-alloy to produce a casting with just under 20% enrichment in ^{235}U and 10wt% Mo. This molten metal charge is then cast to produce a shape.

The eight LEU-10%Mo castings produced at Y-12 in the 2015-2016 time frame were cast in the original triple plate mold with 10" crucible. Analysis of these castings showed a lack of uniformity in the special distribution of ^{235}U that did not meet specifications [1]. The plan for castings in 2017 is to use a revised version of this mold, called the horizontal mold. This work uses process modeling to provide insight into the mixing of the unalloyed uranium and U-Mo master alloy during melting and mold filling of both the original and horizontal triple plate molds. This work builds off of a combination of experiments and modeling done on similar molds [2].

2. Mold Filling from a Stratified Crucible

Consider the situation that occurs during heating of a crucible containing 21% HEU and 79% U-12.7%Mo master-alloy. From the U-Mo phase diagram, the solidus and liquidus of U-12.7wt%Mo is 1205°C and 1280°C respectively [4,5], comparted with the melting point of 1135°C for unalloyed uranium. As the crucible heats up the unalloyed HEU melt first at 1135°C. At this point, there will be solid U-12.7%Mo master-alloy (density 15.3

g/cm^3) floating in a lesser-amount of higher-density unalloyed uranium liquid (density 17.0 g/cm^3) [see Section 2.1.1 for discussion of estimated densities]. As heating continues the greater volume of DU-12.7%Mo master-alloy will melt begin to melt at 1205 and become fully molten at 1280°C. Although there will be some degree of mixing during the melting process, it is easy to imagine that some of the light U-12.7%Mo liquid (15.0 g/cm^3) winds up floating on top of the unalloyed HEU. In the limiting case of no mixing, there will be a crucible with stratified layers of unalloyed uranium on the bottom and U-12.7%Mo on the top. This worst-case stratified crucible is the assumed starting point for the simulations discussed in this section and next. In practice, there will be some mixing, but consideration of the worst-case can help us differentiate what occurs under different processing conditions.

2.1 Simulation Basics

To better understand the solidification behavior during casting of the triple plate molds, the process was simulated using the commercial computational fluid dynamics code Flow-3D [6]. FLOW-3D solves relevant time-dependent heat and fluid flow free-surface problems in three dimensions. The experimentally determined temperature of the mold at pour time was used as the initial conditions and the experimentally determined cooling curves were used to validate the code and parameters used from a thermal perspective in previous work [2]. This simulation also provides a baseline for simulation of other potential design options that will be discussed in later in this report.

Casting simulations typically track fluid flow and heat transfer during mold filling, cooling of the liquid, and solidification. For the simulations in this work tracking the solute (Mo content) was also added. The inclusion of this additional physics proved to be quite troublesome. Pressure iteration convergence often became problematic during run time with resulting small temporal step sizes, pressure iteration failures, simulation instability, and premature solver termination. The combination of small temporal step size and large meshes resulted in long run times for the simulations (on order of several weeks clock time) and solver termination at early time.

The thermophysical properties, interfacial heat transfer coefficients, initial and boundary conditions used are listed in Table 1. Some of the choices are discussed in greater detail below.

2.1.1 Density and Buoyancy

The lack of liquid phase properties of alloys is often problematic for solidification modeling. For this work the lack of density necessitates a number of approximations. Because of the number of approximations taken here, the second order complication of density difference with enrichment will be ignored.

The room temperature density of U-10%Mo is given as 17130 kg/m^3 by Kline [7] and 17120 kg/m^3 by Bridge [8]. This data and values in the Y-12 Technical Datasheets [9] give a linear fit of the room temperature density of U-Mo alloys to be

$$\rho(RT, f_{Mo}) = 18893\ kg/m^3 - 16811 \cdot (f_{Mo}) \quad (1)$$

The density of unalloyed uranium is 18950 kg/m^3 as a solid at room temperature and 16950 kg/m^3 as liquid at its melting temperature [9]. Assuming that the ratio solid densities of unalloyed and U-10%Mo is the same for the ratio of liquid densities at the melting point, the density of U-10%Mo liquid is 15310 kg/m^3.

The density of the liquid as a function of weight fraction Mo is then estimated to be (in the form Flow3D expects the input)

$$\rho(liquid, f_{Mo}) = (15320\ kg/m^3) \cdot [1 - (1.069) \bullet (f_{Mo} - 0.10)] \quad (2)$$

From these two equations, the density of U-12.7%Mo is 16760 kg/m^3 at room temperature and 15000 kg/m^3 as a liquid. These values are used in Section 2.2.2 and 2.3.1 to determine the initial volume of fluid in the crucible.

The density of unalloyed uranium liquid as a function of temperature is

$$\rho(liquid, T) = (17270\ kg/m^3) \cdot [1 - (6.0 \times 10^{-5}\ K^{-1}) \cdot (T - 1406)]$$

from Smithals [10] and

$$\rho(liquid, T) = (16950\ kg/m^3) \cdot [1 - (7.6 \times 10^{-5}\ K^{-1}) \cdot (T - 1406)] \quad (3)$$

from Drotning [11].

Combining equation 2 and 3, the density of the liquid as a function of density and composition is estimated to be (in a form that Flow3D requires as inputs)

$$\rho(liquid, f_{Mo}, T) = (15320\ kg/m^3) \cdot [1 - (1.069) \cdot (f_{Mo} - 0.10) - (6.6 \times 10^{-5}\ K^{-1}) \cdot (T - 1406)]$$

Note that the thermal effect on density is small compared to the solutal effect. For the mold filling simulations, the thermal term will be ignored and only the solutal effect will be included. For the crucible convection simulations discussed in Section 3 both thermal and solutal terms will be included.

2.1.2 Initial thermal gradient

In the instrumented triple plate casting performed at LANL [2] the original mold geometry was used with a 14" crucible. In that casting, the crucible was heated to 1350°C and held for 10 minutes. The observed thermal gradient in the mold at pour time was (1174K/m)·z+1056K. Based on the higher casting temperature (1400°C) and longer hold time (30 minutes), the thermal gradient used in this simulation estimated to be (1256K/m)·z+1173. This mold thermal gradient is similar to the horizontal mold castings poured at 1400°C in the LANL experiments [2]. For sake of comparison the same thermal gradient was used for both mold geometries in this work.

2.1.3 Meshing

The long (200 mm) and thin (5 mm) geometry of this casting makes it very difficult to cast without casting defects. This long and thin geometry also is a challenge to model. To properly capture the mold filling the pates should be at least 5 cells though

thickness. This results in the need to use a 1 mm mesh size in the mold cavity. Slightly larger cells can be used in the graphite but resulting number of cells is quite large.

2.2 Original Y-12 Triple Plate Mold

As mentioned in the introduction, eight LEU-10%Mo plates have been produced by Y-12 using the 3 Plate Stack Assembly (10”). This triple plate mold design in shown in Fig. 1 along with details of the simulation. The Y-12 drawing number for this mold stack is T802077-001.

2.2.1 Mold Geometry

The initial mold design and process parameters were supplied by Y-12 [12]. This design simultaneously casts 3 thin billets and is shown in Fig. 1. The mold stack is comprised of 7 parts: a bottom clamp (T802077-006), top clamp (T802077-005), two outer book mold components (T802077-002), two inner book mold components (T802077-003 and T802077-004), and a crucible on top. The 4 parts of the book mold are held together by the top and bottom mold clamps. The clamps also serve as a heat source on top and a chill on the bottom. The mold forms 3 cavities that are 11.25 inch tall by 8 inch wide by 0.20 inch thick (284 mm tall by 203 mm wide by 5 mm thick). In this design, the center plate is offset by 0.040 inch (1 mm) from the center line of the pour hole.

A standard Y-12 10" diameter crucible is used (350 mm OD by 300 mm ID by 140 mm tall; drawing T2C801217A007) to hold the metal during melting. Bottom discharge of the crucible is controlled by a knockout/rupture disk. This sub-assembly is comprised of the Crucible Knockout Plug (T2C801217A011) with a 0.63 inch diameter discharge hole. It in turn contains the Knockout Rupture Plug (T2C801217A010) and Knockout Butterfly Disk (T2C801217A016).

A 1” Pouring Rod (T2C801217A006) is lowered into the molten metal just before pouring. This Pouring Rod is then struck against the Knockout Rupture Plug to break it and allow the metal to drain into the mold. For the triple plate castings produced in the 2015-2016 time frame, the Pouring Rod was left in the annulus of the Knockout Rupture Plug after breaking the plug. The metal drains out of the crucible between the D-shaped cut outs in the Pouring Rod and the ID of the Knockout Rupture Plug. Based on the cross section of the various flow restrictions in the path of the Crucible Knockout Plug subassembly, it is believed that the crucible discharge rate is limited by the Pour Rod in the broken Knockout Rupture Plug. As such, this portion of the mold geometry was simplified to only include the Pouring Rod and the ID of Knockout Rupture Plug.

2.2.2 Simulation Details

This triple plate mold design in shown in Fig. 1 along with details of the simulation. For convenience, the geometry (solid model) was defined in units of inches, but converted to SI units when read into the simulation. To minimize the mesh size the geometry was divided into 4 mesh blocks. The red lines in Fig. 1 show the extent of the four mesh regions. The purple lines on the left-hand side of Fig. 1 indicate the initial temperatures

used. As discussed in section 2.1 the thermal gradient is based on the thermal gradient experimentally observed at pour time in the castings.

Because the mold cavities are not symmetric about X=0, but are symmetric about Y=0, a half symmetry mesh can be used. Using 1 mm cells in the regions where there was fluid flow and 1.5 mm in the graphite yielded a half symmetry mesh with 3.1 million cells.

The 10” crucible used is shown in Fig. 2 with the pour rod down. To provide the correct casting charge there needs to be 43.67 in^3 of unalloyed uranium and 10.37 in^3 of U-12.7%Mo initially in the crucible. Because of the geometrical complexity of the crucible with the pour rod down, a CAD program was used determine the appropriate fluid depths to give the needed volume of two layers of metal. Those initial fluid levels are shown in the crucible in Fig. 2.

Many of the other details of the simulation were similar to the simulations discussed previously in [2].

2.2.3 Simulation Results

In Figure 3, simulation results are shown as a function of time for the original triple plate mold with the pour rod down. The results are read like a comic strip with time running left to right (and onto the continuing pages). The results are viewed in 3D from the negative X-Y quadrant looking in a positive X-Y direction. The left plate is in the foreground and right plate is in rear. For clarity, the mold is not displayed. Temperature is shown along the top row, solid fraction on the center row, and the Mo concentration on the bottom row.

The same information is presented in a different manner in Figures 4 though 7. In these figures the results are presented as 2D Y-Z slices though the center of the left, center and right plates respectively. Figure 4 shows temperature, Fig. 5 solid fraction, and Fig. 6 concentration of Mo. Figure 7 shows the concentration of Mo as a X-Y section of the mold (orthogonal to Fig. 6). Figure 8 shows 2D Y-Z slices with the velocity magnitude shown as colors and the velocity (in the Y-Z) plane shown as vectors. The multiple meshes used in this simulation imprint an artifact on the rendering of the velocity vectors that is visible in Fig. 8, but this is a post processing artifact only.

Filling is similar for the three plates, with a great deal of splashing as the metal falls from the crucible and hits the inner mold separating the 3 plates. Because of the top of inner molds are angled away from the center, the streams into the right and left plates have a stronger flow down the center cavity (but still with significant splashing), while filling of the center plate is dominated by splashing. There is some preference for the filling of the right plate. The right plate fills in 7 seconds while the center and left plate take 10 seconds to fully fill. As can be seen from the temperature and solid fraction, the metal super-heat is rapidly lost during filling with all 3 plates showing a significant fraction solidified by the end of filling (11 seconds).

The crucible starts with the unalloyed U (0% Mo) as a bottom layer of fluid and 12.7% Mo on the top. As can best be seen in Figs. 3 and 7, during the first few seconds of pouring both the top and bottom layers are drawn into the crucible discharge and mixing occurs. The smaller quantity of pure U is quickly exhausted, and the composition exiting the crucible shifts from the approximately 7% observed in the first 2 seconds to 12.7% at 4 seconds. The momentum of the falling stream results in hot Mo-rich liquid plunging deep into the casting. The momentum and plunging liquid sets up a circulation down the center, along the bottom, and up the sides of the mold cavity. This mixing is quickly doused by the solidifying solid's increasing viscosity and liquid immobility at the critical fraction solid (f_s).

The plunging high-Mo liquid that enters late in the filling process results in an overall composition that is blotchy through thickness (Fig. 7) as well as in the plane of the plate (Fig. 8). Given time, the momentum of the filling would allow some additional mixing to occur, but as can be seen in Fig. 8 the metal velocity of the quickly-solidifying thin-plates quickly drops to zero.

This mold filling is of course complicated by the fact that the fraction solid is a function of both temperature and composition. The later arriving Mo-rich fluid solidifies at a higher temperature and small regions of high Mo become frozen in place. Toward the top of the casting, the slower solidification allows some of the late arriving Mo-rich fluid to undergo some degree of mixing.

The temperature of mold and metal as a function of time for the original mold with the pour rod down is shown in Fig. 9. Shown is a X-Z slice along Y=0. The molten metal quickly loses it super heat to the mold which heats up. Because of the thick nature of the outer mold components they heat up only slowly, while the inner components become isothermal with the solidifying metal.

2.3 Horizontal Triple Plate Mold

As with the original triple plate mold, the mold design and process parameters were supplied by Y-12. This design simultaneously casts 3 thin billets and is shown in Fig. 10. 3 Plate (90°) Stack Assembly (3 Pour) drawing T802077-0016 [11]. The major difference in this mold is

(1) the presence of a distributor to control filling into the plates,

(2) horizontal orientation of plates to reduce filling and feeding distance,

(3) the presence of a hot top on each cast plate to provide feeding during solidification.

The horizontal stack is comprised of 8 parts: a bottom clamp (Y-12 mold drawing T802077-028), top clamp (T802077-0027), a distributor (T802077-0026), two outer book mold components (T802077-0029), two inner book mold components (T802077-0030), and a 14" crucible on top. The 4 parts of the book mold are held together by the top and bottom mold clamps. The clamps also serve as a heat source on top and a chill on the bottom. The mold forms 3 cavities that are 8.5 in. tall by 9.75 in. wide by 0.20 in. thick

(216 mm tall by 248 mm wide by 5 mm thick). On the top of each plate is a 2 in. tall by 0.5 in. thick hot top that runs the full width of the cast plate.

A standard Y-12 14" Crucible is used (drawing T2C801217A008). As with the 10" crucible the pour is affected by breaking the Knockout Rupture Plug. Instead of the Crucible Knockout Plug the Fast Pour Crucible Plug will be used (T2C801217A011). The intent is to break the Knockout Rupture Plug with the Pour Rod and then withdraw the Pour Rod. The limiting cases with respect to filling and crucible discharge times are:

(a) Pour Rod remains in the Knockout Rupture Plug while the metal drains (slow crucible discharge) and

(b) Pour Rod is pulled immediately (fast crucible discharge)

These two cases are considered separately below.

2.3.1 Simulation Details

Simulation setup for the horizontal triple plate mold with the pour rod down is shown in Fig. 10. As before, the mold geometry, initial temperature distribution, mesh/simulation boundaries, and initial fluid levels are shown. To minimize the mesh size the geometry was divided into 4 mesh blocks. The red lines in Fig. 10 show the extent of the four mesh regions. The purple lines on the left-hand side of Fig. 10 indicate the initial temperatures used. Although this horizontal mold with a 14" crucible is likely to couple with the induction heating differently, the same thermal gradient as used in the previous simulation was used.

The center plate is centered on X=0 and as such the plate cavities are symmetric about X-Z. But because the distributor does not have 4-fold symmetry, the simulation had to be run in half symmetry about Y=0. This is as opposed to the original mold which was simulated in a half symmetry mesh about X=0. Again 1 mm cells where used in regions where there was fluid flow and 1.5 mm cells in the graphite yielded a half symmetry with 5.6 million cells.

The volume of the 3 plates with their hot tops half-filled is 68.07 in^3. Crucible detail for the horizontal triple plate mold with 14" crucible and pour rod down is shown in Fig. 11. To provide the correct casting charge there needs to be 55.04 in^3 of unalloyed uranium and 13.03 in^3 of U-12.7%Mo initially in the crucible. Because of the geometrical complexity of the crucible with the pour rod down, a CAD program was used determine the appropriate fluid depths to give the needed volume of two layers of metal. Those initial fluid levels are shown in the crucible in Fig. 11.

2.3.2 Pour Rod Down Simulation Results (Slow Crucible Discharge)

In Figure 12, simulation results are shown as a function of time for the horizontal triple plate mold with the pour rod down. The results are viewed in 3D from the negative X-Y quadrant looking in a positive X-Y direction. The center plate is in the foreground and right plate is in rear. For clarity, the mold is not displayed. Temperature is shown along

the top row, solid fraction on the center row, and the Mo concentration on the bottom row.

The same information is presented in a different manner in Figures 13 though 15. In these figures the information is presented as 2D Y-Z slices though the center of the center and right plates respectively. Figure 13 shows temperature, Fig. 14 solid fraction, and Fig. 15 concentration of Mo. Figure 16 shows the concentration of Mo as a X-Z section (orthogonal to Fig. 15) at three locations; the top row is through the center Y=0, middle row is below the distributor discharge hole Y=0.030 m, and bottom row is near edge at Y=0.107 m. In this X-Z slice, the mirror symmetry of the simulation is used to produce merged image of the simulation. This is done so that the metal in the center plate can more easily be observed. Figure 17 shows 2D Y-Z slices with the velocity magnitude shown as colors and the velocity (in the Y-Z) plane shown as vectors. The multiple meshes used in this again simulation imprint an artifact on the rendering of the velocity vectors.

The initial metal is discharged from the crucible and begins to fill the distributor. At the same time metal flows from the distributor into the mold. Filling is similar for the two plates with a great deal of splashing when the metal transitions from falling in the hot top (between distributor and mold cavity). There is some preference for the filling of the right plate which may be an artifact of having the symmetry boundary condition down the center of the center plate. The center plate fills and then begins to overflow into the right plate.

As can be seen from the temperature and solid fraction, not much of the metal super-heat is lost in the distributor. But super-heat is rapidly lost as metal fills the thin plates. Both plates showing significant degree of solid and are well into the mushy zone by the end of filling (13 seconds).

The crucible starts with the unalloyed U (0% Mo) as a bottom layer of fluid and 12.7% Mo on the top. As can best be seen in Figs. 12 and 15, during the first few seconds of pouring both the top and bottom layers are both drawn into the crucible discharge and mixing occurs. The smaller quantity of pure U is quickly exhausted and the composition exiting the crucible shifts from the approximately 7% observed in the first 2 seconds to 12.7% at 4 seconds. There is some additional mixing in the distributor, but by in large the metal is not retained for very long in the distributor and the composition coming in is the composition that goes out.

The momentum of the stream of metal falling from the distributor into the mold cavity, results in hot Mo-rich liquid plunging deep into the casting. The momentum and plunging liquid sets up a circulation down the center, along the bottom, and up the sides. Since the stream is more well defined entering the mold cavity from the distributor, as opposed to splashing into the cavity as was the case for the original mold, the degree of circulation is greater. This mixing is quickly doused by the solidifying solid's increasing viscosity and liquid immobility at the critical fraction solid (f_s).

The plunging high-Mo liquid late in the filling process results in an overall composition that is blotchy through thickness (Fig. 16) as well as in the plane of the plate (Fig. 15). Given time the momentum of the filling would allow some additional mixing to occur but as can be seen in Fig. 17 the metal velocity of the quickly-solidifying thin-plates quickly drops to zero.

The temperature of mold and metal as a function of time for the horizontal mold with the pour rod down is shown in Fig. 18. Shown is a X-Z slice along Y=0. As can also be seen in Fig 15, the molten metal quickly loses it super heat to the mold which heats up. Because of the thick nature of the outer mold components they heat up only slowly, while the inner components become isothermal with the solidifying metal. Figure 19 also shows that the mold temperatures are more uniform in a horizontal direction showing a more balance heat flow from each side of the casting due to the balanced mold thickness of the mold design.

2.3.3 Pour Rod Removed Simulation Results (Fast Crucible Discharge)

Simulation setup for the horizontal triple plate mold with the pour rod withdrawn. is shown in Fig. 19. As before, the mold geometry, initial temperature distribution, mesh/simulation boundaries, and initial fluid levels are shown. This simulation differs from the Pour Rod Down Simulation, of the previous section, in that:

- Pour rod is not present
- Knockout Rupture Plug has been replaced with a representation of the Fast Pour Crucible Plug and it's three 0.5" diameter discharge holes.

In Figure 20, simulation results are shown as a function of time for the horizontal triple plate mold with the pour rod down. The results are viewed in 3D from the negative X-Y quadrant looking in a positive X-Y direction. The center plate is in the foreground and right plate is in rear. The mold not displayed for clarity. Temperature is shown along the top row, solid fraction on the center row, and the Mo concentration on the bottom row.

The same information is presented in a different manner in Figures 21 though 23. In these figures the information is presented as 2D Y-Z slices though the center of the center and right plates respectively. Figure 21 shows temperature, Fig. 22 solid fraction, and Fig. 23 concentration of Mo. Figure 24 shows the concentration of Mo as a X-Z section (orthogonal to Fig. 23) at three locations; the top row is through the center Y=0, middle row is below the distributor discharge hole Y=0.030 m, and bottom row is near edge at Y=0.107 m. In this X-Z slice, the mirror symmetry of the simulation is used to produce merged image of the simulation. This is done so that the metal in the center plate can more easily be observed. Figure 25 shows 2D Y-Z slices with the velocity magnitude shown as colors and the velocity (in the Y-Z) plane shown as vectors. The multiple meshes used in this again simulation imprint an artifact on the rendering of the velocity vectors.

The initial metal is discharged from the crucible and begins to fill the distributor. At the same time metal flows from the distributor into the mold. Because of the higher

discharge rate from the crucible than from the crucible, metal begins to backup in the crucible by about 3 seconds. The resulting turbulence and mixing in the distributor does an effective job of compositionally mixing the metal. Filling is similar for the two plates with a great deal of splashing when the metal transitions from falling in the hot top (between distributor and mold cavity). There is some preference for the filling of the right plate which may be an artifact of having the symmetry boundary condition down the center of the center plate. The center plate fills and then begins to overflow into the right plate.

The crucible is empty at 5 seconds, compared to 12 seconds for the pour rod down case. The distributor is empty at 11 seconds, compared to about 13 seconds for the pour rod down case. Thus, the greater amount of residence time of metal in the distributor is due to faster crucible discharge and not slower discharge from the distributor. To a first approximation the molds fill in a similar manner to that of the pour rod down case.

The crucible starts with the unalloyed U (0% Mo) as a bottom layer of fluid and 12.7% Mo on the top. As can best be seen in Figs. 20 and 23, during the first few seconds of pouring both the top and bottom layers are both drawn into the crucible discharge and mixing occurs. The smaller quantity of pure U layer quickly is exhausted and the composition exiting the crucible shifts from the approximately 7% observed in the first 2 seconds to 12.7% at 4 seconds. Because of the great residence time in the distributor the differing metal compositions from the crucible have a chance to mix in the distributor. The problem comes in that some of the high-Mo metal that gets though the distributor (just before it really chokes off) and into the mold at about 3 or 4 seconds remains unmixed. This is especially evident in the right plate.

The temperature of mold and metal as a function of time for the original mold with the pour rod down is shown in Fig. 26. Shown is a X-Z slice along Y=0. As can also be seen in Fig 15, the molten metal quickly loses it super heat to the mold which heats up. Because of the thick nature of the outer mold components they heat up only slowly, while the inner components become isothermal with the solidifying metal. Figure 19 also shows that the mold temperatures are more uniform in a horizontal direction showing a more balance heat flow from each side of the casting due to the balanced mold thickness of the mold design.

2.4 Discussion

The crucible empties in 5 seconds for the fast-discharge pour rod up simulation, compared to 12 seconds for the slow discharge pour rod down case. The distributor is empty at 11 seconds for the pour rod up simulation, compared to about 13 seconds for the pour rod down case. This results in greater residence time of metal in the distributor for the fast-pour case. In Fig. 27 of composition distribution at the end of filling for the three different situations considered is shown. For ease of comparison the mirror symmetry of the original mold is utilized. The distribution of Mo is poor in the original

mold with no distributor. The addition of the distributor helped the Mo distribution in the horizontal mold with pour rod down case. The horizontal mold with pour rod up has the best Mo distribution; though only marginally over the pour rod down case.

The actual degree of mixing during mold filling is strongly dependent on the crucible discharge rate which controls mold filling and mold temperature at pour time which controls solidification rate. The initial mold temperature is approximately known from prior work. In this work, the range of crucible discharge rates has been bounded by the simulations with the pour rod down and pour rod withdrawn. The actual temperature and discharge rate has not been experimentally measured and as such actual mixing is cannot be quantitatively predicted.

3. Convective Stirring in the Crucible

The simulations above assume a worse case stratified crucible. During mold heating there is a thermal gradient from the outer rim of the crucible (which is coupling with the induction heating), to the crucible center (which is not coupling). This thermal gradient in the crucible may lead to temperature differences in the molten metal, that may in turn induce thermal buoyancy and mixing. If such thermal buoyancy can result in significant mixing then the Mo distribution in the crucible may be improved. Also, there might be advantages to overshooting the crucible temperature (spiking) to encourage more mixing. This portion of the work looks at the degree of stirring produced by thermal buoyancy and its impact on metal distribution in the crucible.

3.1 Simulation Details

The simulation setup uses the same 10" crucible as used in the original mold pouring simulations. In Fig. 28 the simulation setup for the crucible convection simulations in the original Y-12 triple plate mold is shown. Shown is the mold geometry, mesh/simulation boundaries, and initial fluid levels. Since the pour rod is only placed in the metal late in the melting process, it has been left out of the simulation, and the solid plug of the Knockout Plug keeps the metal in the crucible.

Three situations are considered

1) Isothermal hold at 1400°C for 35 minutes
2) Heat from 1300°C to 1400°C in 5 minutes (0.33°C/s) and hold for 30 minutes.
3) Heat from 1300°C to 1500°C in 10 minutes, cool back to 1400°C in 5 minutes, then held at 1400°C for 20 minutes.

The actual induction heating of the crucible is not simulated, rather this imposed boundary condition is achieved by specifying temperature as a function of time for the outer layer of the crucible. The thermal profile of outer surface of crucible as function of time is shown in Fig. 29. The 0.33°C/s heating rate used is estimated based on the Y-12 observed overall heating rate of RT to 1400°C in 40 minutes (0.57°C/s). Although the overall heating rate appears Y-12 is higher, in general for a fixed power setting the initial

heating rate will be higher and then begin to slow as radiation becomes important. The 0.33°C/min used in the simulation is thus an estimated heating rate near 1400°C.

The same simulation and thermophysical values used for the mold filling simulations are used here and are as given in Table 1. The same volume and metal depth in the crucible of unalloyed uranium and U-12.7Mo are used as in Fig. 2. To avoid problems with numerically induced surface waves, no free surface is used in this simulation. As discussed in Section 2.1.1 the liquid density is estimated to be

$$\text{rho(liquid, } f_{Mo}, T) = (15320\ kg/m^3)\cdot[1 - (1.069)\cdot(f_{Mo} - 0.10) - (6.6\times10^{-5}\ K^{-1})\cdot(T - 1406)]$$

as a function of Mo fraction (f_{Mo}) and temperature (T).

The results of the isothermal simulation will not be discussed separately, but instead will be discussed in comparison to the other two cases.

3.2 Crucible heat up and hold

The simulation results for the crucible heated from 1300°C to 1400°C in 5 minutes (0.33°C/s) and held for 30 minutes is shown in Fig. 30. The results are presented as X-Z slices along the Y=0 axis, with data at equal time increments presented in columns and the rows as different forms of the data. Temperature is shown in the first row, metal velocity magnitude (with in plane velocity vectors) is shown in the second row, the Mo composition is shown on the third row, and the macroscopic density is shown on the bottom row.

At time zero, the high density unalloyed uranium is on the bottom with the lower density U-12.7Mo on the top in an isothermal crucible at 1300°C. As the outer rim of the crucible heats the heat conducts into the crucible radially creating a thermal gradient. This temperature gradient sets up a slight thermal gradient in the liquid metal. The thermal gradient in the liquid is predominantly in the horizontal direction with a minor top to bottom thermal gradient. The warmer less-dense fluid rises along the vertical side of the crucible and then flows axially in. This creates a modest circulation along the outer wall. Once the outer crucible reaches 1400°C and the crucible becomes once again isothermal (at times greater than about 900 seconds), the buoyancy induced metal flow dies out and only diffusive mixing occurs.

The temperature and velocity plots are shown side-by-side at early time in Fig. 31. Because the thermal change in density, is very small compared to the compositional density, the metal circulation is restricted to the upper lower-density U-Mo layer.

3.3 Crucible overheat, cool, and hold

The simulation results for the crucible heated from 1300°C to 1500°C in 10 minutes, cooled back to 1400°C in 5 minutes, then held at 1400°C for 20 minutes is shown in Fig. 32. Again, the results are presented as X-Z slices alone Y=0 axis, with data at equal time increments presented in columns and the rows as different forms of the data.

Temperature is shown in the first row, metal velocity magnitude (with in plane velocity vectors) is sown in the second row, the Mo composition is shown on the third row, and the macroscopic density is shown on the bottom row.

At time zero, the high density unalloyed uranium is on the bottom with the lower density U-12.7Mo on the top in an isothermal crucible at 1300°C. As the outer rim of the crucible heats the heat conducts into the crucible radially creating a thermal gradient. This temperature gradient sets up a slight thermal gradient in the liquid metal. The thermal gradient in the liquid is predominantly in the horizontal direction with a minor top to bottom thermal gradient. The warmer less-dense fluid rises along the vertical side of the crucible and then flows axially in. This creates a modest circulation along the outer wall.

As the temperature of the crucible begins to cool back down from 1500°C to 1400°C, the radial thermal gradient inverts. The cooler metal at the crucible edge now begins to sink, creating a reversed circulation. The density of this descending liquid is still lower than the unalloyed uranium, so it does not skink below the upper layer of metal. As the temperature returns to isothermal (at times greater than about 1200 seconds), the buoyancy induced metal flow dies out and only diffusive mixing occurs.

The temperature and velocity plots are shown side-by-side at early time in Fig. 33. Because of the greater temperature excursions, the degree of mixing is higher than in the heat up and old case. Again, because the thermal change in density is very small to the compositional density difference, the metal circulation is restricted to the upper lower-density U-Mo layer.

In Fig. 34 the composition of Mo at the center line (along the Z axis), is plotted as a function of time. As shown in the color plots of Fig. 32, there is some mixing but that mixing and the composition at the bottom of the crucible rises from 0 at time zero to about 3% at 35 minutes.

3.4 Discussion

Although not shown here, the isothermal crucible case showed essentially no flow. But where was some limited homogenization of the initial bi-modal step function in Mo content. In Fig. 35 the Mo composition at the initial time and for the 3 cases

1) Isothermal hold at 1400°C for 35 minutes
2) Heat from 1300°C to 1400°C in 5 minutes (0.33°C/s) and hold for 30 minutes.
3) Heat from 1300°C to 1500°C in 10 minutes, cool back to 1400°C in 5 minutes, then hold at 1400°C for 20 minutes.

are shown at 35 minutes (2100 seconds). These same results are replotted in Fig. 36 as composition along the center line.

Clearly there has been a degree of homogenization of the Mo content for all three cases. The most homogenization has occurred for the third case where there was the

most mixing, while the least amount of homogenization has occurred for the first (isothermal) case. The fact that all three Mo distributions are quite similar suggests that numerical diffusion is the predominate effect and that thermal induced convection had a minimal effect on mixing in the crucible.

4. Summary and Recommendations

This work uses process modeling to provide insight into the mixing of the unalloyed uranium and U-Mo master alloy during melting and mold filling of a triple plate casting. Two different sets of situations are considered: (1) mixing during mold filling from a compositionally stratified crucible and (2) convective mixing of a compositionally stratified crucible during mold heating. The mold filling simulations are performed on the original Y-12 triple plate mold and the horizontal triple plate mold.

4.1 Summary

Mixing During Mold Filling

In this work, as a worst-case situation, it has been assumed that the crucible starts with stratified layers of unalloyed U at the bottom and 12.7% Mo on top. For both the original and horizontal mold designs, during the first few seconds of pouring both the top and bottom layers are drawn into the crucible discharge and mixing occurs. The smaller quantity of pure U is quickly exhausted, and the composition exiting the crucible shifts from medium-Mo to Mo-rich. The late exiting Mo-rich liquid is most problematic.

The momentum of the falling stream results in hot Mo-rich liquid plunging deep into the casting. The momentum and plunging liquid sets up a circulation down the center, along the bottom, and up the sides of the mold cavity. This mixing is quickly doused by the by solidification and the late exiting Mo-rich liquid is locked in place. This results in an overall composition that is blotchy through thickness as well as in the plane of the casting.

For the horizontal mold the presence of the distributor allows additional mixing to occur and the blotchy compositional variation is reduced. For the horizontal mold pouring rate also had a large effect on mixing. A fast crucible discharge rate allows metal to mix in the distributor because there is greater residence time and late-versus-early crucible discharge compositional versions could be averaged out though mixing.

Convective Stirring in the Crucible

The thermal gradient in the crucible can set up thermal buoyancy driven convection in the crucible, but does not result in significant mixing. The Mo distribution from a crucible with and without buoyancy driven mixing was quite similar suggesting that numerical diffusion is the predominate effect and that thermal induced convection had a minimal effect on mixing in the crucible.

Although not explicitly considered, since the melt pool is shallower in the 14” cubicle than in the 10” crucible considered, it is expected that there would be even less convective mixing in the larger crucible.

4.2 Recommendations for Further work.

Actual mold temperature and crucible discharge rates are not known. The actual degree of mixing during mold filling is strongly dependent on the crucible discharge rate which controls mold filling and mold temperature at pour time which controls solidification rate any further work needs to understand and be bounded by actual experimental data.

Smaller discharge holes in the horizontal mold distributor could allow longer residence time and improved mixing in the crucible. But such longer residence time would have to be balanced with heat loss and potential premature freezing in the distributor. Observation of the skull and degree of metal backup in the distributor of castings can help inform degree of metal back up in the distributor. Knowing the actual mold temperature and crucible discharge rates (discussed above) would also inform considerations to change the distributor discharge hole size.

The electric current induced by the induction heating mainly flows at "skin" of the conductor between the outer surface and a level called the skin depth. Thus, the majority of the heating is deposited within the skin depth. If the crucible is significantly thinner than the skin depth, the alternating magnetic field can penetrate the crucible and cause stirring of the metal. At low to moderate frequencies, the skin depth is given by

$$\delta = \sqrt{\frac{1}{\pi \mu_o \sigma f}}$$

where μ_o is 4π x 10^{-7}, σ-1 is the electrical resistivity (1.65×10^{-5} Ω•m), and *f* is the frequency. For graphite at 3 kHz the skin depth is 3.7 cm (1.5 inch). For the 10” Y-12 crucible the crucible wall is 0.75 inches thick, while the 14” crucible is 1 inch thick. As such there may be some Lorentz stirring. But with the very shallow melt pools associated with these castings (especially the 14” crucible) it is unclear if induction mixing is possible. Modeling of induction induced stirring would be helpful to inform possible crucible and induction frequency changes and determine if Lorentz stirring is a feasible option.

5. Acknowledgement

This work is supported financially by the U.S. Department of Energy/National Nuclear Security Administration’s M3 Reactor Conversion Program. Los Alamos National Laboratory, and affirmative action equal opportunity employer, is operated by Los Alamos National Security, LLC for DOE/NNSA under contract DE-AC52-06NA25396.

6. References

[1] Private communication Jim Henkel, Y-12 Nat. Security Complex, Oak Ridge, TN, USA.

[2] R.M. Aikin Jr., “Triple Plate Mold Final Report: Optimization of the Mold Design and Casting Parameters for a Thin U-10mo Fuel Casting”, LA-UR-17-20036 (2017).

[4] P.C.L. Pfeil, J. Inst. Metals, v 77, pp. 553-570 (1950).

[5] S.P. Garg and R.J. Ackermann, J Nucl. Mater., v. 64, pp. 265-274 (1977).

[6] Flow-3D by Flow Science Inc., Santa Fe, NM USA.

[7] J.L. Klein, “Uranium and Its Alloys,” in Nuclear Reactor Fuel Elements, ed. A.R. Kaufmann, Wiley, New York-London, p. 31 (1962).

[8] J.R. Bridge, C.M. Schwartz, D.A. Vaughan, “X-Ray Diffraction Determination of the Coefficient of Expansion of Alpha-Uranium”, Trans AIME, v. 206, p. 1282 (1956).

[9] “Y-12 Technical Datasheets”, ed. V.C. Hemperly, Union Carbide Corp. (1978).

[10] Smithals Metals Reference Book 8th Edition, Ed. W.F. Gale and T.C. Totemeier, Elsevier (2004)

[11] W.D. Drotning, “Density and Thermal Expansion of Liquid U-Nb Alloys”, High Temp. High Press., v. 14, p. 253 (1982).

[12] Baseline mold design and process parameters private communication H.A. Longmire, Y-12 Nat. Security Complex, Oak Ridge, TN, USA.

[13] Thermophysical Properties of High Temperature Solid Materials, Vol. 1: Elements, The MacMillian Co. (1967)

[14] I. Barin, “Thermochemical Data of Pure Substances”, 3rd Ed., VCH (1995).

[15] Graphite Design Handbook, DOE-HTGR-88111 (1988).

[16] “Grade HLM Extruded Typical Physical Properties for 10-14 inch diameter”, Great Lakes Carbon Corp Technical Data Sheet 2330.

[17] “Typical Effect of Temperature on the Thermal Conductivity of Graphite”, Great Lakes Carbon Corp Technical Data Sheet 9050.

Tables

Table 1
Boundary Conditions and Thermophysical Properties use for Filling Simulations.

Initial and boundary conditions

MESHING
Use 3 mesh blocks
Break mold body into upper and lower objects to minimize simulation size
Grid size = 1.5 mm in most areas; 1 mm in mold cavities

INITIAL CONDITIONS:
Simulation dependent; see Figures 19, 23, and 32

BOUNDARY CONDITIONS
Metal pour temperature = 1673 K (100 deg superheat)
Temperature at top of mesh = 1673 K
Temperature at bottom of mesh simulation dependent; see Figures 1, 23, and 32
No radiation from mold surface

Interfacial Heat Transfer Coefficients:
Fluid/Mold IHTC = 2000 W/m^2•K above liquidus
Fluid/Mold IHTC linear from 2000 to 500 between liquidus and solidus
Fluid/Mold IHTC = 500 W/m^2•K below solidus
Crucible/Mold IHTC = 200 W/m^2•K
Mold/Mold IHTC = 100 W/m^2•K

Thermophysical - Fluid

See Section 2.1.1 for discussion of density

Used pure U viscosity and surface temperature properties from Smithals [10] since U-Mo data is unavailable
viscosity of liquid = 0.0065 kg/m•s (see best guess values for mushy zone effects)
surface tension coefficient = 1.55 N/m
surface tension coefficient temp sensitivity = -0.14E-3

Thermal conductivity of pure U from TPRC [13]

Temperature (K)	Therm. Cond. (W/m•K)
300	23.85
1100	42.26
1463	50.61
1504	25.3
2000	25.3

Enthalpies of U-Mo estimated from pure U data from Barin [14]
latent heat of transformation = 4.616E4 J/kg
specific heat of liquid = 201.3 J/kg•K
specific heat of solid = 181.1 J/kg•K

Solidus and liquidus based on linearized phase diagram informed by ref [5-6]
liquidus temperature =1503 K
solidus temperature =1433 K
reference temperature = 1408 K (tstar in Flow3D)
reference composition =0.10 (cstar in Flow3D)
partition coefficient = C_L/C_S = 1.727

Best guess values
static contact angle for fluid wall adhesion = 90 deg
dendrite coherency point = 0.16
critical fraction solid above with there is no fluid flow = 0.66
viscosity of liquid at dendrite coherency point = 0.0095 kg/m•s
molecular diffusion coefficient of the solute mass concentration = 1.4E4 kg/m•s

Thermophysical - Graphite Mold

For specific heat times density use properties of grade 2020 from Graphite Design Handbook (1988) [15]. Since 2020 and HLM density are similar these values should be a good approximation.

T (K)	Specific heat x Density ($J/K•kg^2$)
250	1.0201E+06
300	1.2687E+06
400	1.7628E+06
500	2.1674E+06
600	2.474E+06
700	2.7053E+06
800	2.8826E+06
900	3.0211E+06
1000	3.1314E+06
1100	3.2208E+06
1200	3.2943E+06
1300	3.3556E+06
1400	3.4073E+06
1500	3.4514E+06
1600	3.4893E+06
1700	3.5222E+06
1800	3.5509E+06
1900	3.5761E+06
2000	3.5984E+06

For the simulations done here the thermal conductivity of HLM grade was used for all mold objects was used. These values were approximated by taking the room

temperature data from Great Lakes Carbon Corp Technical Data Sheet 2320 [16] and then adjusting it as a function of temperature by correction curve given in Great Lakes Carbon Corp Technical Data Sheet 9050 [17].

Temperature (K)	Against-Grain Therm. Cond. (W/m•K)	With-Grain Therm. Cond. (W/m•K)
273	121.0	195.0
300	115.0	185.3
400	94.6	152.5
500	81.3	131.1
600	71.9	115.9
700	64.8	104.4
800	59.2	95.4
900	54.6	88.1
1000	50.9	82.0
1100	47.7	76.9
1200	45.0	72.5
1300	42.6	68.6
1400	40.5	65.3
1500	38.7	62.3
1600	37.0	59.6
1700	35.5	57.2
1800	34.2	55.1
1900	320.9	53.1
2000	31.8	51.3

The vertical axis of the crucible, top clamp and bottom clamp mold components would typically be machined parallel to the long axis (extrusion axis) of the HLM log. The book mold components would be machined with the long axis of the graphite log normal to the flat faces of the mold (along the horizontal direction). Since the thermal conductivity of HLM is 60% higher in the long axis direction than in the radial direction, these orientations are important to keep in mind when simulation of the heat flow in the casting is discussed.

Flow3D cannot take the anisotropic nature of the thermal conductivity of HLM graphite into account. The heat flow from the plates is across the metal/mold interface and then in the vertical direction down the thermal gradient. The heat flow in the book mold portion of the mold is thus primarily in a vertical direction. Since this direction is in the radial direction of the graphite log from which the mold was machined, the against-grain value of the thermal conductivity was used in the simulation. Simulations of this same geometry that used either the with-grain thermal conductivity or an average thermal conductivity produced experiment-simulation matches that were less in agreement with the experimental data.

Figures

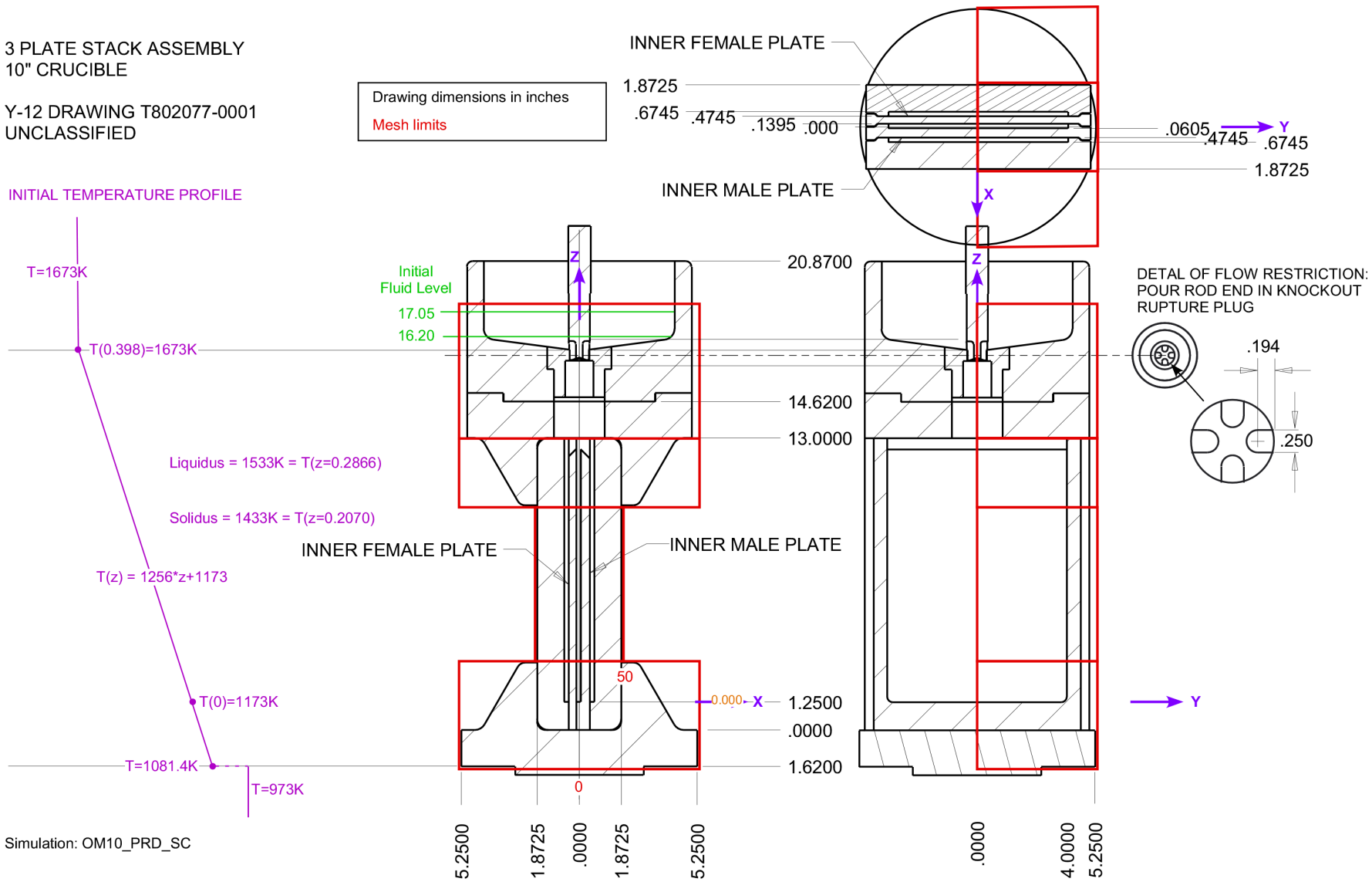

Fig. 1 Simulation setup for the original Y-12 triple plate mold with the pour rod down. Shown is the mold geometry, initial temperature distribution, mesh/simulation boundaries, and initial fluid levels.

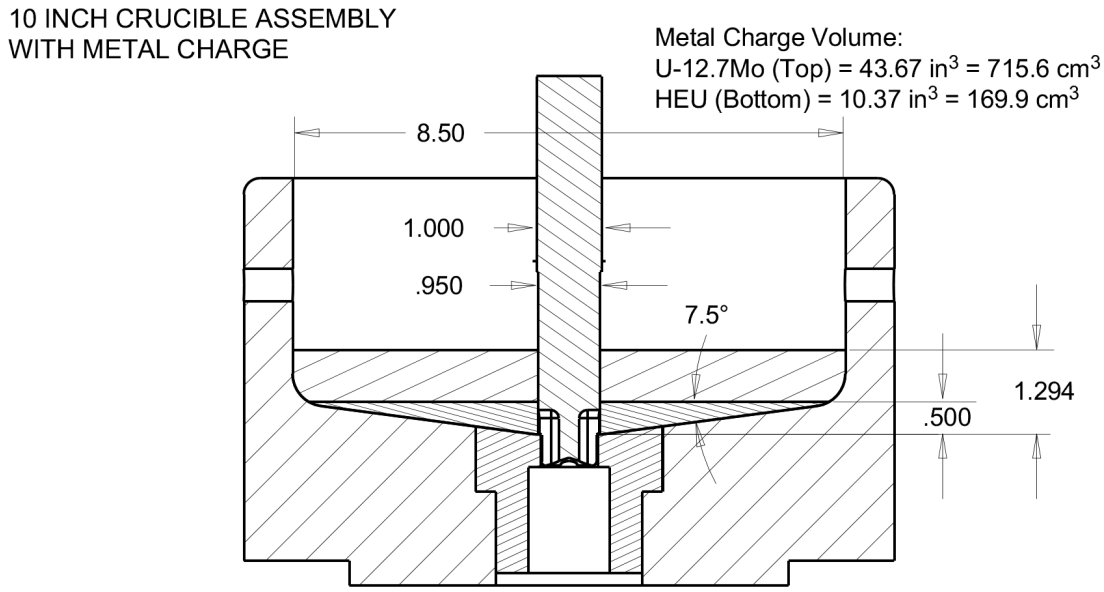

Fig. 2 Crucible detail for the original Y-12 triple plate mold with the pour rod down. Shown is the crucible and pour rod with the initial fluid levels.

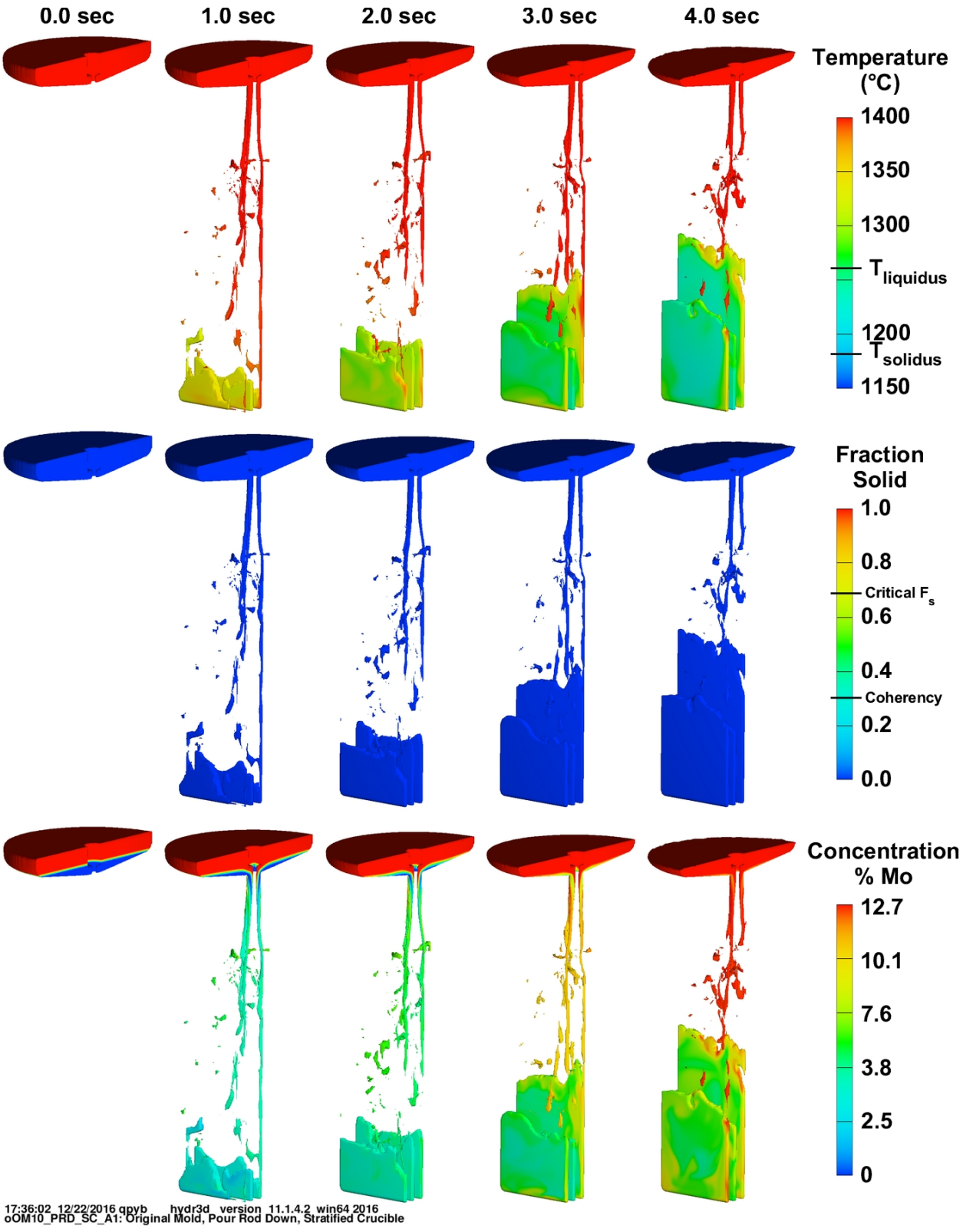

Fig. 3 Simulation results showing temperature, solid fraction and Mo concentration as a function of time for the original Y-12 triple plate mold with the pour rod down.

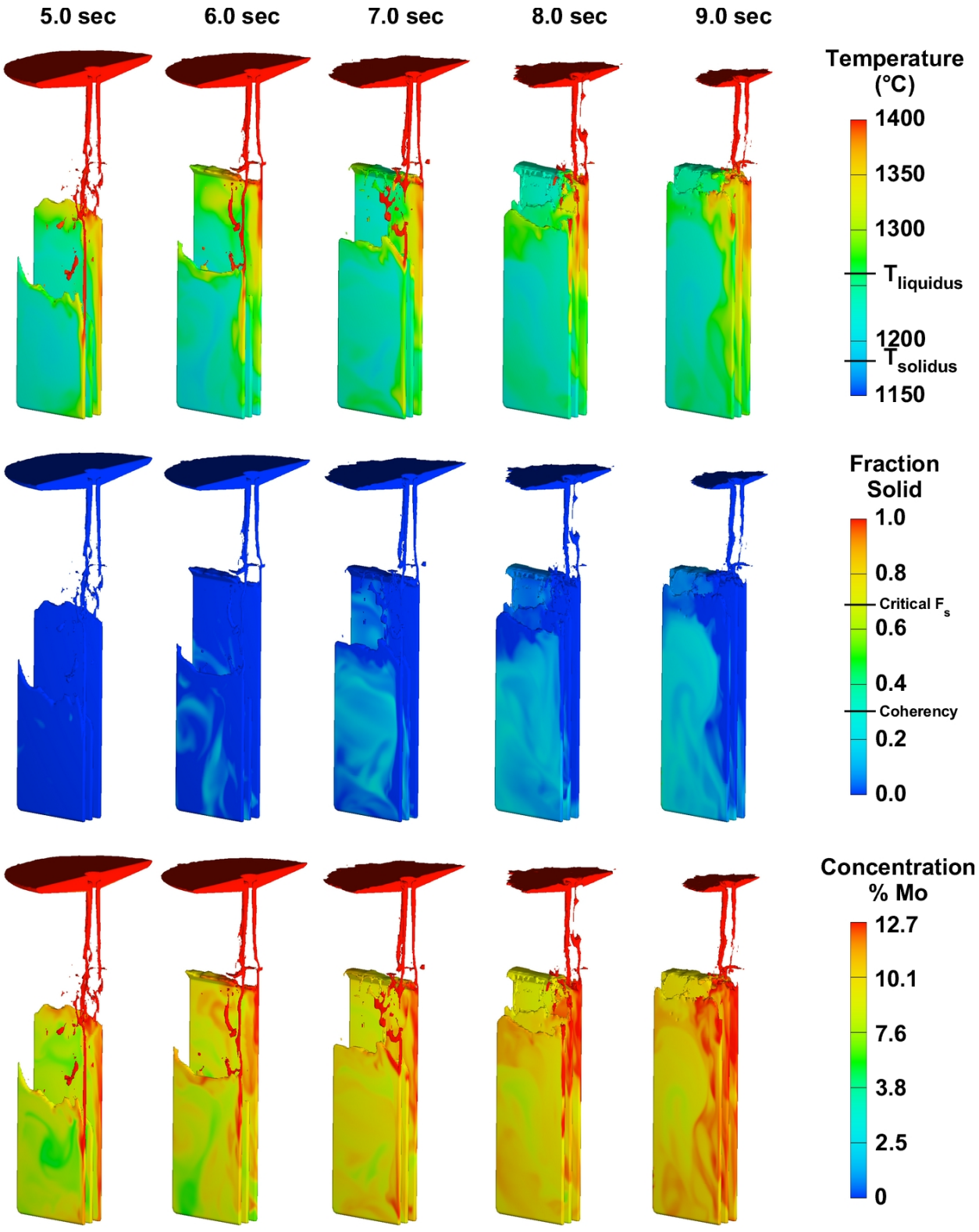

Fig. 3 (cont.) Simulation results showing temperature, solid fraction and Mo concentration as a function of time for the original Y-12 triple plate mold with the pour rod down.

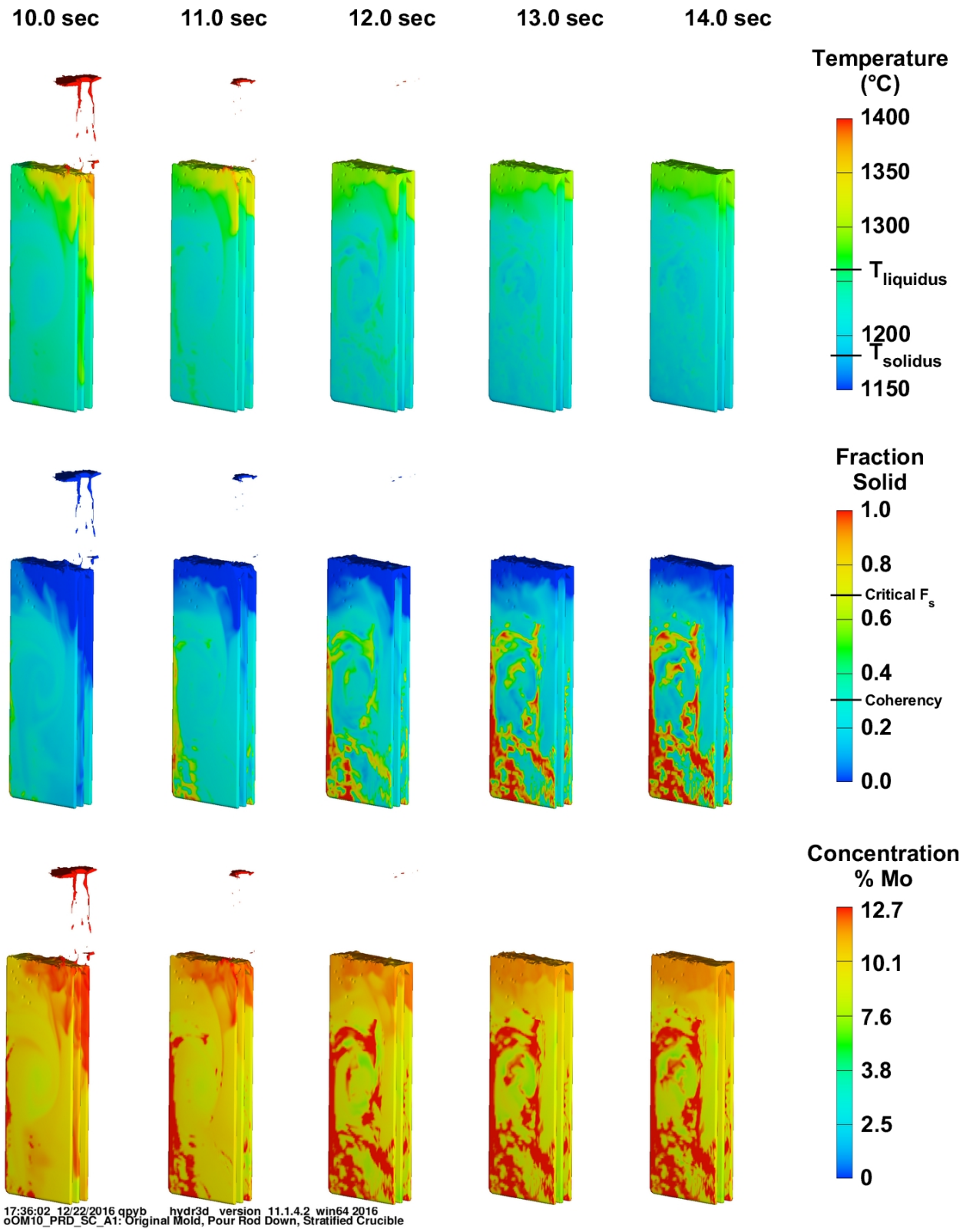

Fig. 3 (cont.) Simulation results showing temperature, solid fraction and Mo concentration as a function of time for the original Y-12 triple plate mold with the pour rod down.

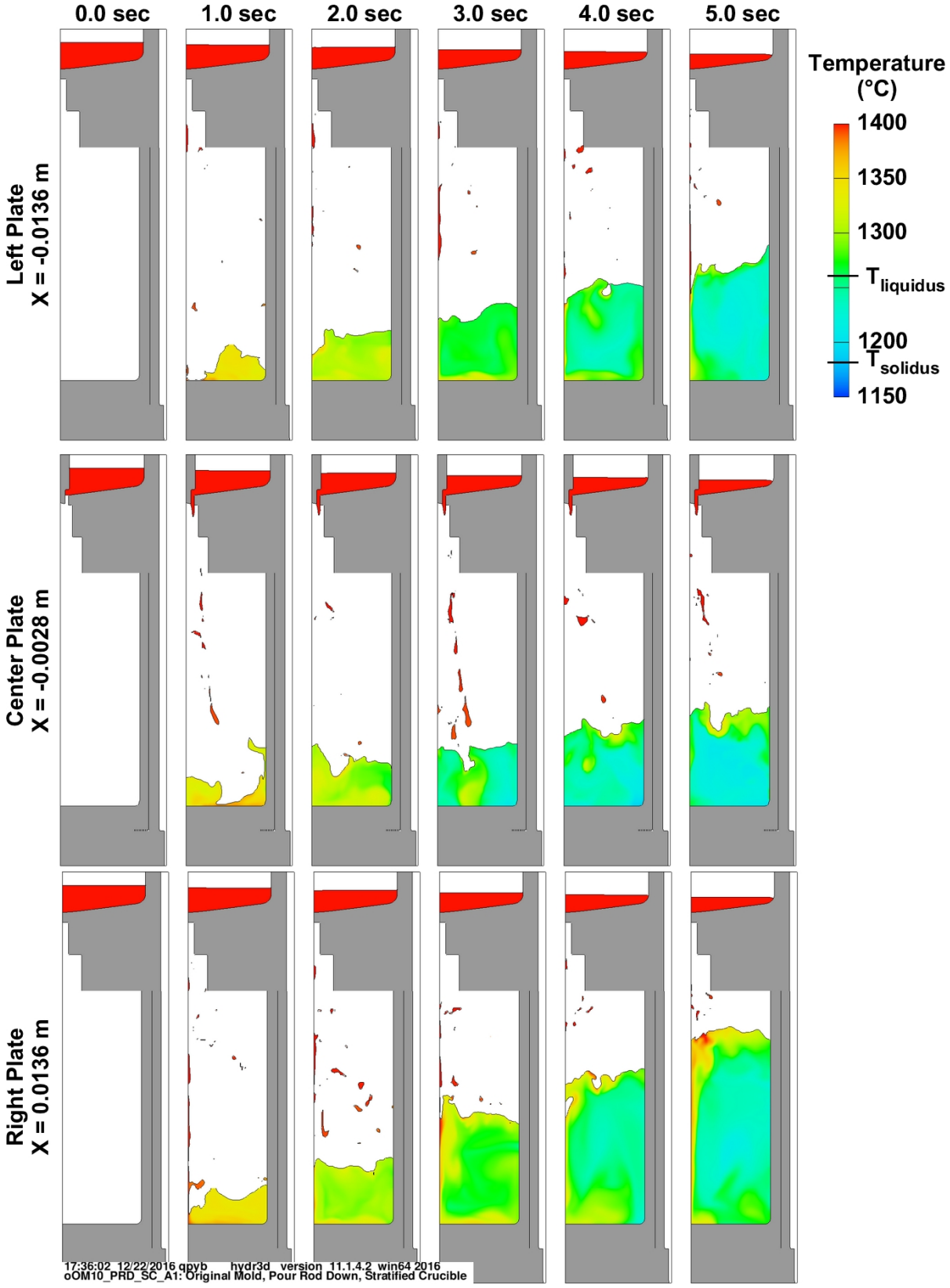

Fig. 4 Temperature as a function of time for the original mold with the pour rod down. Top row is through center of left plate, middle row is through the center plate, and bottom is through the right plate.

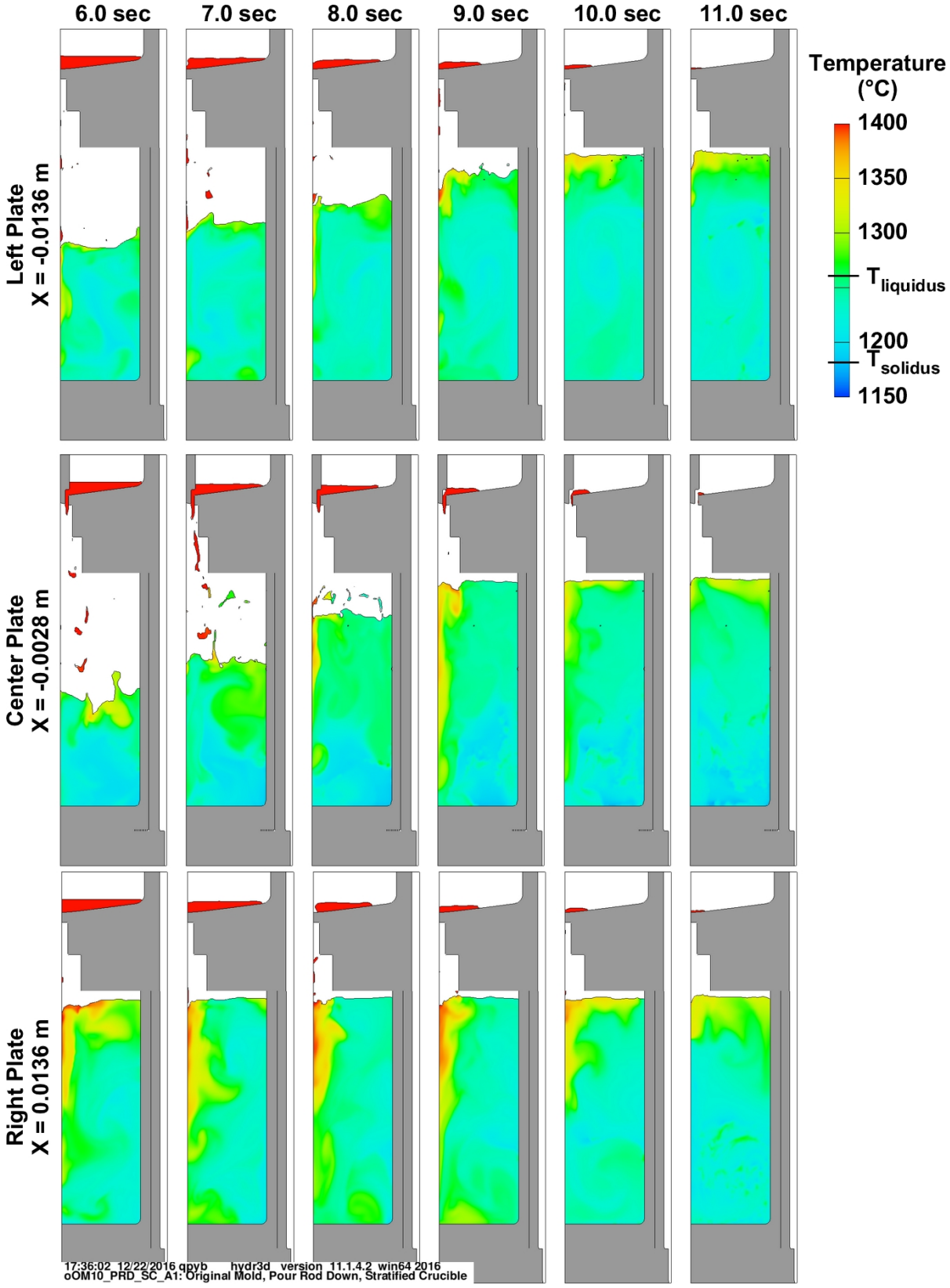

Fig. 4 (cont.) Temperature as a function of time for the original mold with the pour rod down. Top row is through center of left plate, middle row is through the center plate, and bottom is through the right plate.

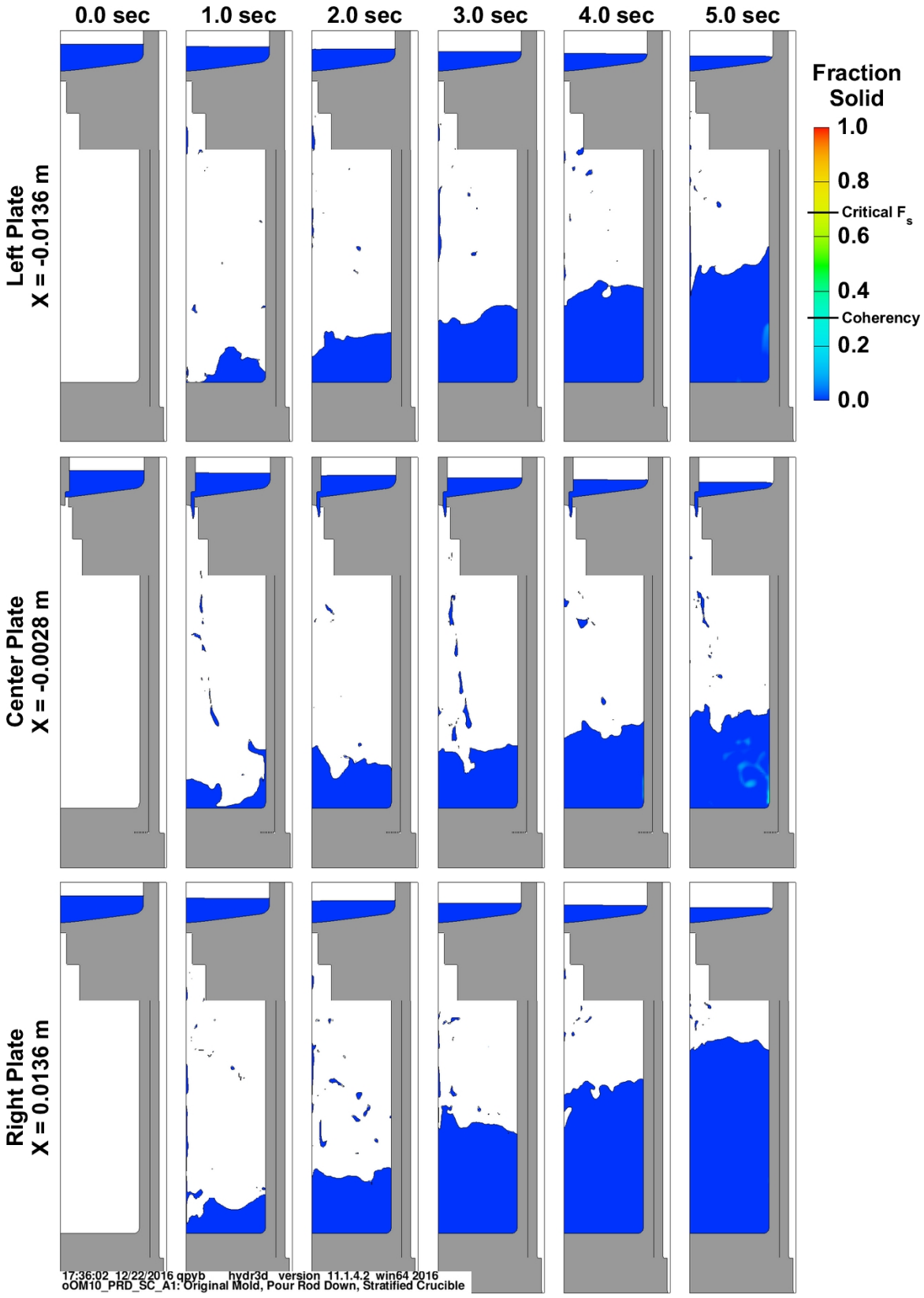

Fig. 5 Solid fraction as a function of time for the original mold with the pour rod down. Top row is through center of left plate, middle row is through the center plate, and bottom is through the right plate.

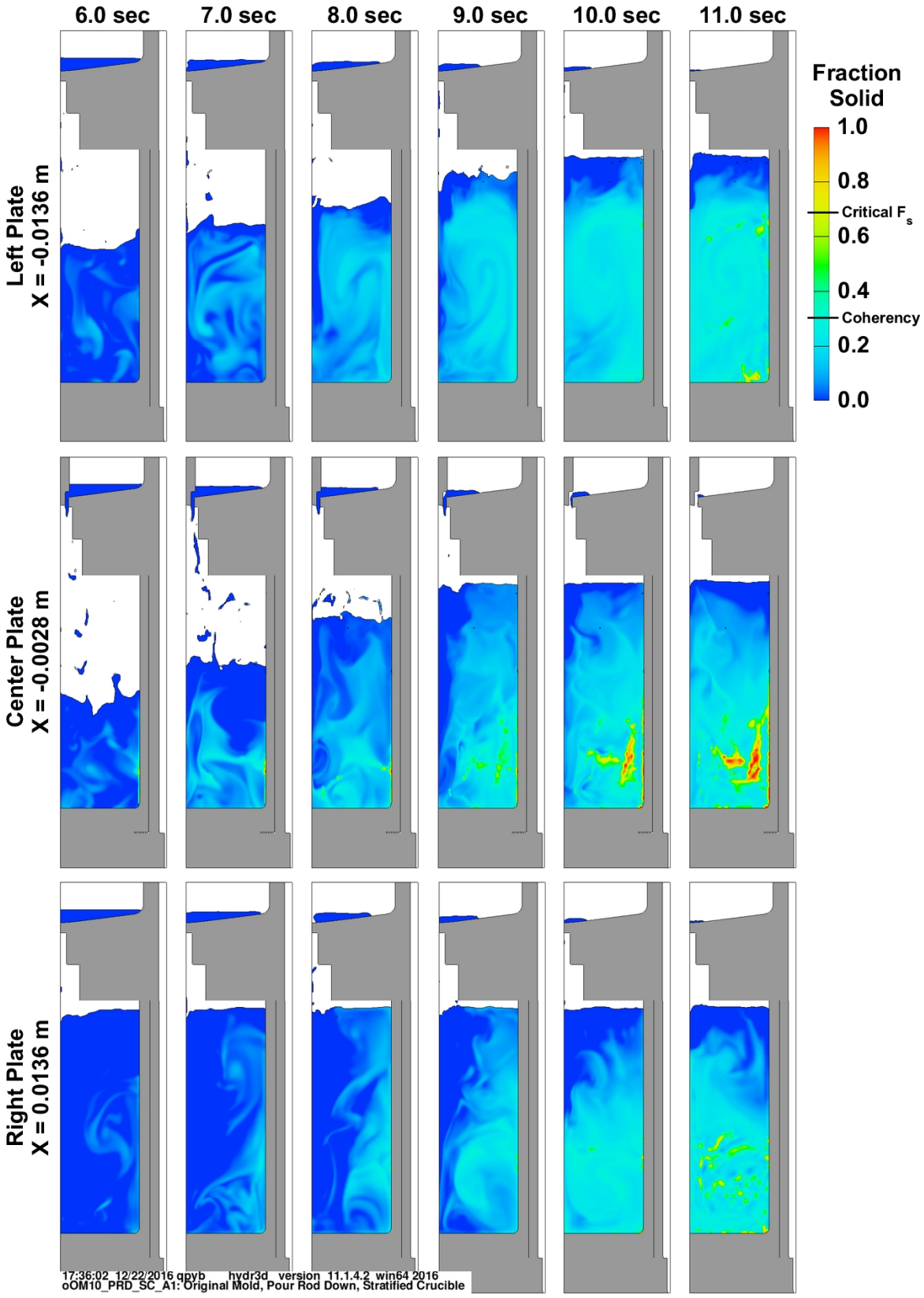

Fig. 5 (cont.) Solid fraction as a function of time for the original mold with the pour rod down. Top row is through center of left plate, middle row is through the center plate, and bottom is through the right plate.

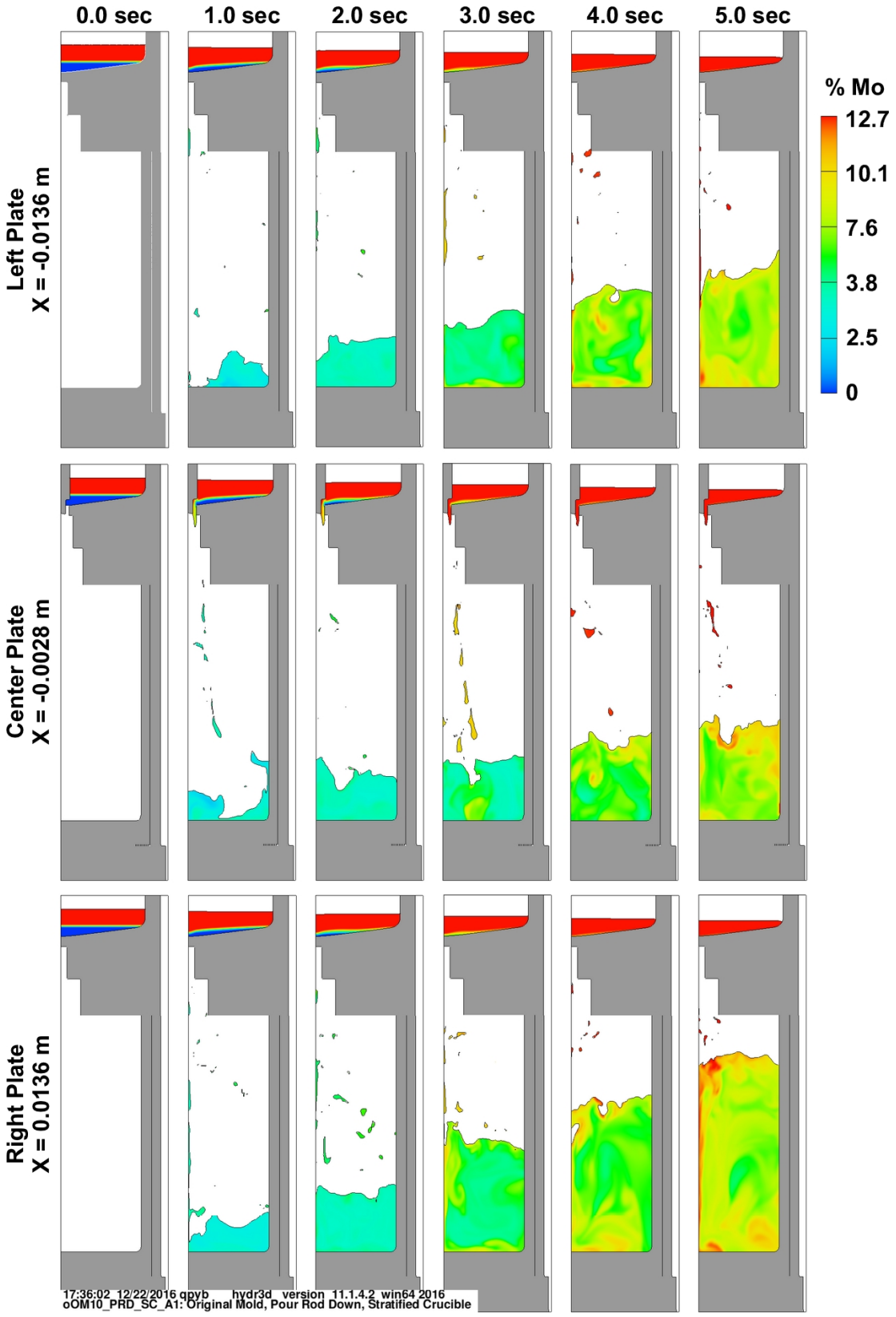

Fig. 6 Concentration of Mo as a function of time for the original mold with the pour rod down. Top row is through center of left plate, middle row is through the center plate, and bottom is through the right plate.

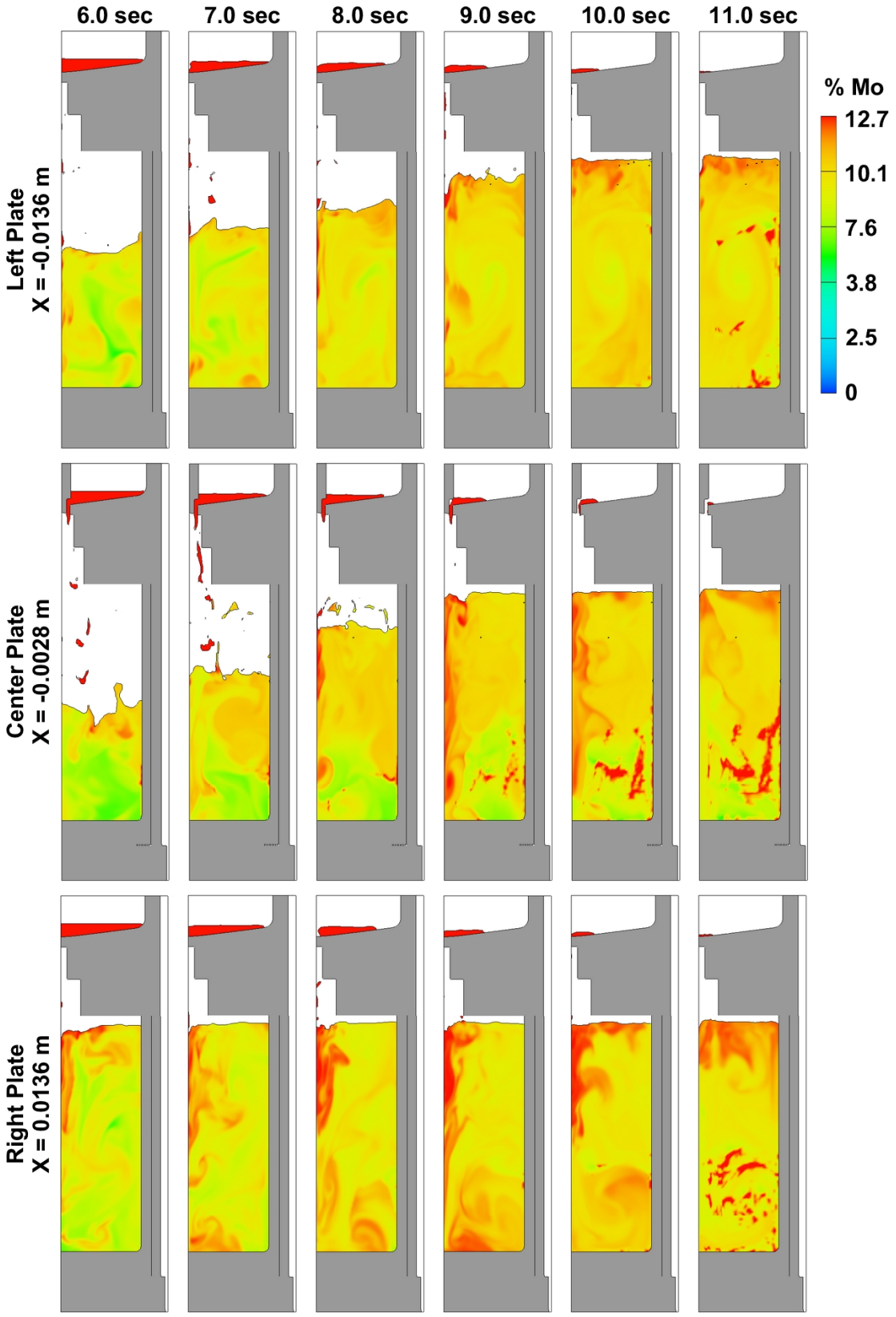

Fig. 6 (cont.) Concentration of Mo as a function of time for the original mold with the pour rod down. Top row is through center of left plate, middle row is through the center plate, and bottom is through the right plate.

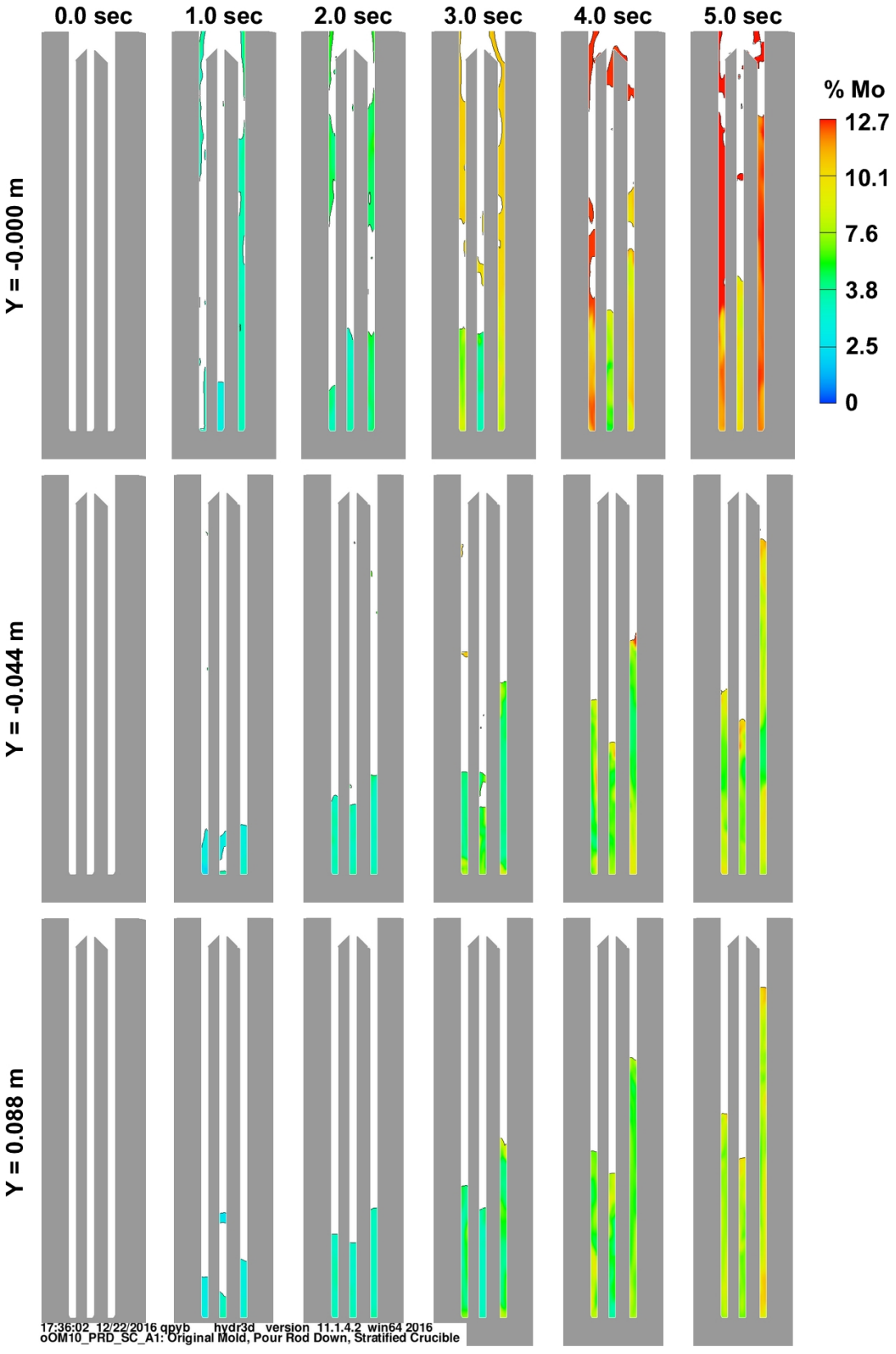

Fig. 7 X-Y cross-section of concentration of Mo as a function of time for the original mold with the pour rod down. Top row is through Y=0, middle row is through Y=0.044m, and bottom is through Y=0.088 m.

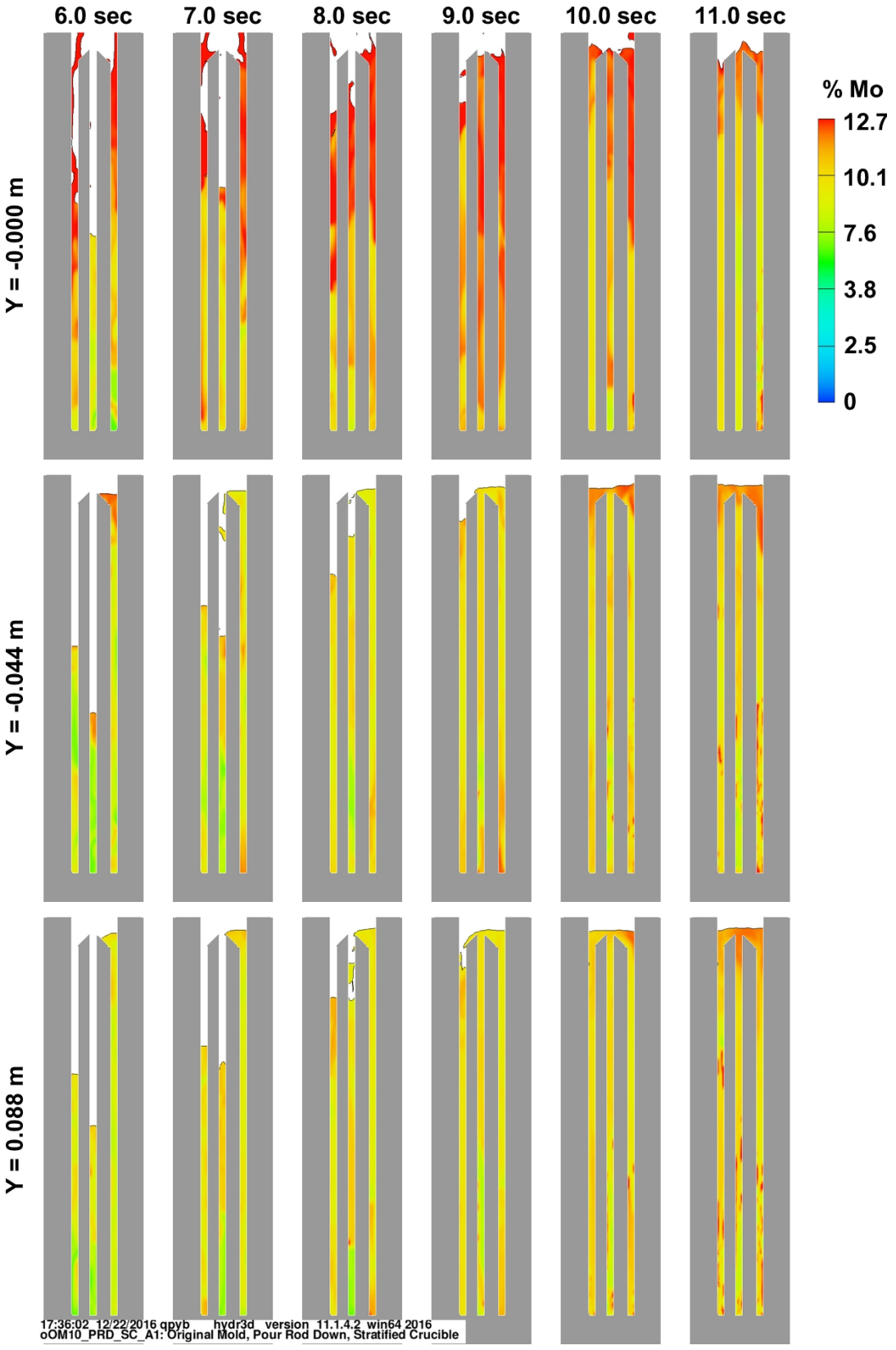

Fig. 7 (cont.) X-Y cross-section of concentration of Mo as a function of time for the original mold with the pour rod down. Top row is through Y=0, middle row is through Y=0.044m, and bottom is through Y=0.088 m.

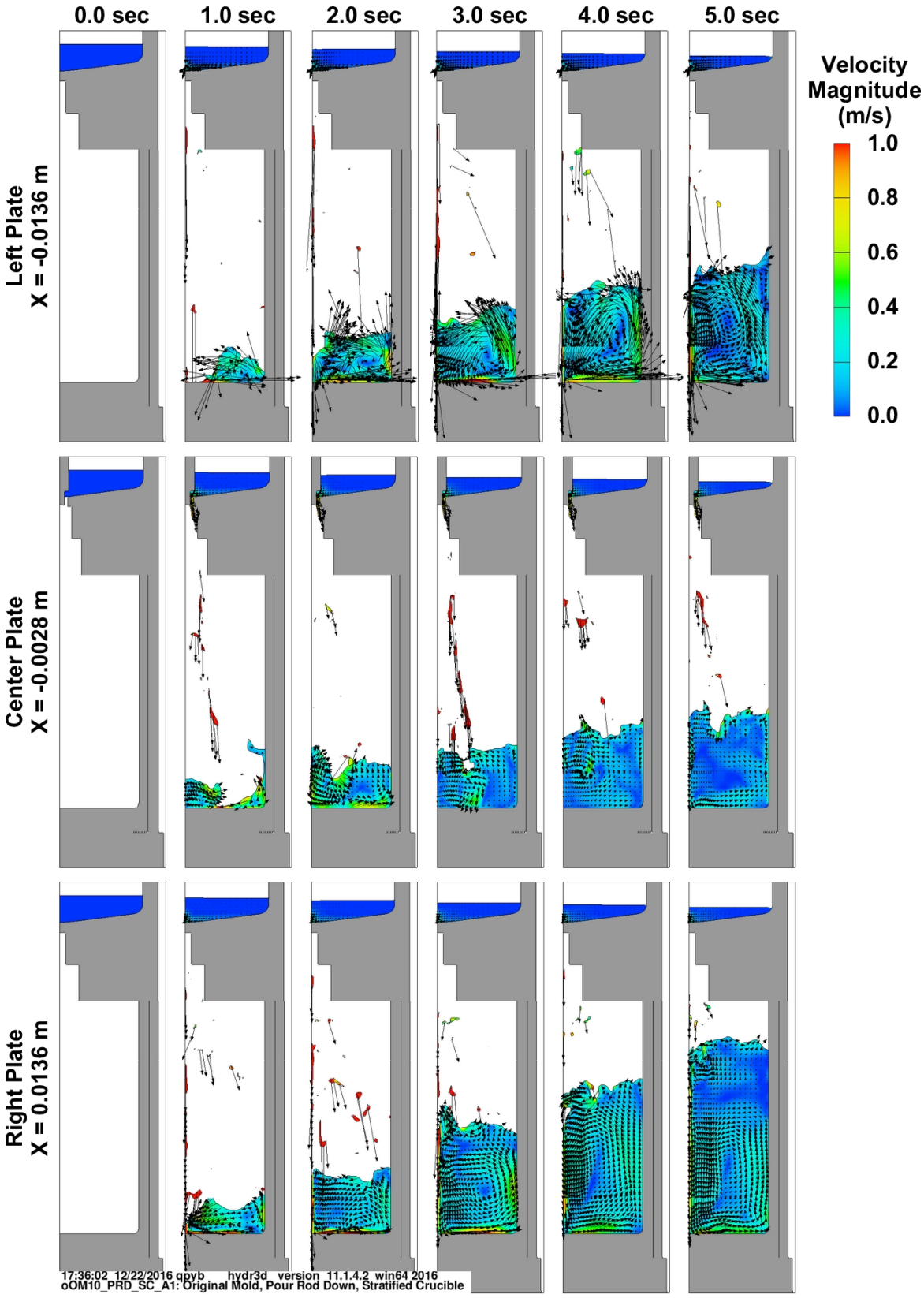

Fig. 8 Velocity magnitude and flow direction a function of time for the original mold with the pour rod down. Top row is through center of left plate, middle row is through the center plate, and bottom is through the right plate.

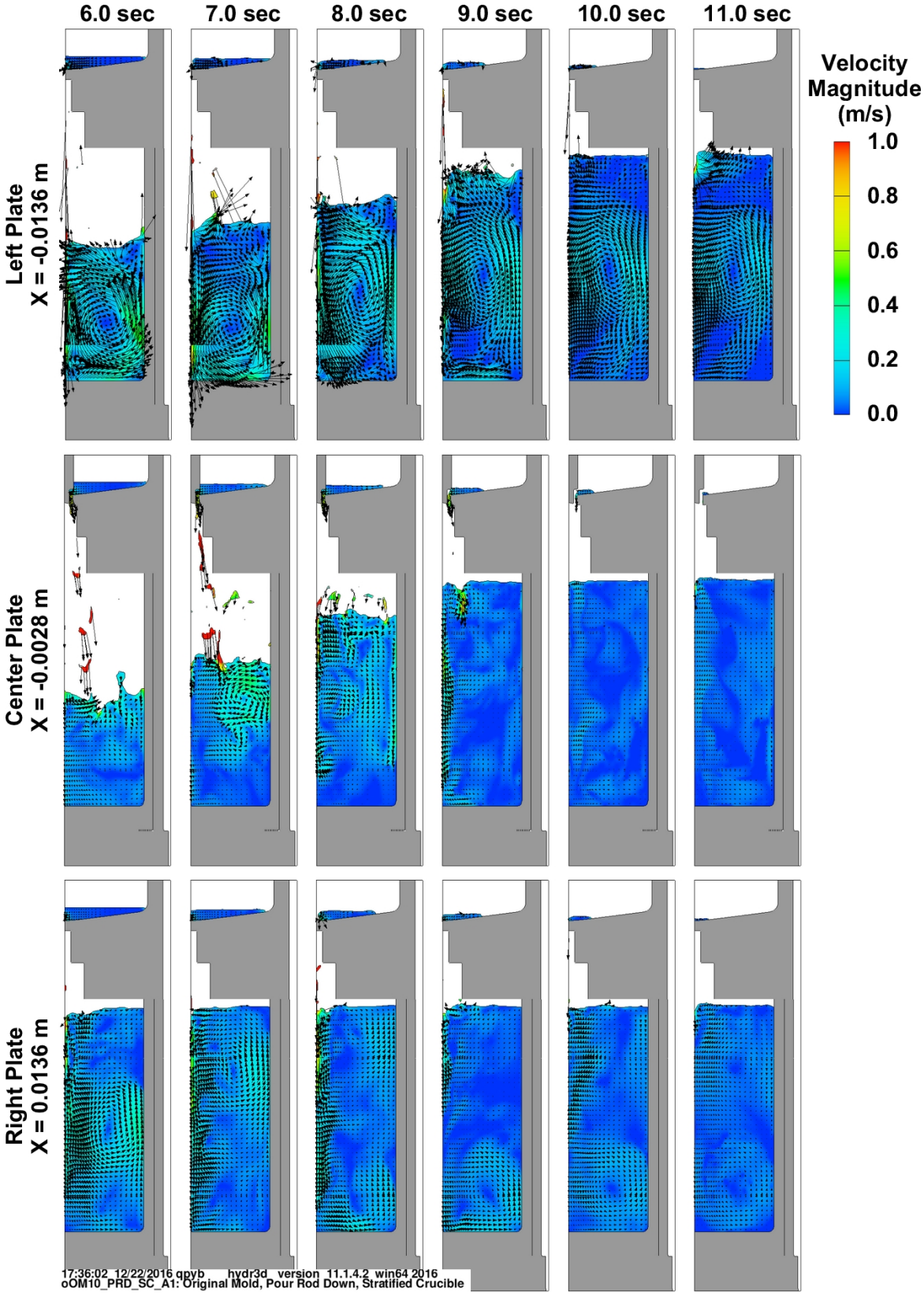

Fig. 8 (cont.) Velocity magnitude and flow direction a function of time for the original mold with the pour rod down. Top row is through center of left plate, middle row is through the center plate, and bottom is through the right plate.

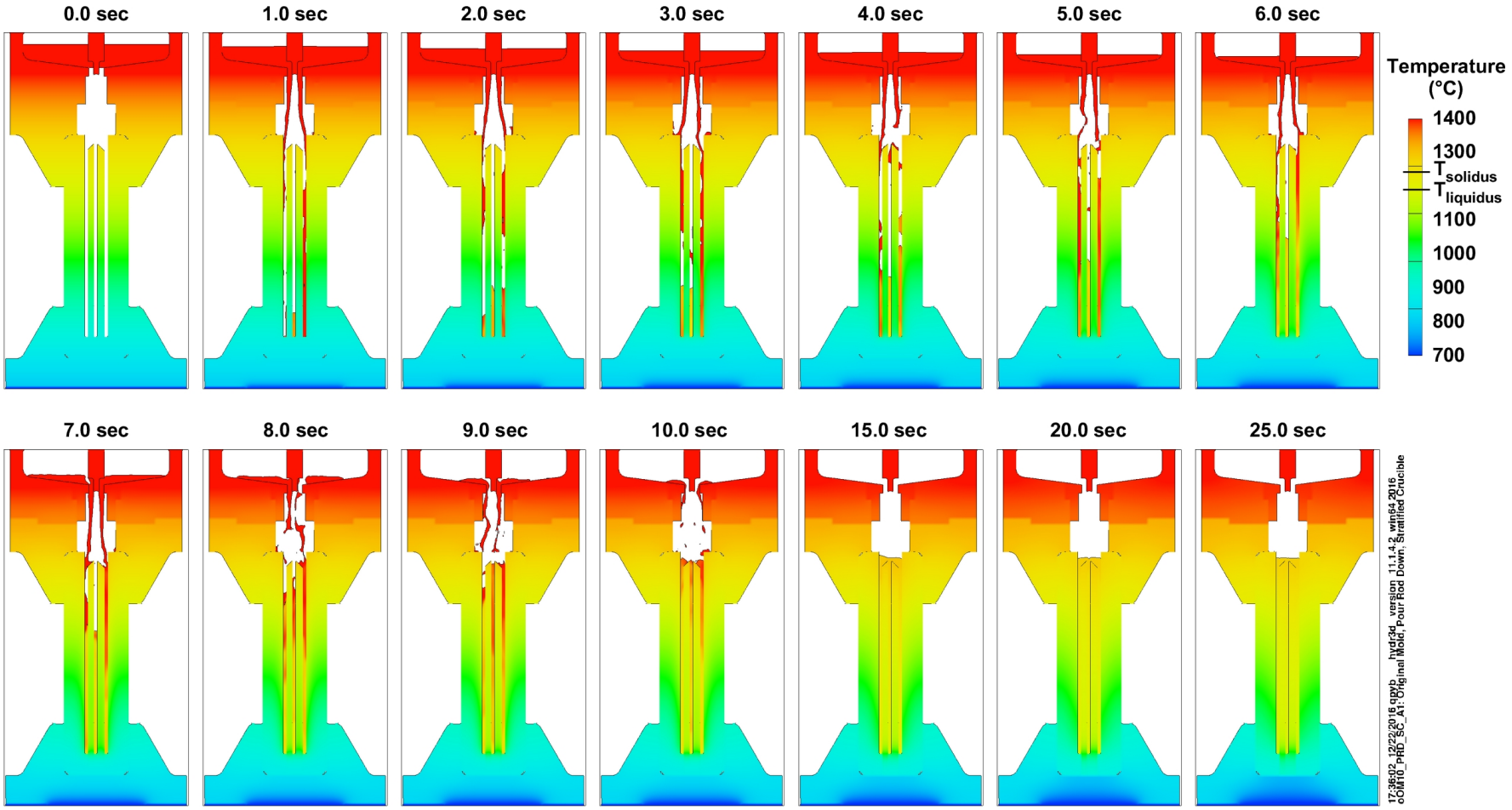

Fig. 9 Temperature of mold and metal as a function of time for the original mold with the pour rod down. Shown is a X-Z slice along Y=0.

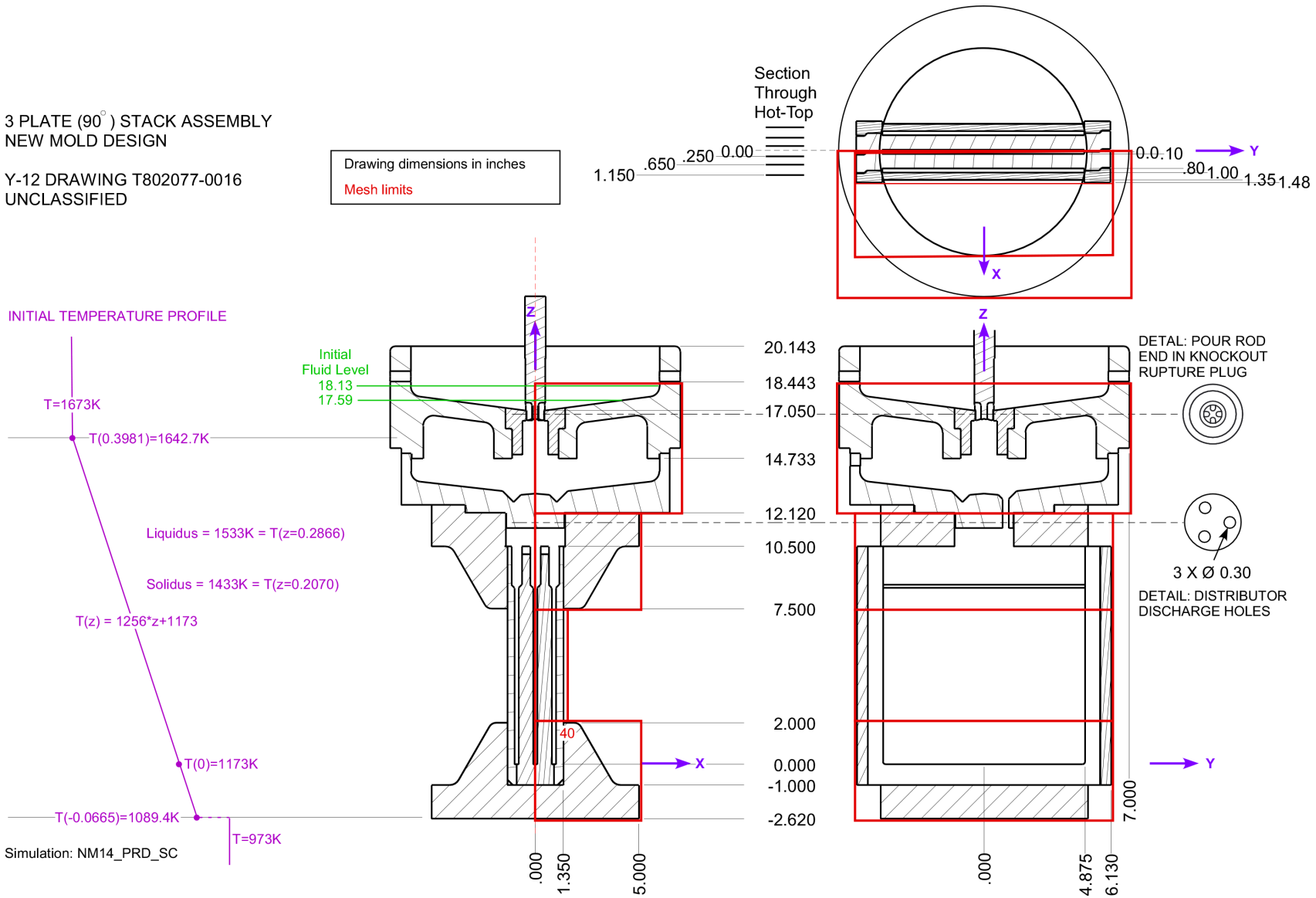

Fig. 10 Simulation setup for the horizontal triple plate mold with the pour rod down. Shown is the mold geometry, initial temperature distribution, mesh/simulation boundaries, and initial fluid levels.

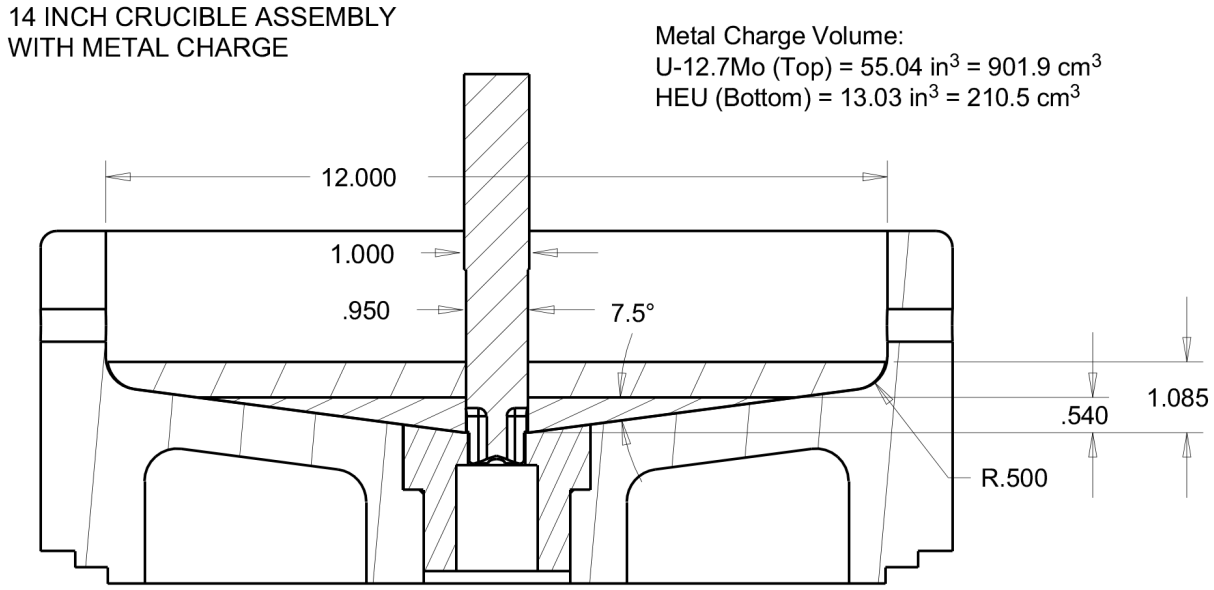

Fig. 11 Crucible detail for the horizontal triple plate mold with the pour rod down. Shown is the crucible and pour rod with the initial fluid levels.

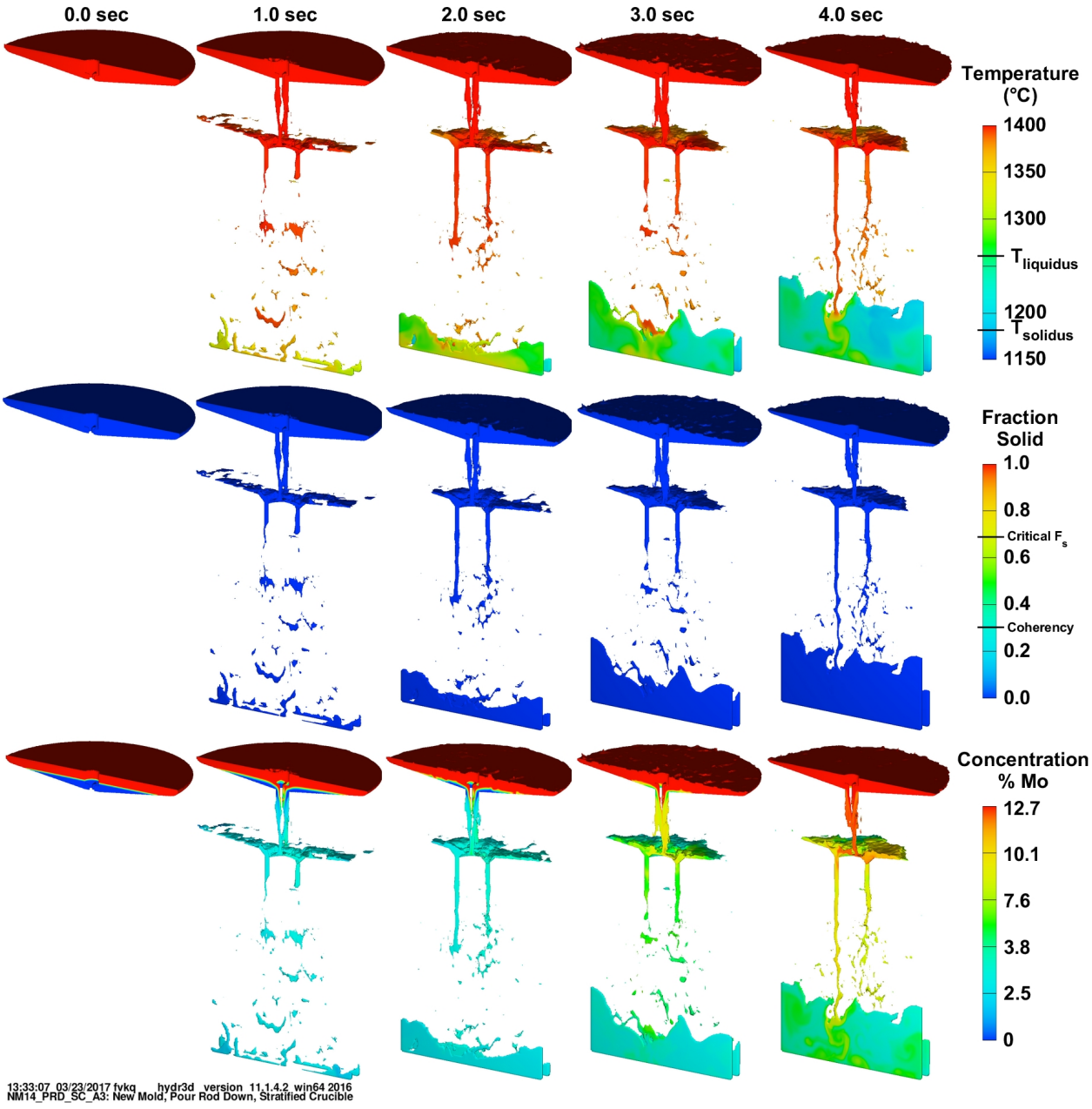

Fig. 12 Simulation results showing temperature, solid fraction and Mo concentration as a function of time for the horizontal triple plate mold with the pour rod down.

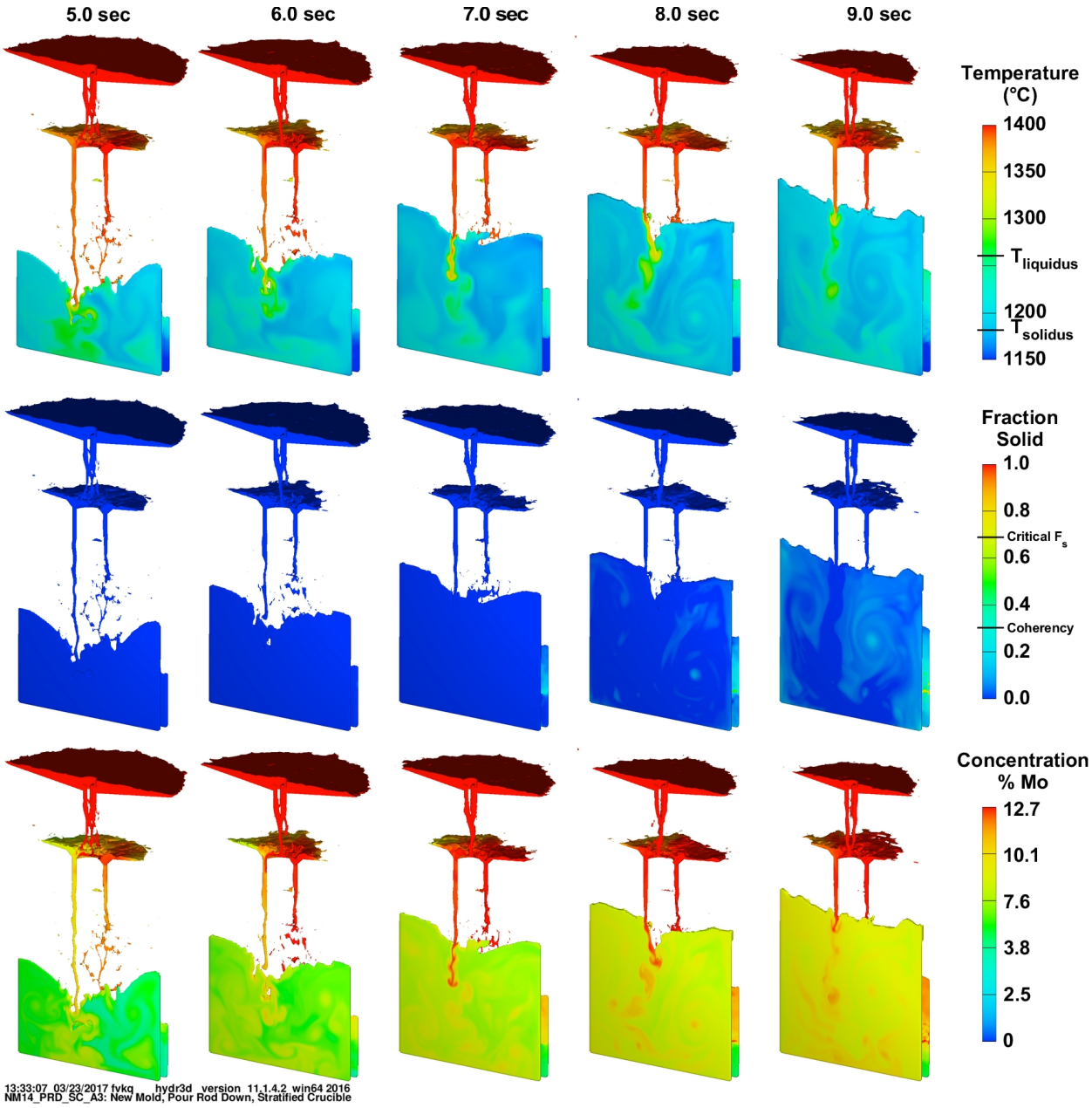

Fig. 12 (cont.) Simulation results showing temperature, solid fraction and Mo concentration as a function of time for the horizontal triple plate mold with the pour rod down.

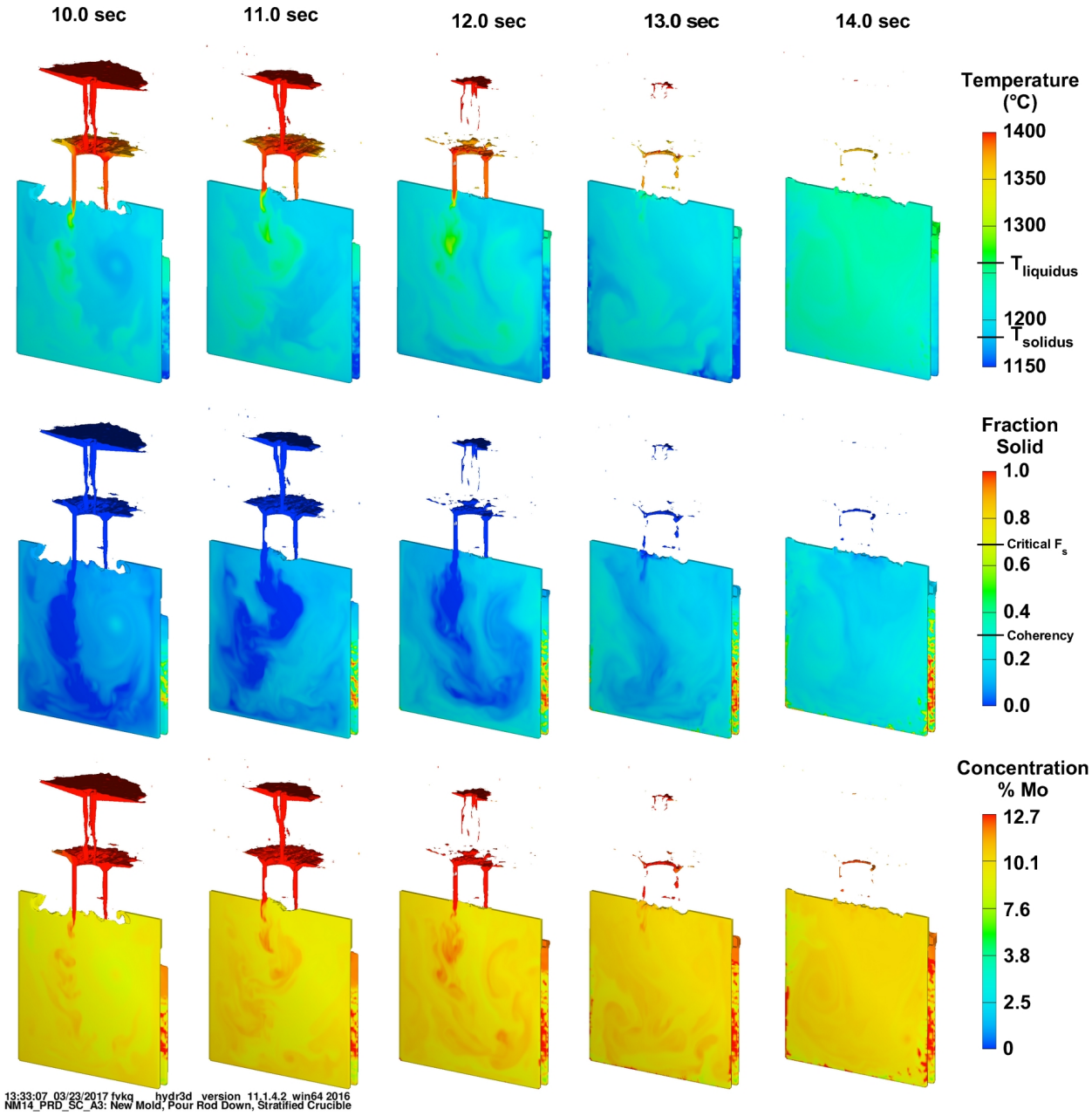

Fig. 12 (cont.) Simulation results showing temperature, solid fraction and Mo concentration as a function of time for the horizontal triple plate mold with the pour rod down.

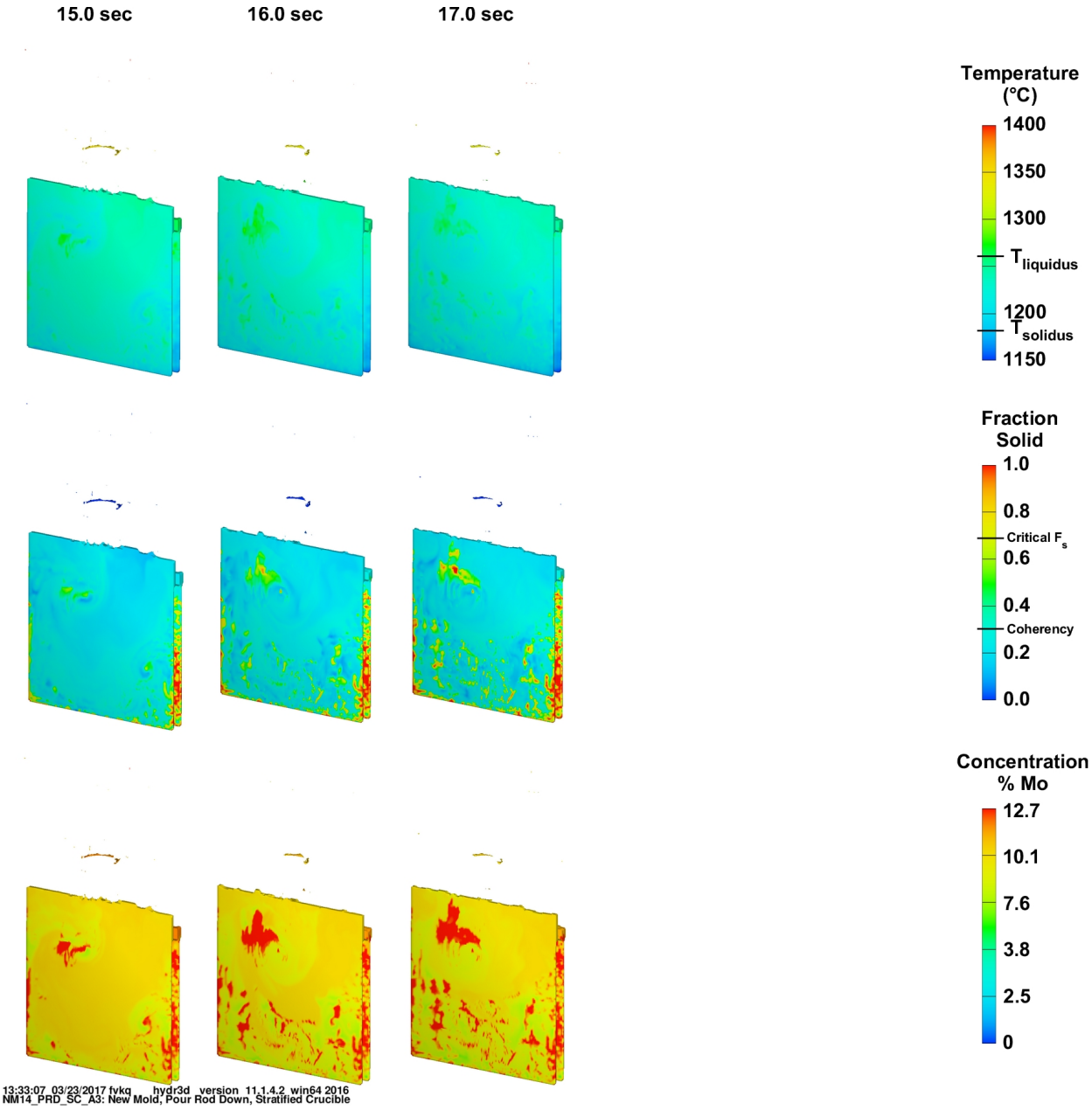

Fig. 12 (cont.) Simulation results showing temperature, solid fraction and Mo concentration as a function of time for the horizontal triple plate mold with the pour rod down.

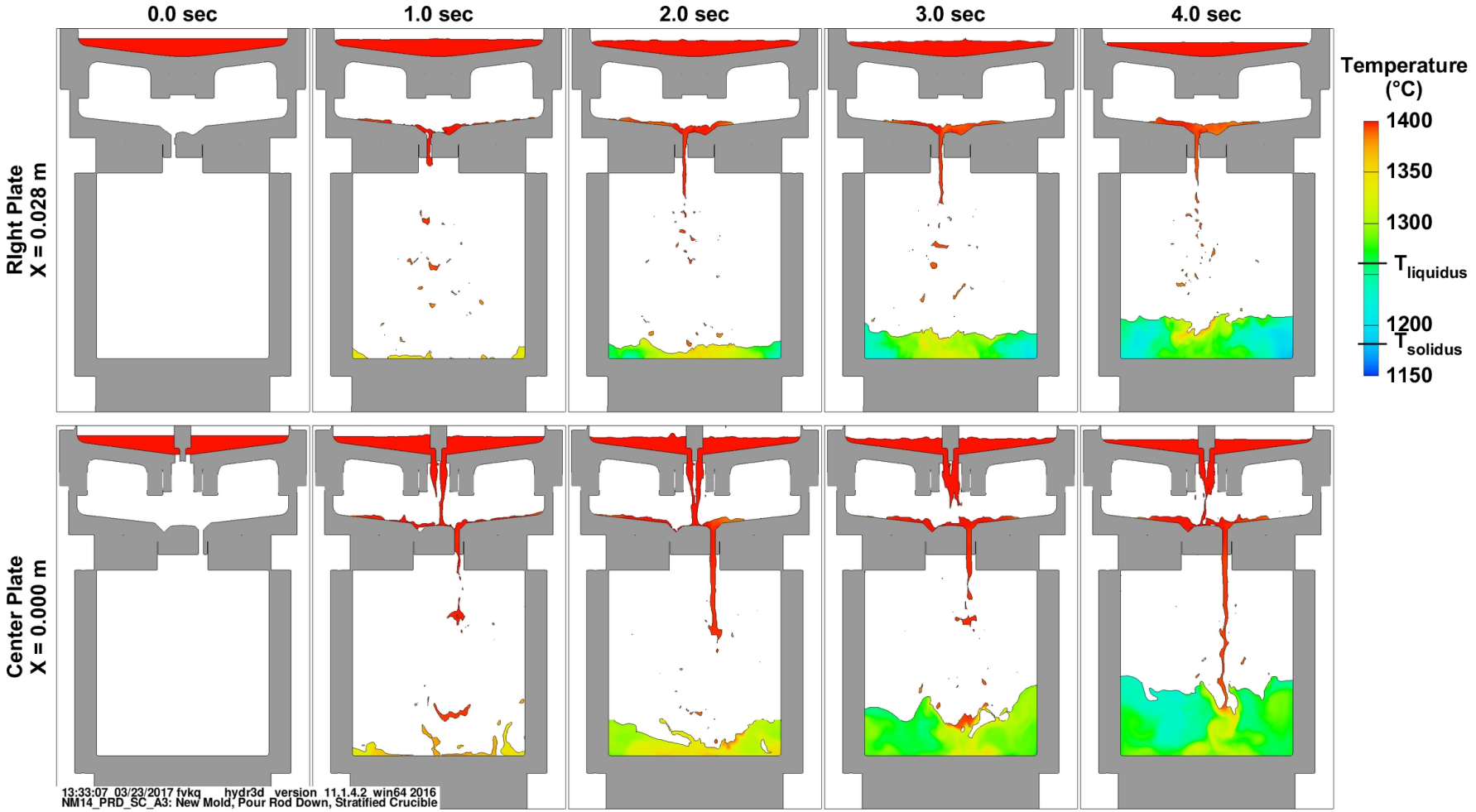

Fig. 13 Temperature as a function of time for the horizontal mold with the pour rod down. Top row is through the center of the left plate and the bottom row is through the center plate.

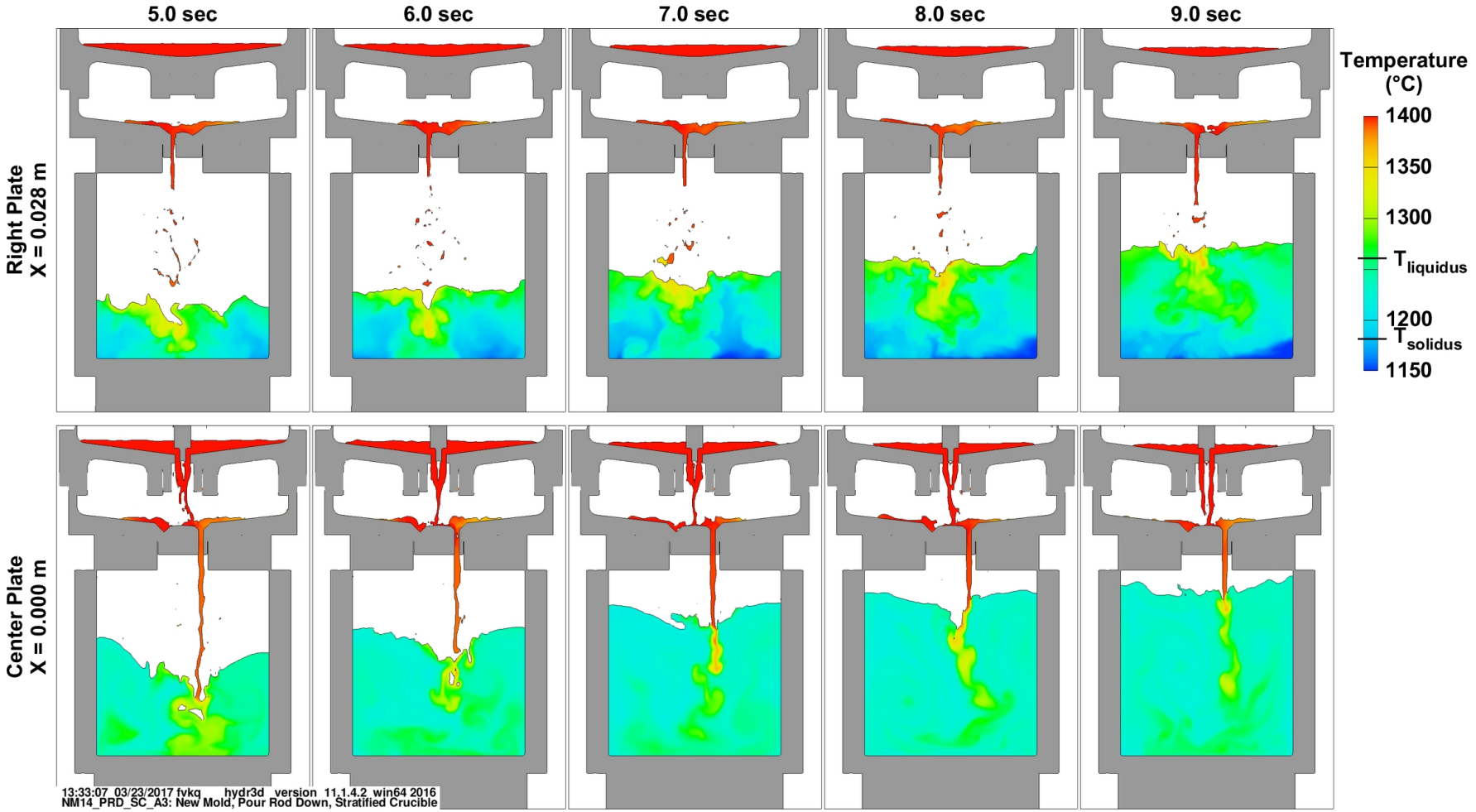

Fig. 13 (cont.) Temperature as a function of time for the horizontal mold with the pour rod down. Top row is through the center of the left plate and the bottom row is through the center plate.

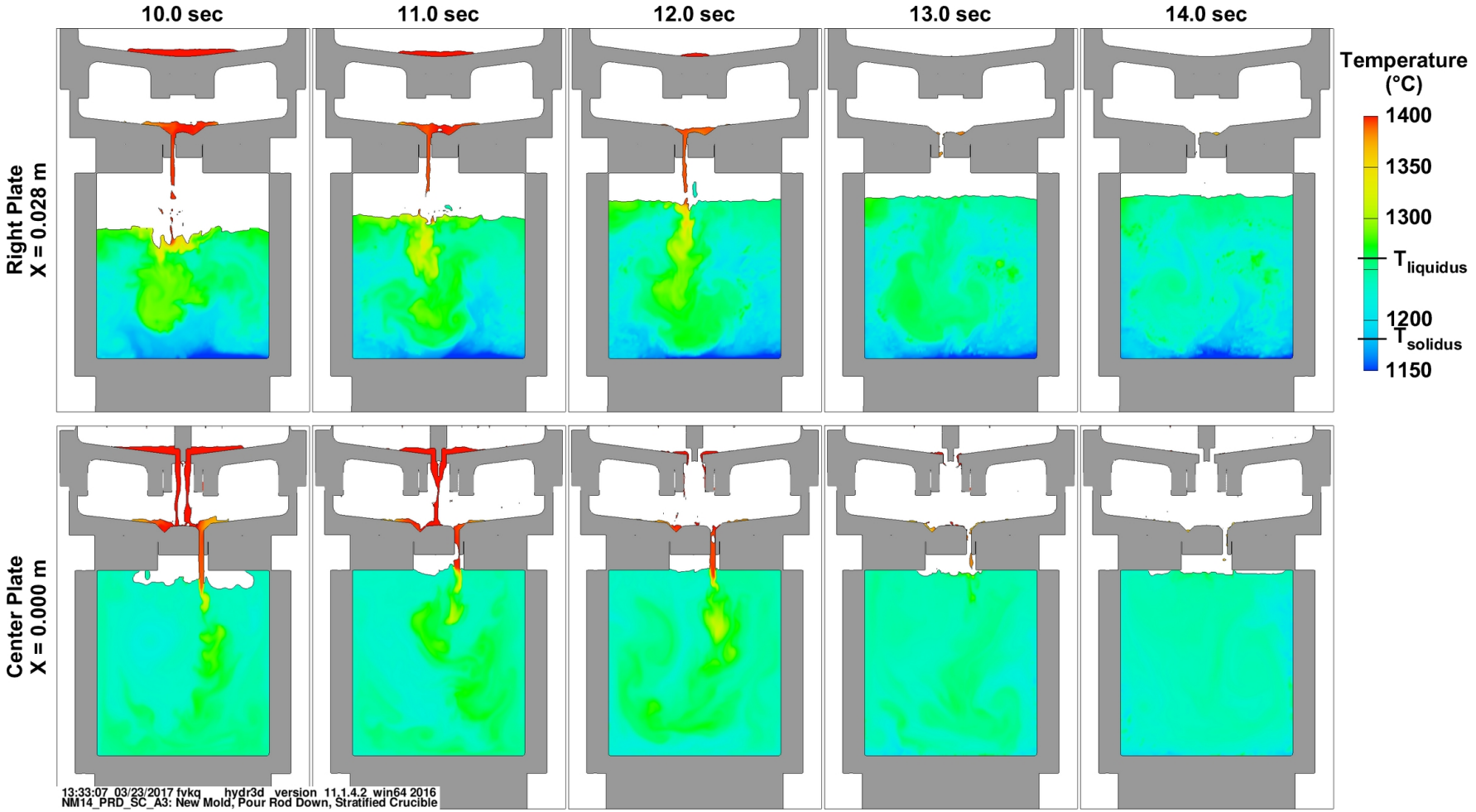

Fig. 13 (cont.) Temperature as a function of time for the horizontal mold with the pour rod down. Top row is through the center of the left plate and the bottom row is through the center plate.

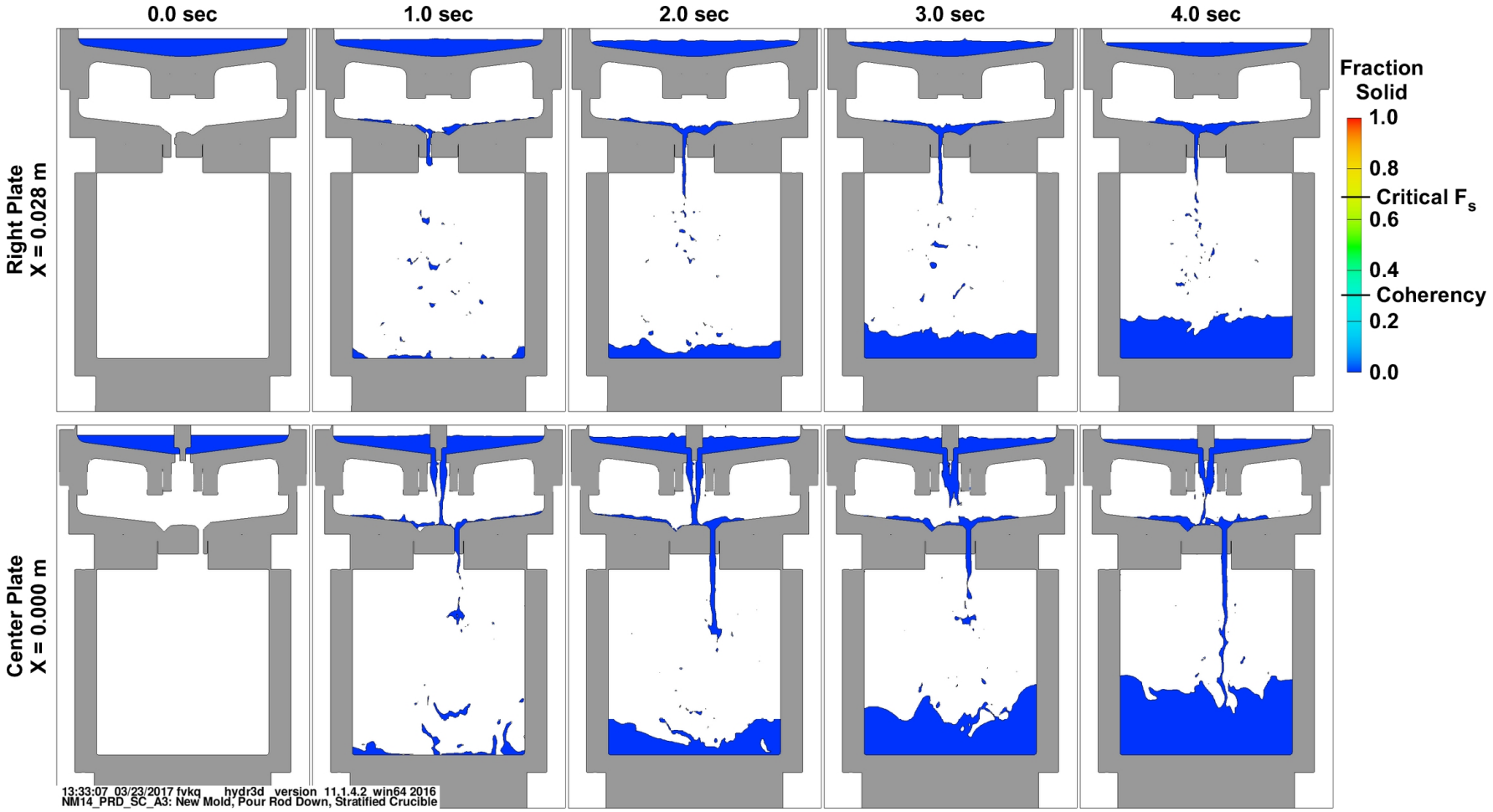

Fig. 14 Solid fraction as a function of time for the horizontal mold with the pour rod down. Top row is through the center of the left plate and the bottom row is through the center plate.

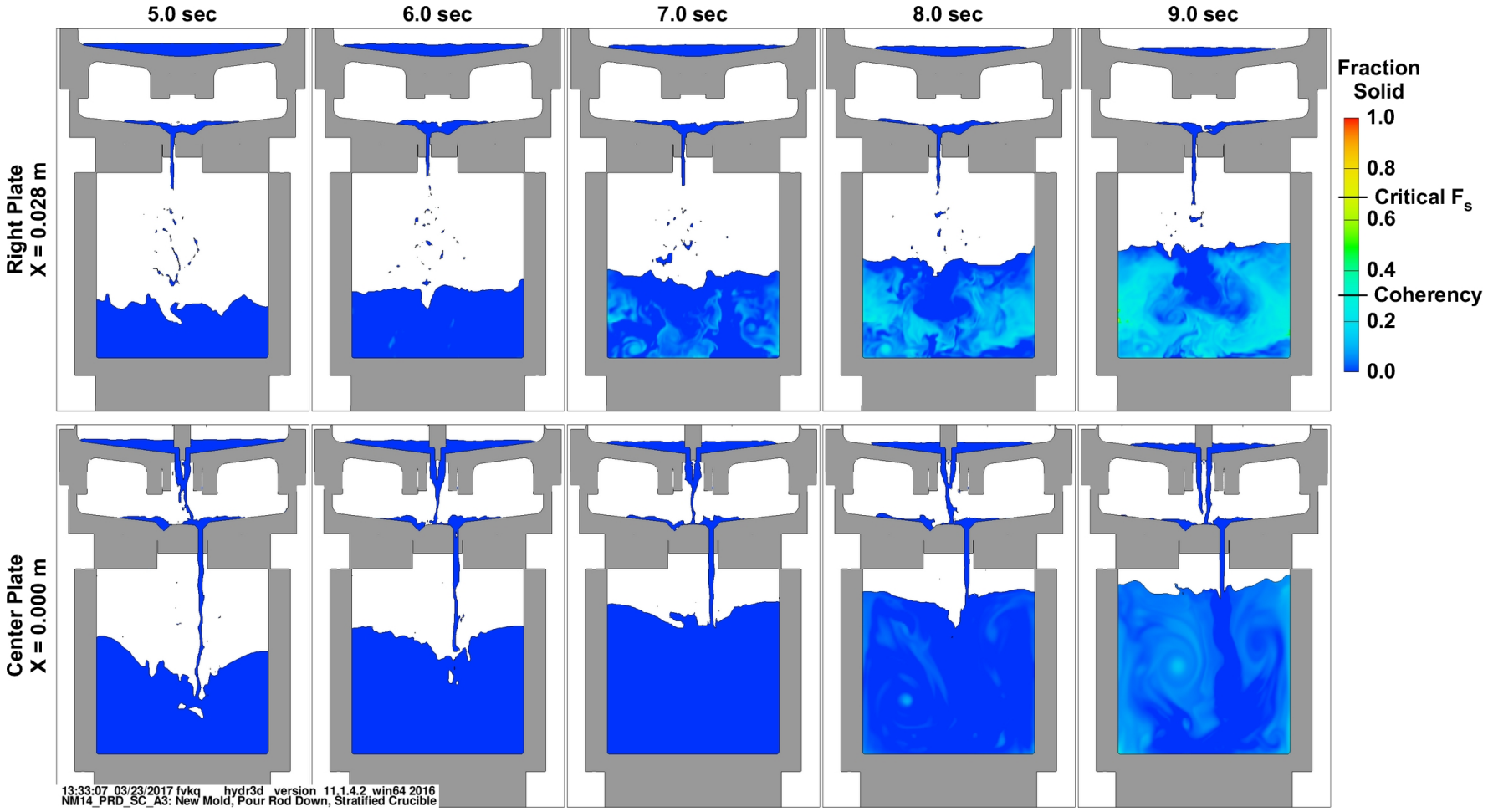

Fig. 14 (cont.) Solid fraction as a function of time for the horizontal mold with the pour rod down. Top row is through the center of the left plate and the bottom row is through the center plate.

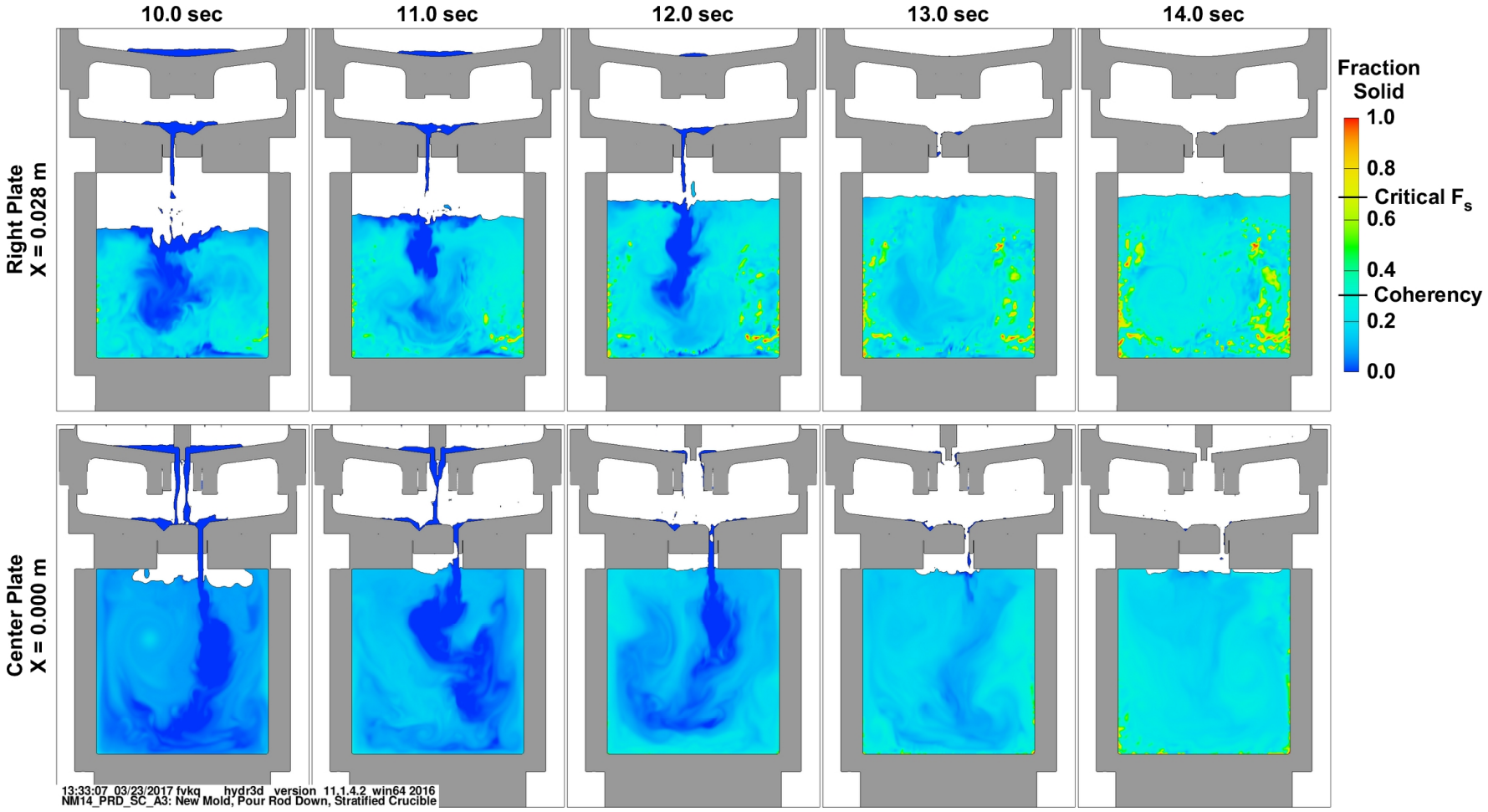

Fig. 14 (cont.) Solid fraction as a function of time for the horizontal mold with the pour rod down. Top row is through the center of the left plate and the bottom row is through the center plate.

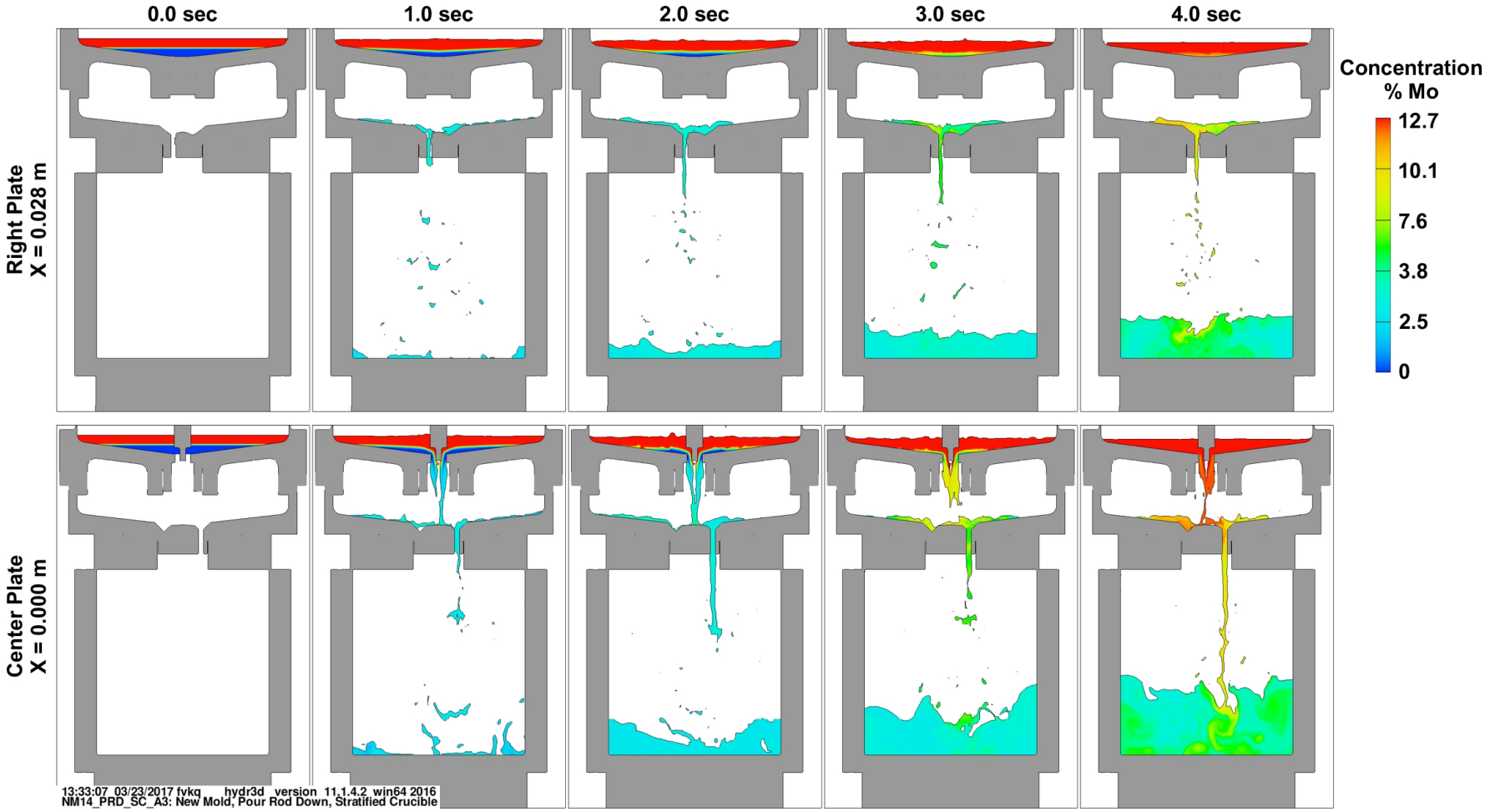

Fig. 15 Concentration of Mo as a function of time for the horizontal mold with the pour rod down Top row is through the center of the left plate and the bottom row is through the center plate.

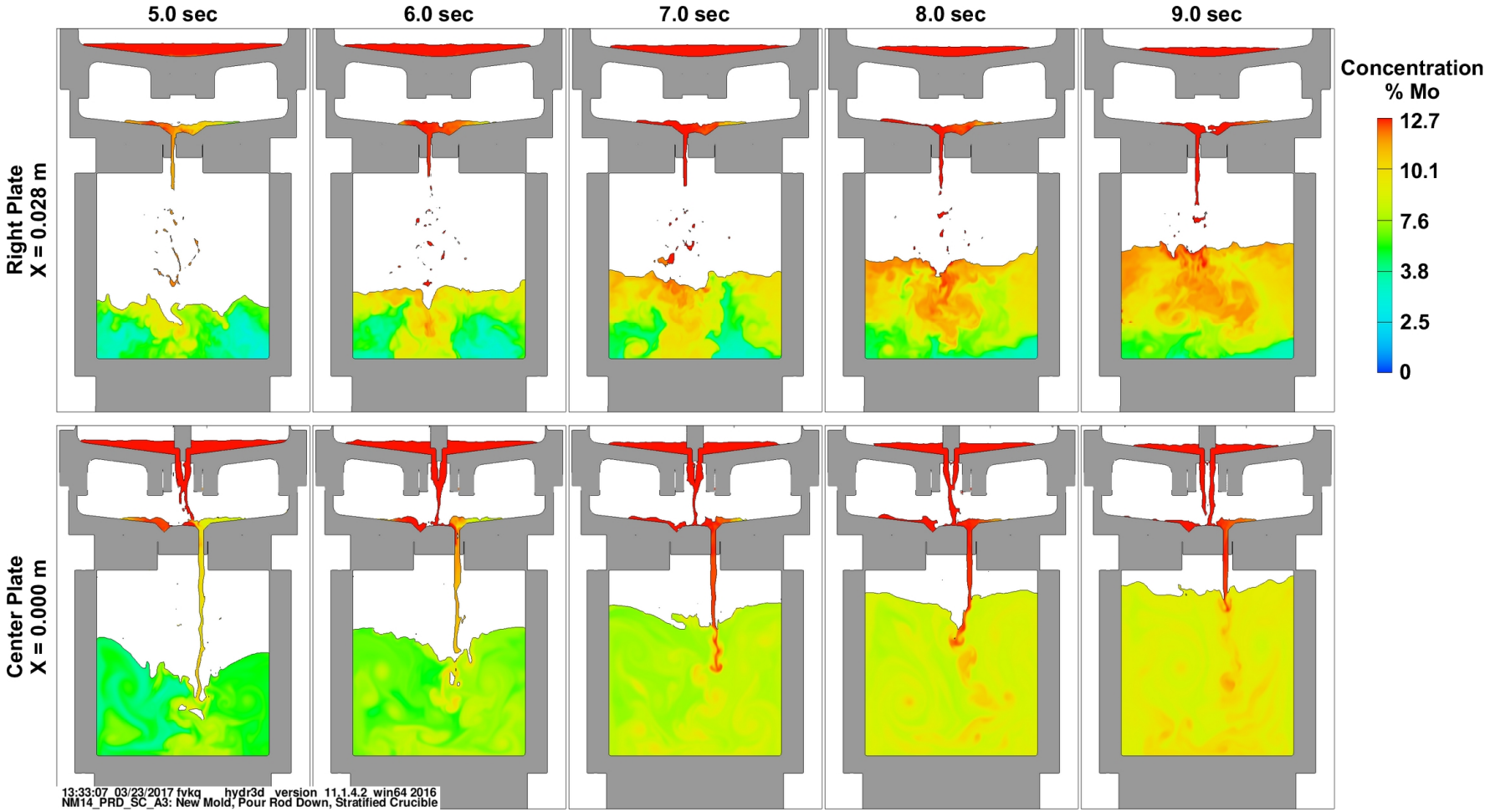

Fig. 15 (cont.) Concentration of Mo as a function of time for the horizontal mold with the pour rod down. Top row is through the center of the left plate and the bottom row is through the center plate.

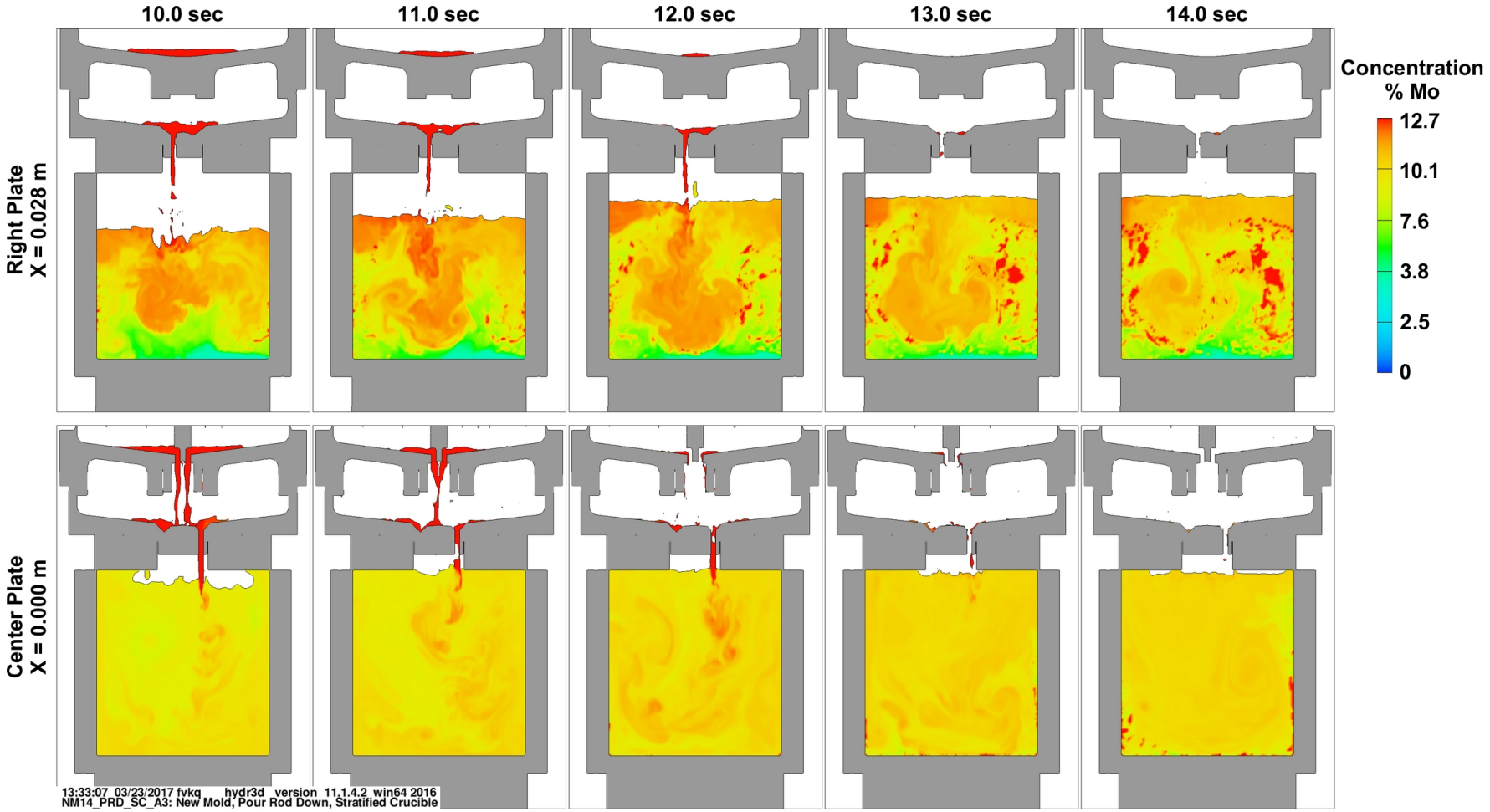

Fig. 15 (cont.) Concentration of Mo as a function of time for the horizontal mold with the pour rod down. Top row is through the center of the left plate and the bottom row is through the center plate.

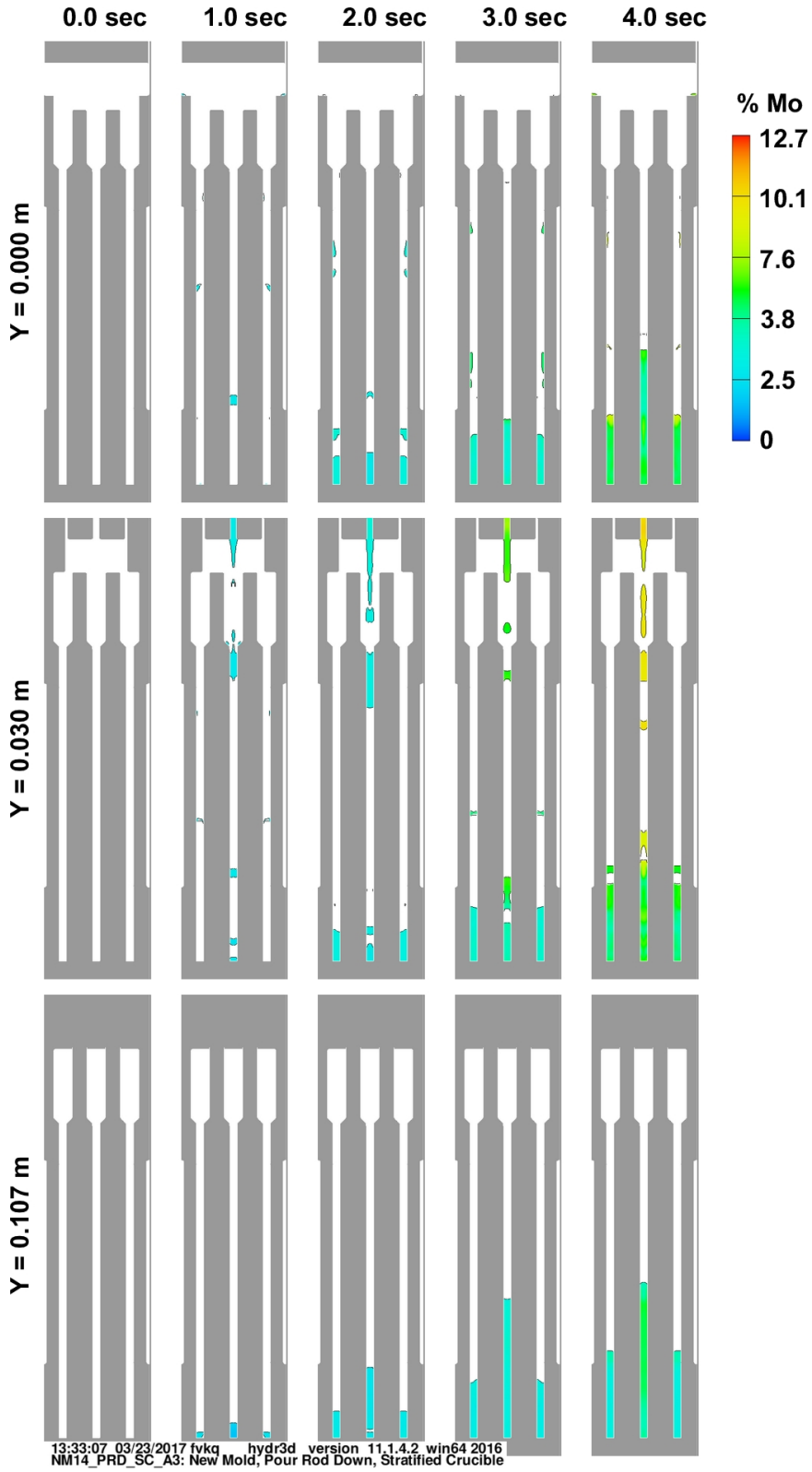

Fig. 16 X-Y cross-section of concentration of Mo as a function of time for the horizontal mold with the pour rod down. Top row is through the center Y=0, middle row is below the distributor discharge hole Y=0.030m, and bottom row is near edge at Y=0.107m.

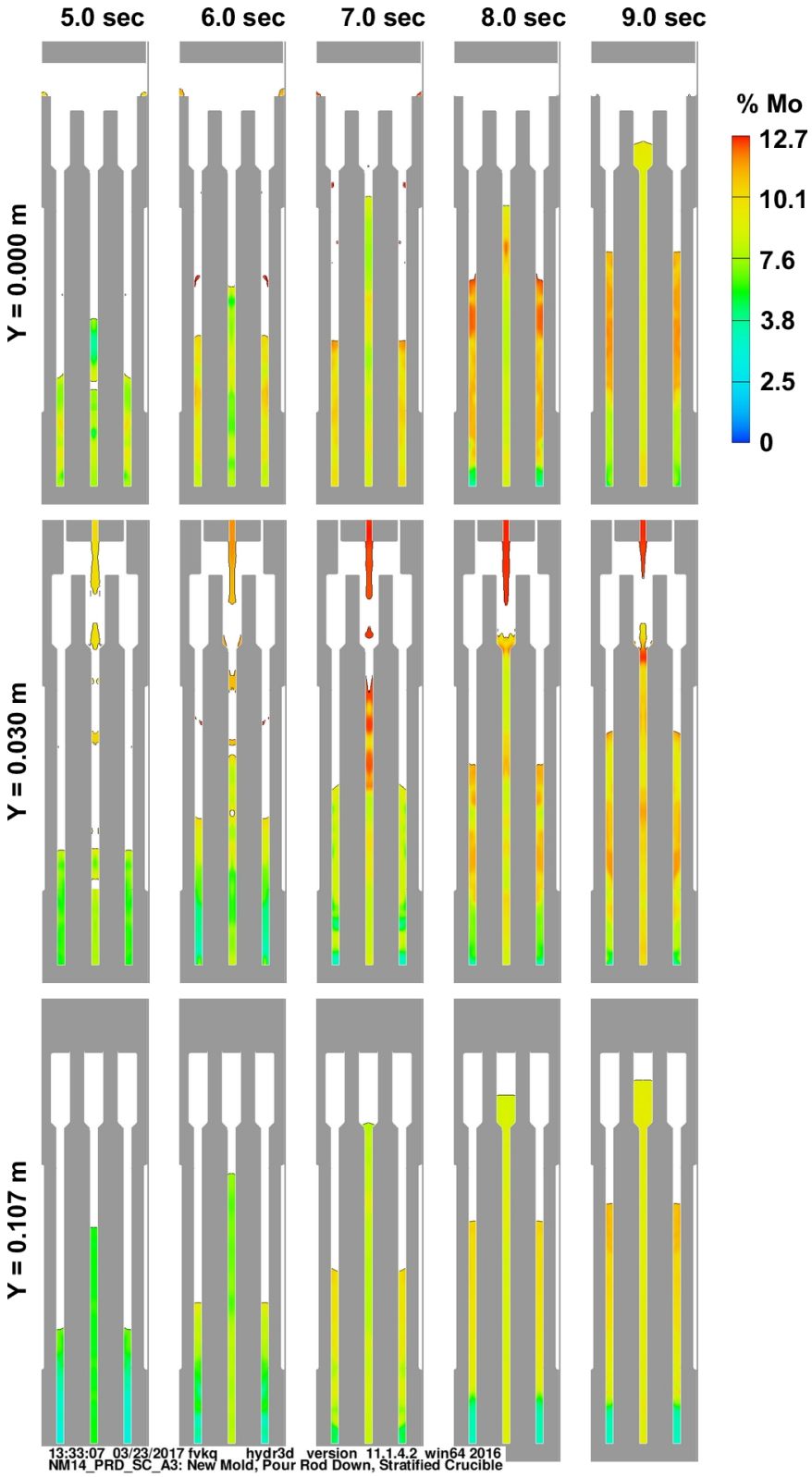

Fig. 16 (cont.) X-Y cross-section of concentration of Mo as a function of time for the horizontal mold with the pour rod down. Top row is through the center Y=0, middle row is below the distributor discharge hole Y=0.030m, and bottom row is near edge at Y=0.107m.

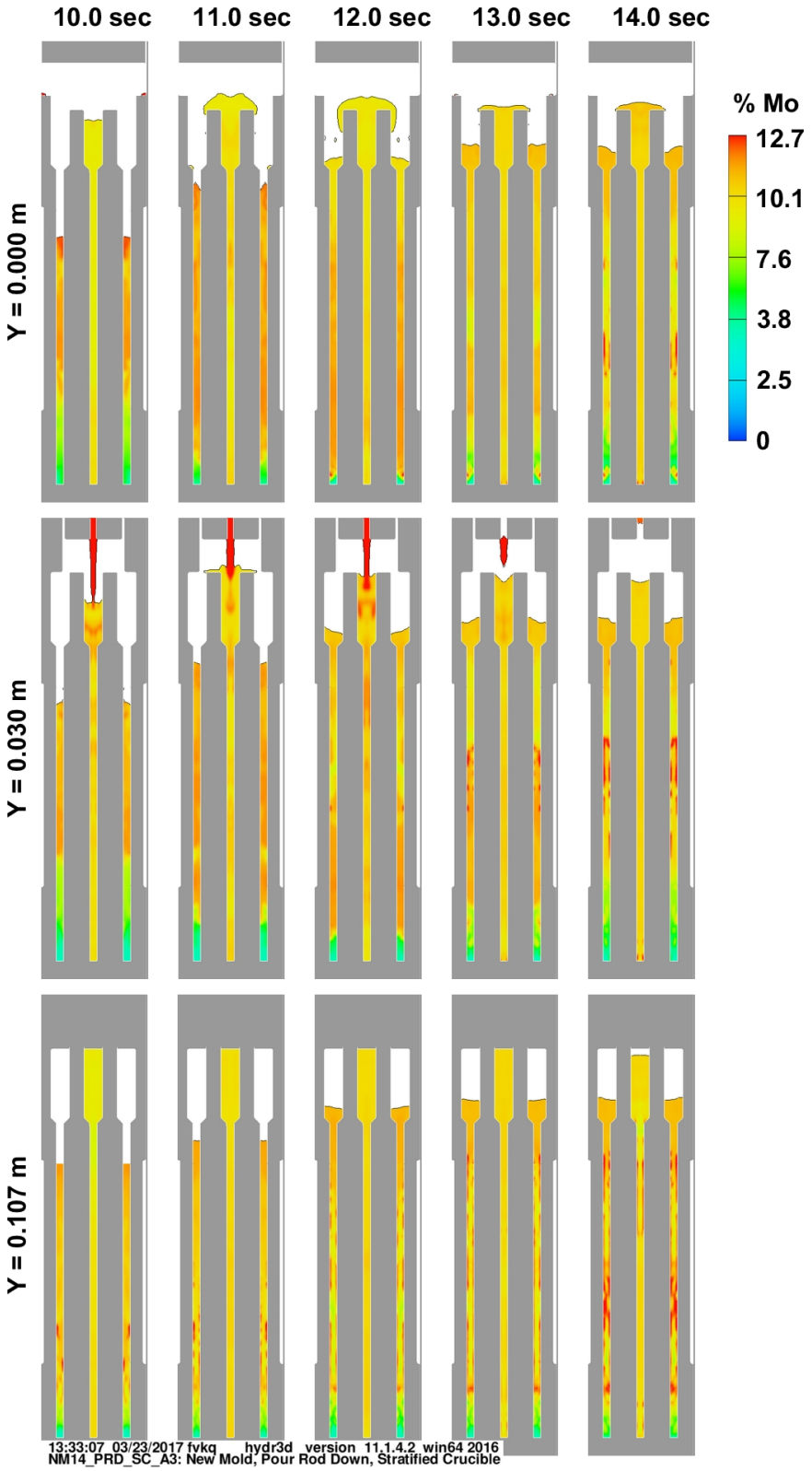

Fig. 16 (cont.) X-Y cross-section of concentration of Mo as a function of time for the horizontal mold with the pour rod down. Top row is through the center Y=0, middle row is below the distributor discharge hole Y=0.0m, and bottom row is near edge at Y=0.107m.

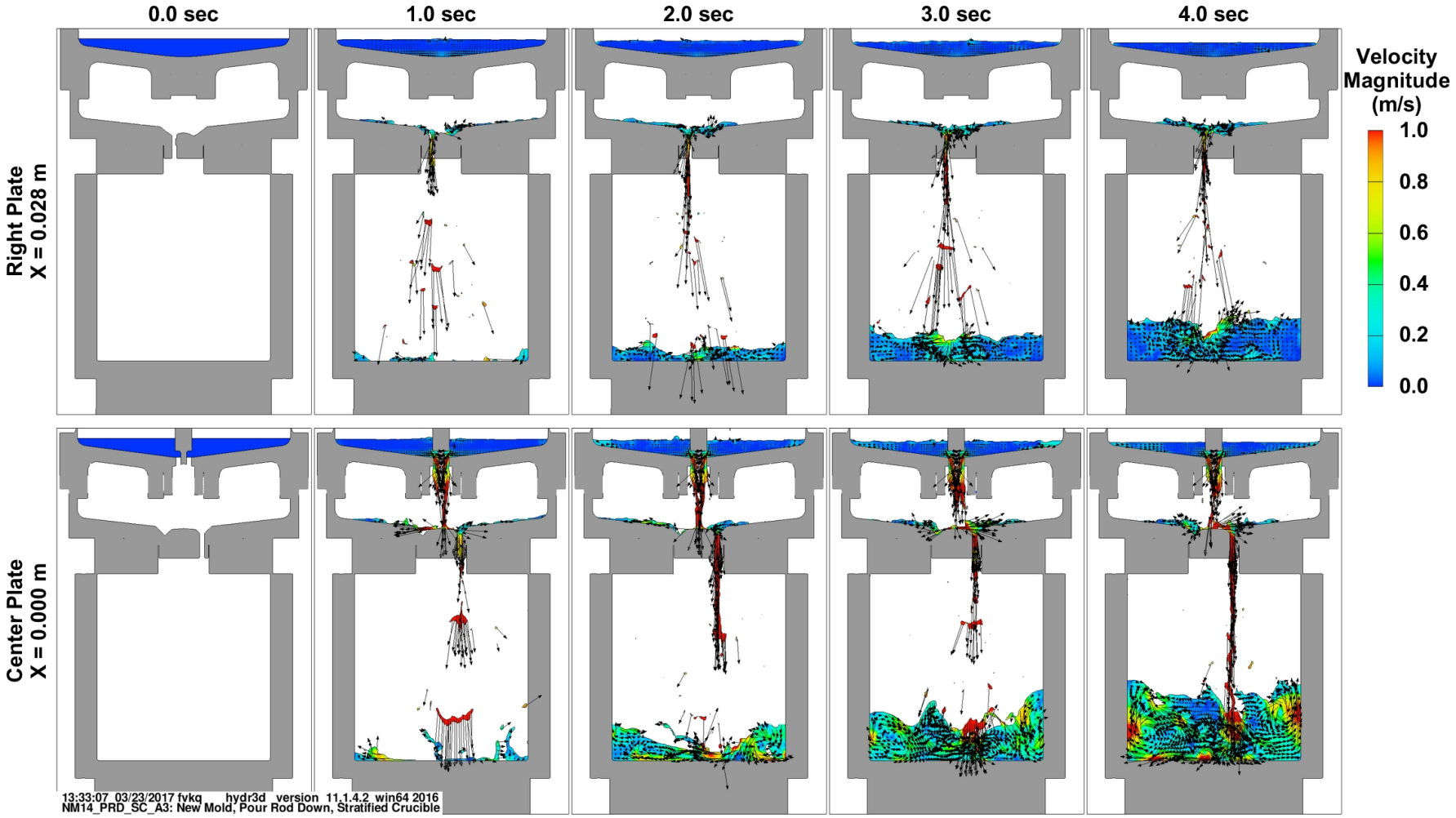

Fig. 17 Velocity magnitude and flow direction as a function of time for the horizontal mold with the pour rod down. Top row is through the center of the left plate and the bottom row is through the center plate.

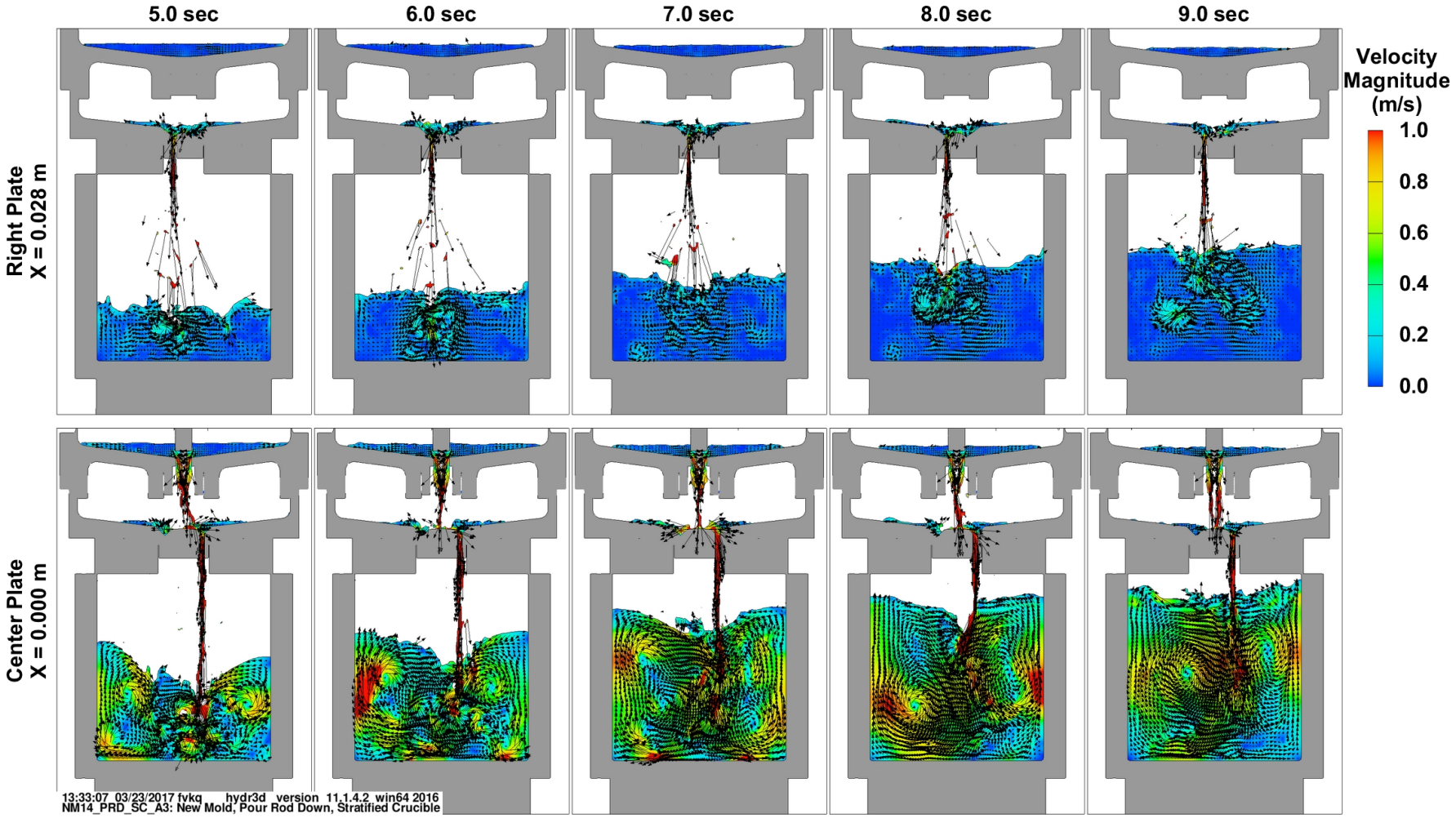

Fig. 17 (cont.) Velocity magnitude and flow direction as a function of time for the horizontal mold with the pour rod down. Top row is through the center of the left plate and the bottom row is through the center plate.

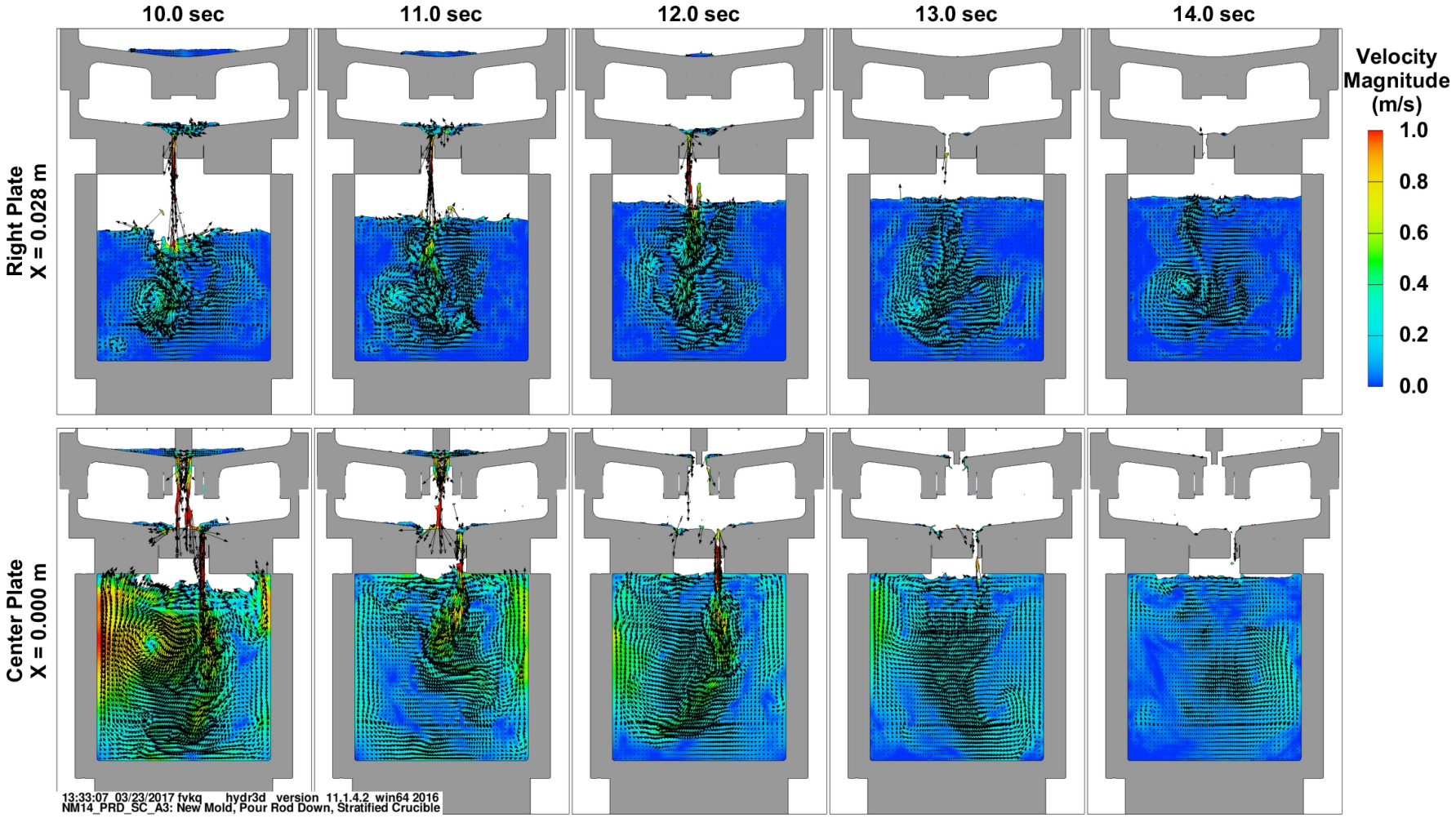

Fig. 17 (cont.) Velocity magnitude and flow direction as a function of time for the horizontal mold with the pour rod down. Top row is through the center of the left plate and the bottom row is through the center plate.

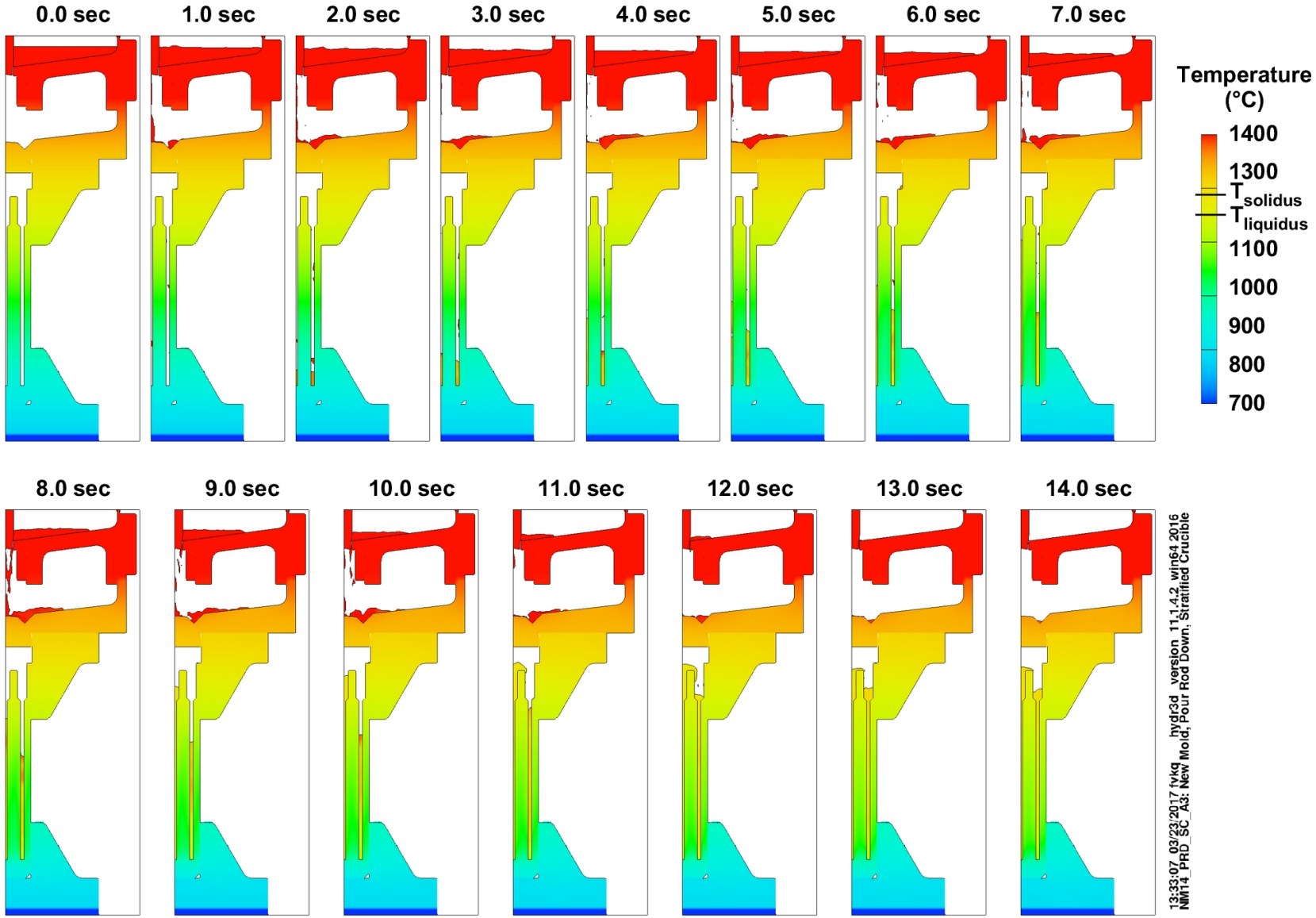

Fig. 18 Temperature of mold and metal as a function of time for the horizontal mold with the pour rod down. Shown is a X-Z slice along Y=0.

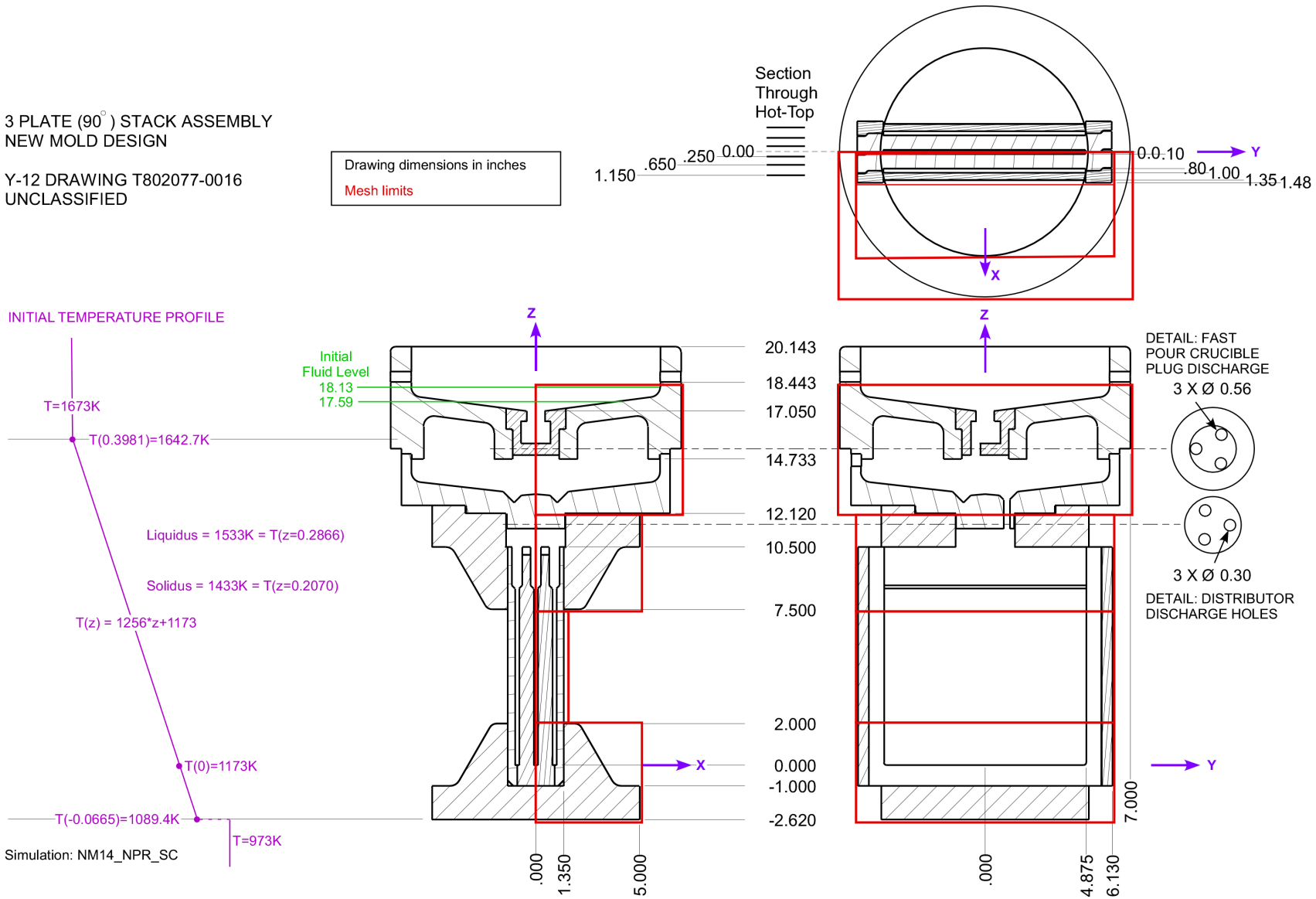

Fig. 19 Simulation setup for the horizontal triple plate mold with the pour rod removed. Shown are the mold geometry, initial temperature distribution, mesh/simulation boundaries, and initial fluid levels.

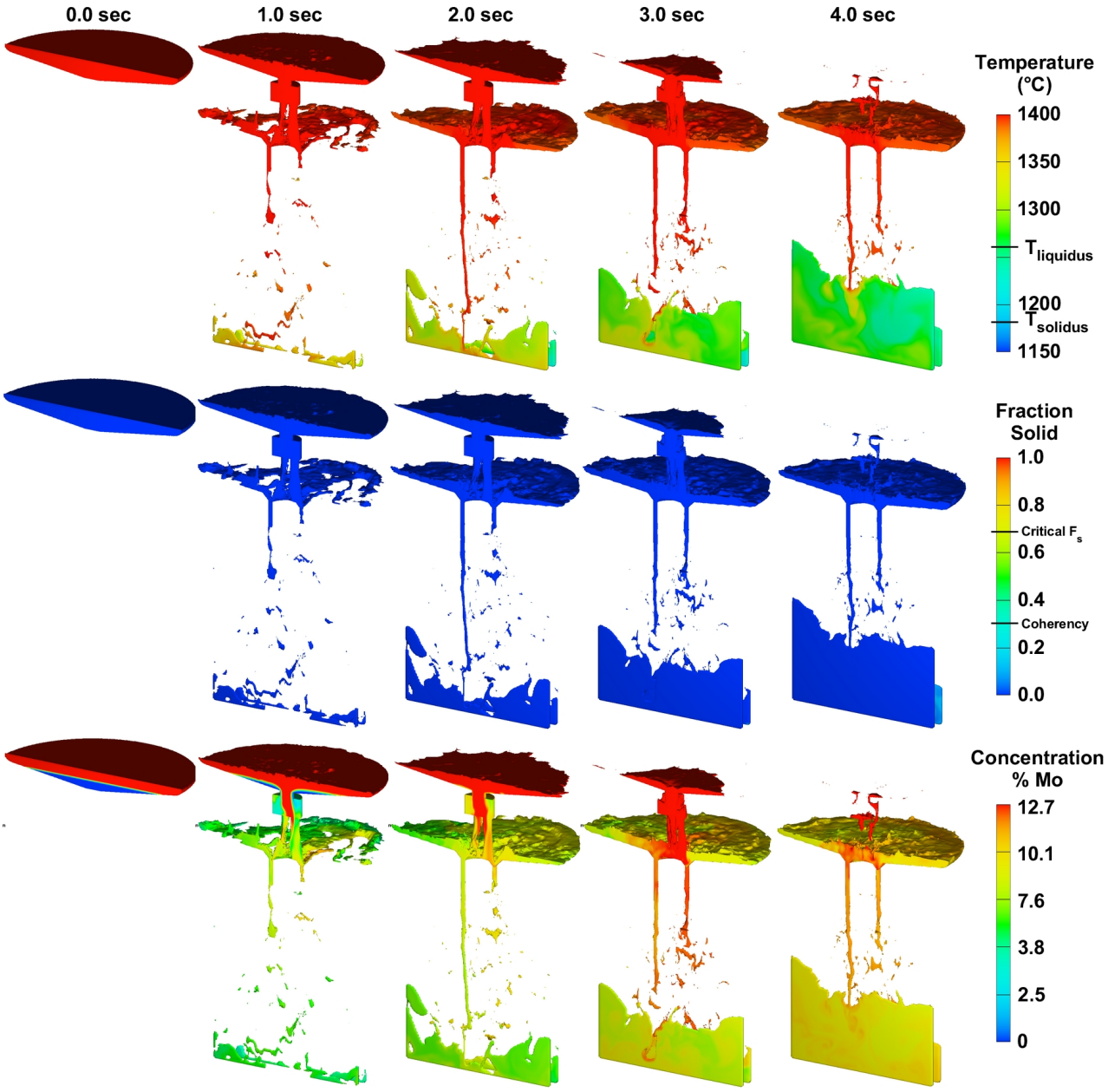

Fig. 20 Simulation results showing temperature, solid fraction and Mo concentration as a function of time for the horizontal triple plate mold with the pour rod removed.

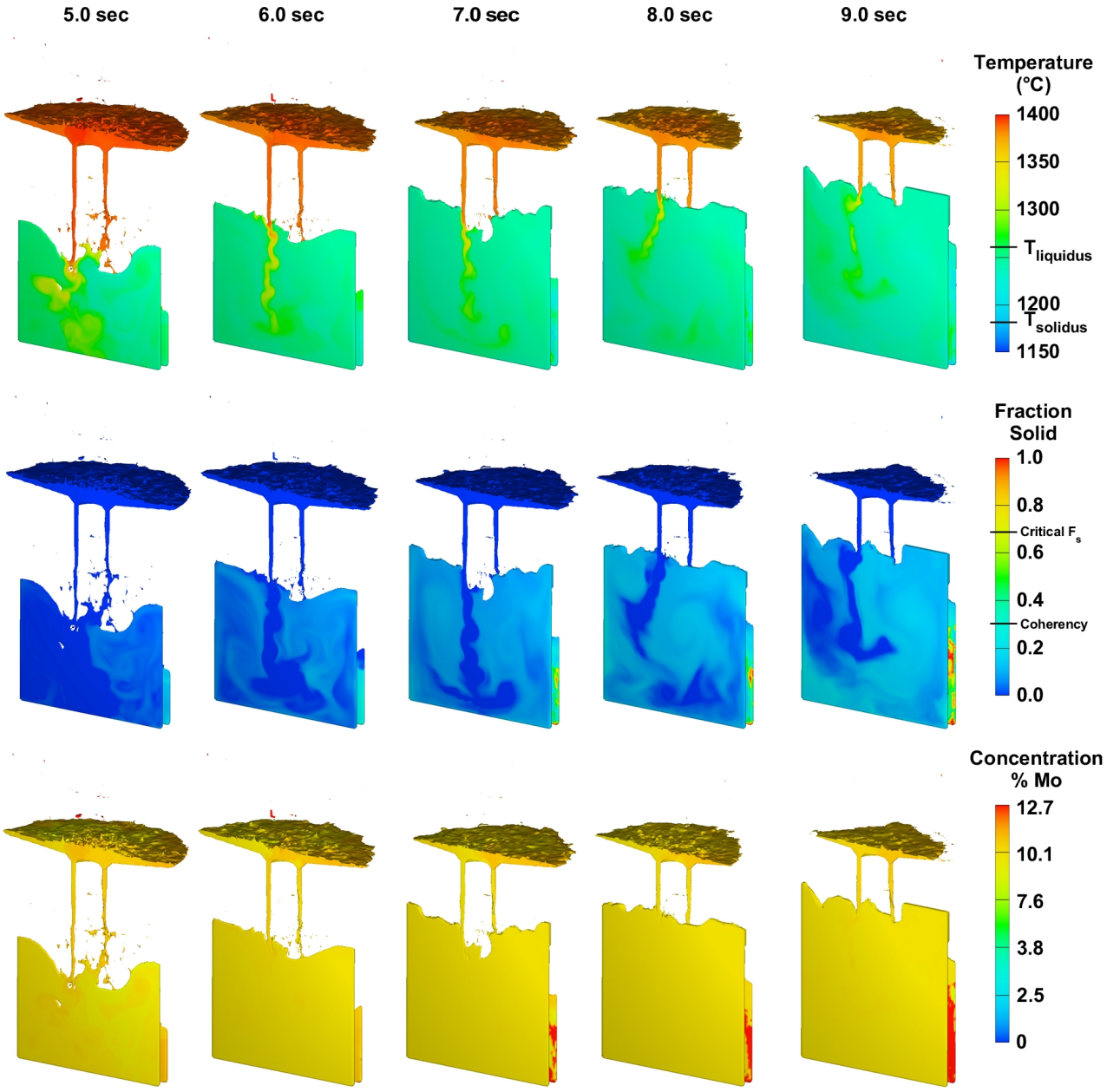

Fig. 20 (cont.) Simulation results showing temperature, solid fraction and Mo concentration as a function of time for the horizontal triple plate mold with the pour rod removed.

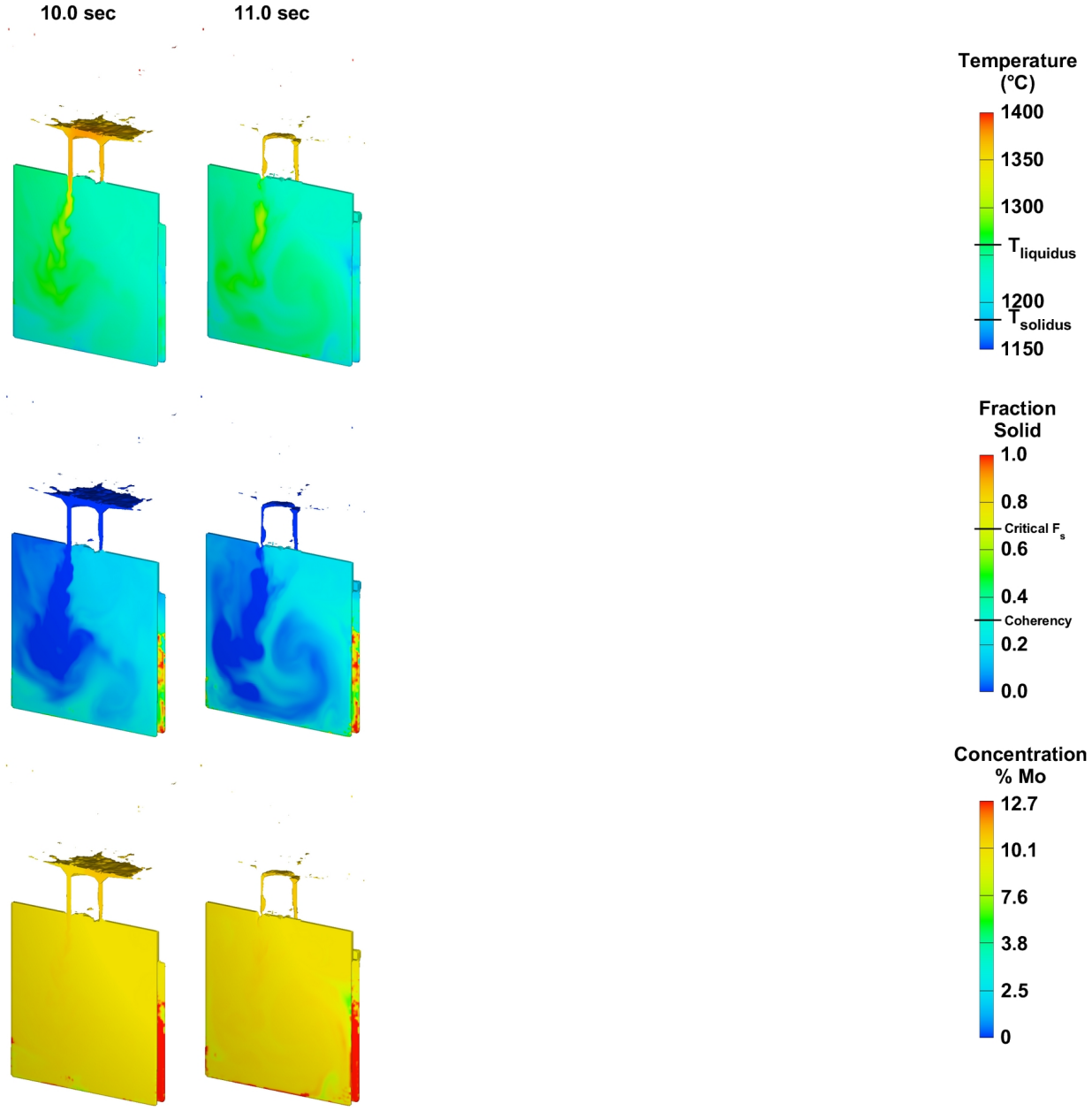

Fig. 20 (cont.) Simulation results showing temperature, solid fraction and Mo concentration as a function of time for the horizontal triple plate mold with the pour rod removed.

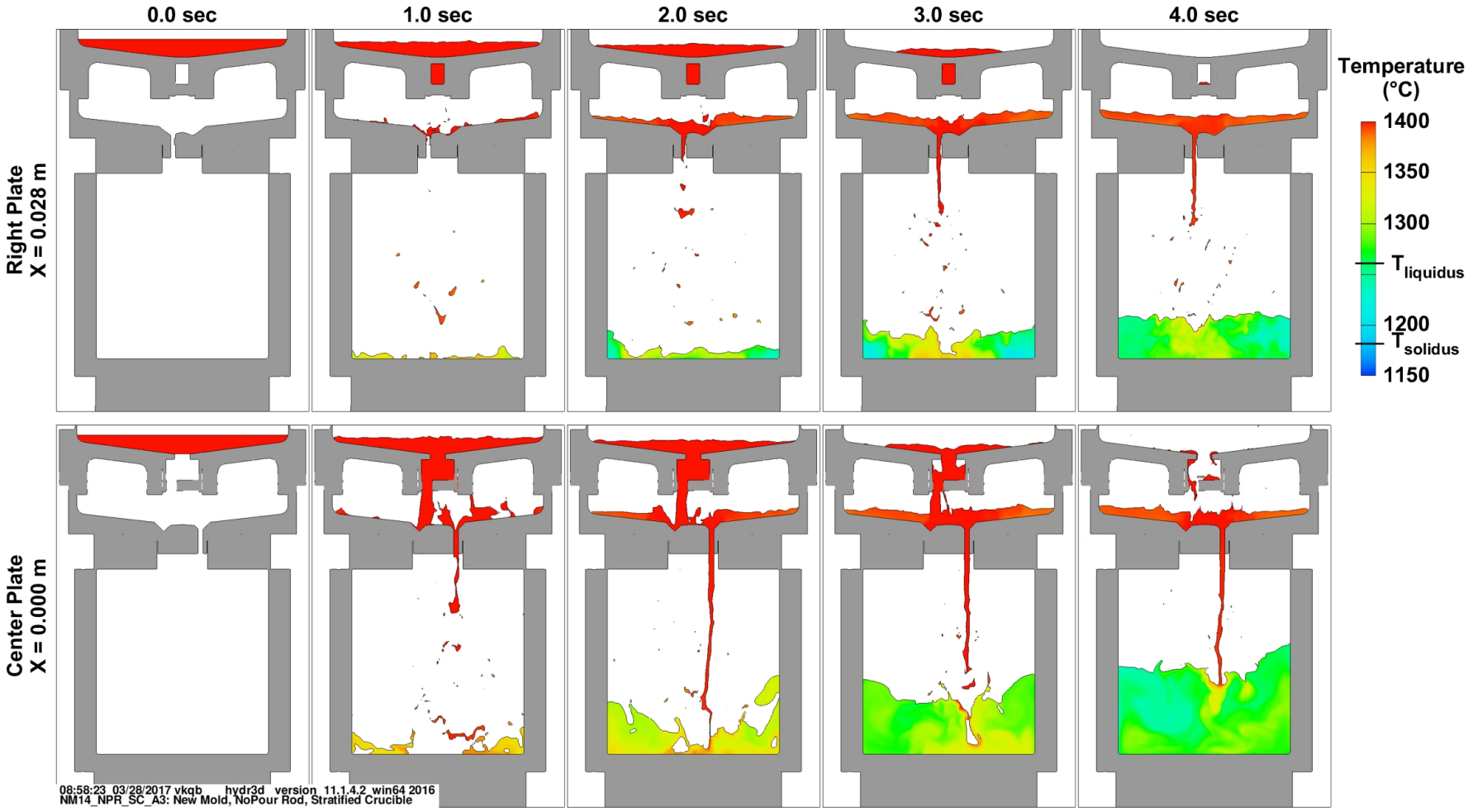

Fig. 21 Temperature as a function of time for the horizontal mold with the pour rod removed. Top row is through the center of the left plate and the bottom row is through the center plate.

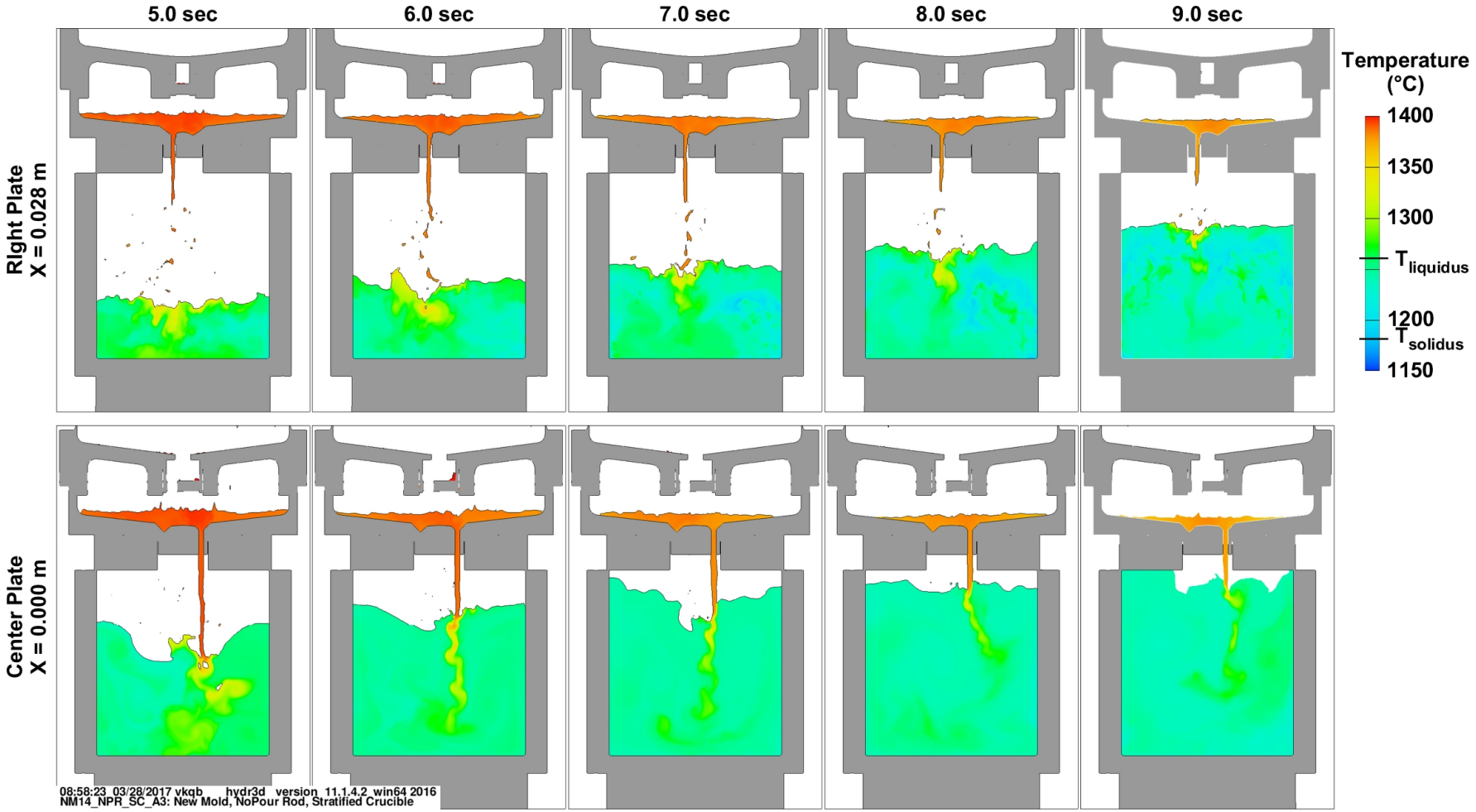

Fig. 21 (cont.) Temperature as a function of time for the horizontal mold with the pour rod removed. Top row is through the center of the left plate and the bottom row is through the center plate.

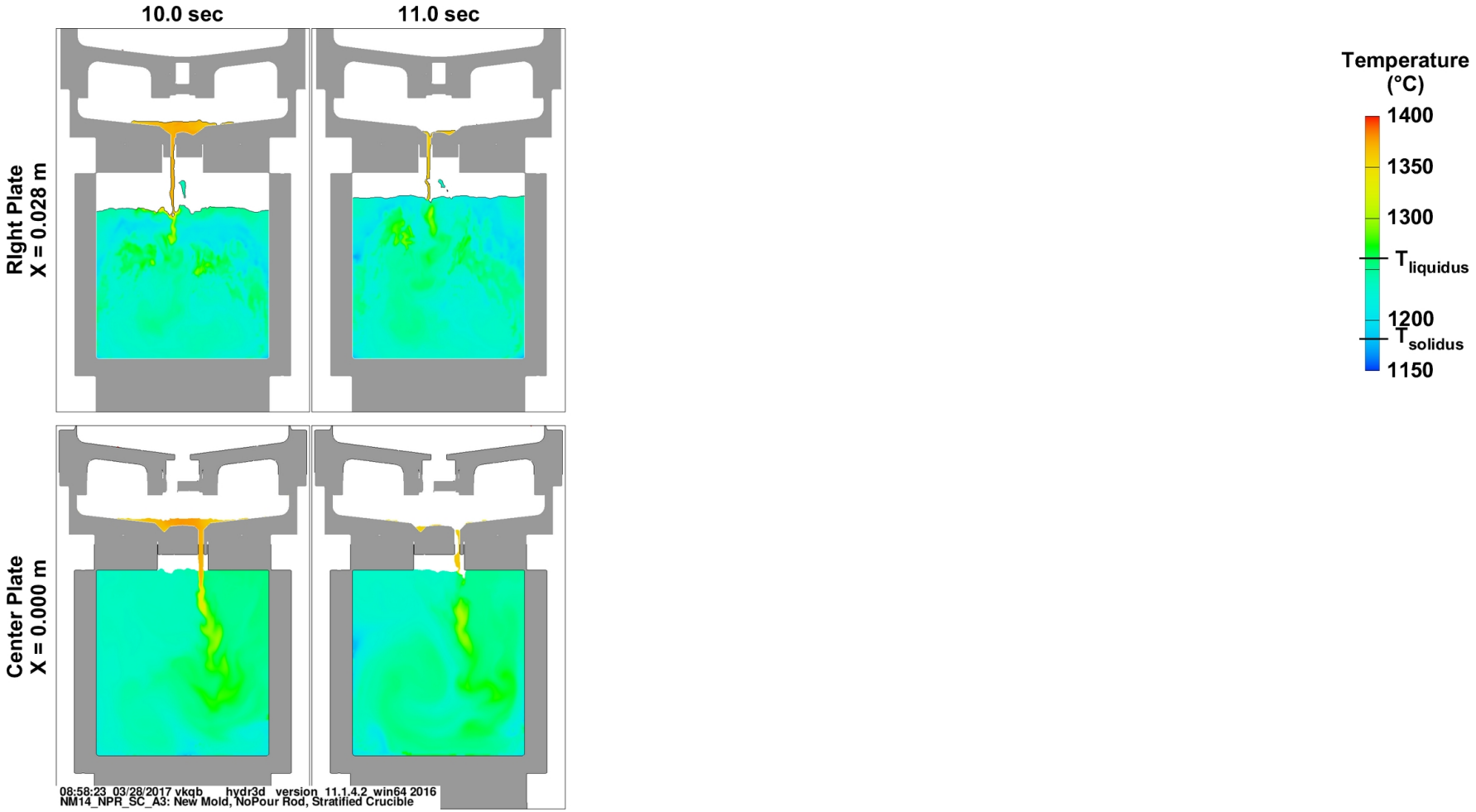

Fig. 21 (cont.) Temperature as a function of time for the horizontal mold with the pour rod removed. Top row is through the center of the left plate and the bottom row is through the center plate.

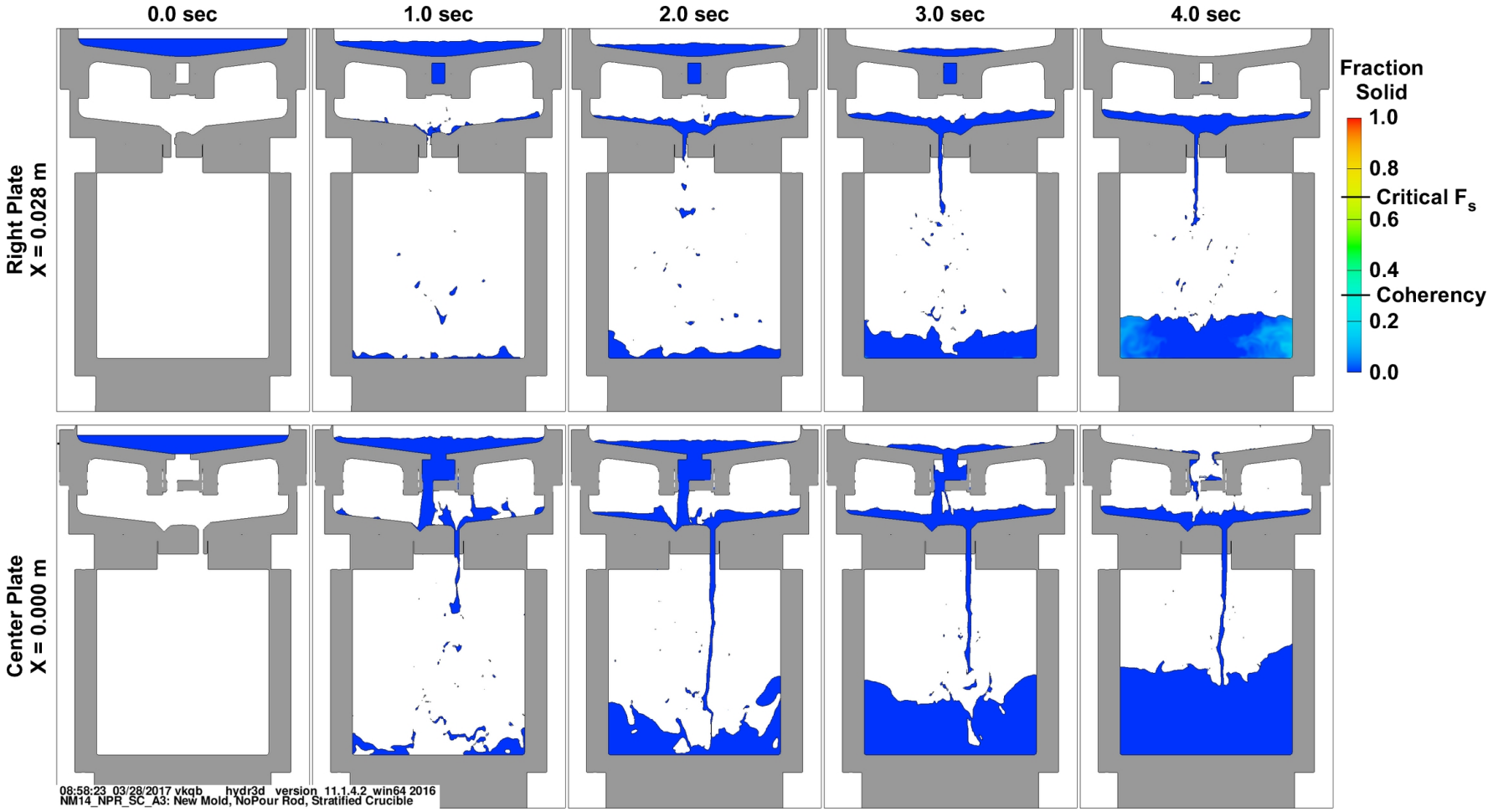

Fig. 22 Solid fraction as a function of time for the horizontal mold with the pour rod removed. Top row is through the center of the left plate and the bottom row is through the center plate.

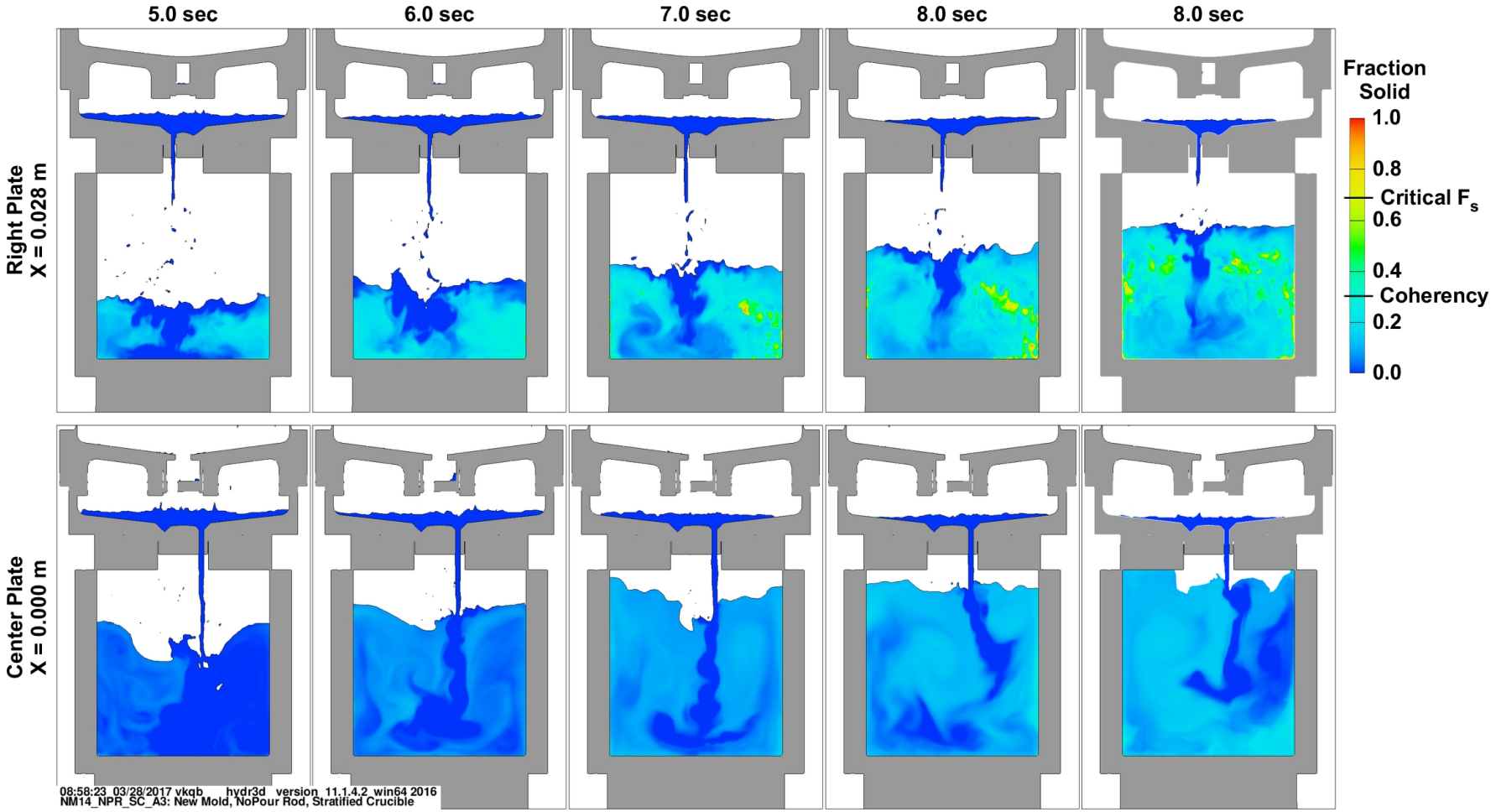

Fig. 22 (cont.) Solid fraction as a function of time for the horizontal mold with the pour rod removed. Top row is through the center of the left plate and the bottom row is through the center plate.

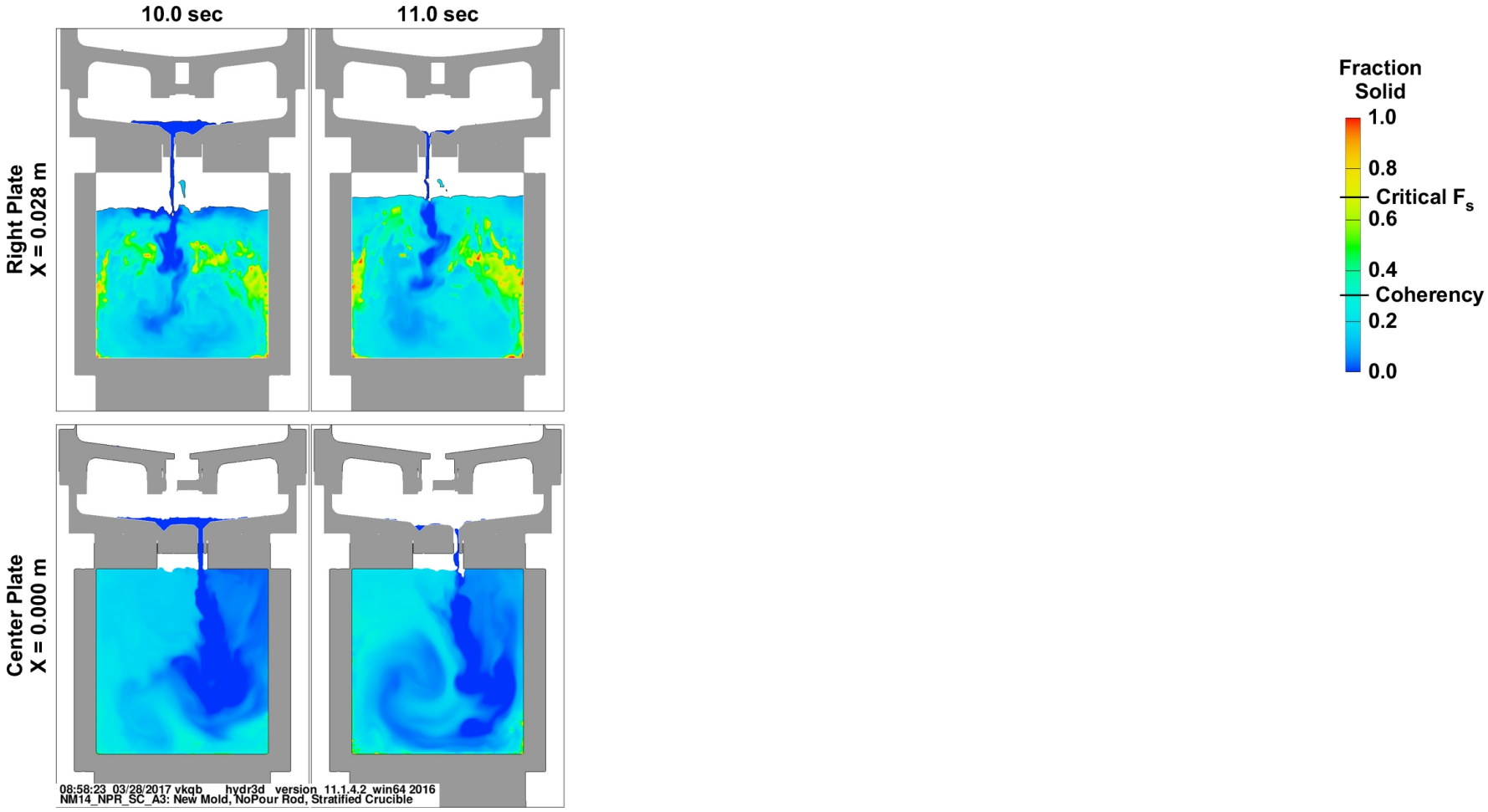

Fig. 22 (cont.) Solid fraction as a function of time for the horizontal mold with the pour rod removed. Top row is through the center of the left plate and the bottom row is through the center plate.

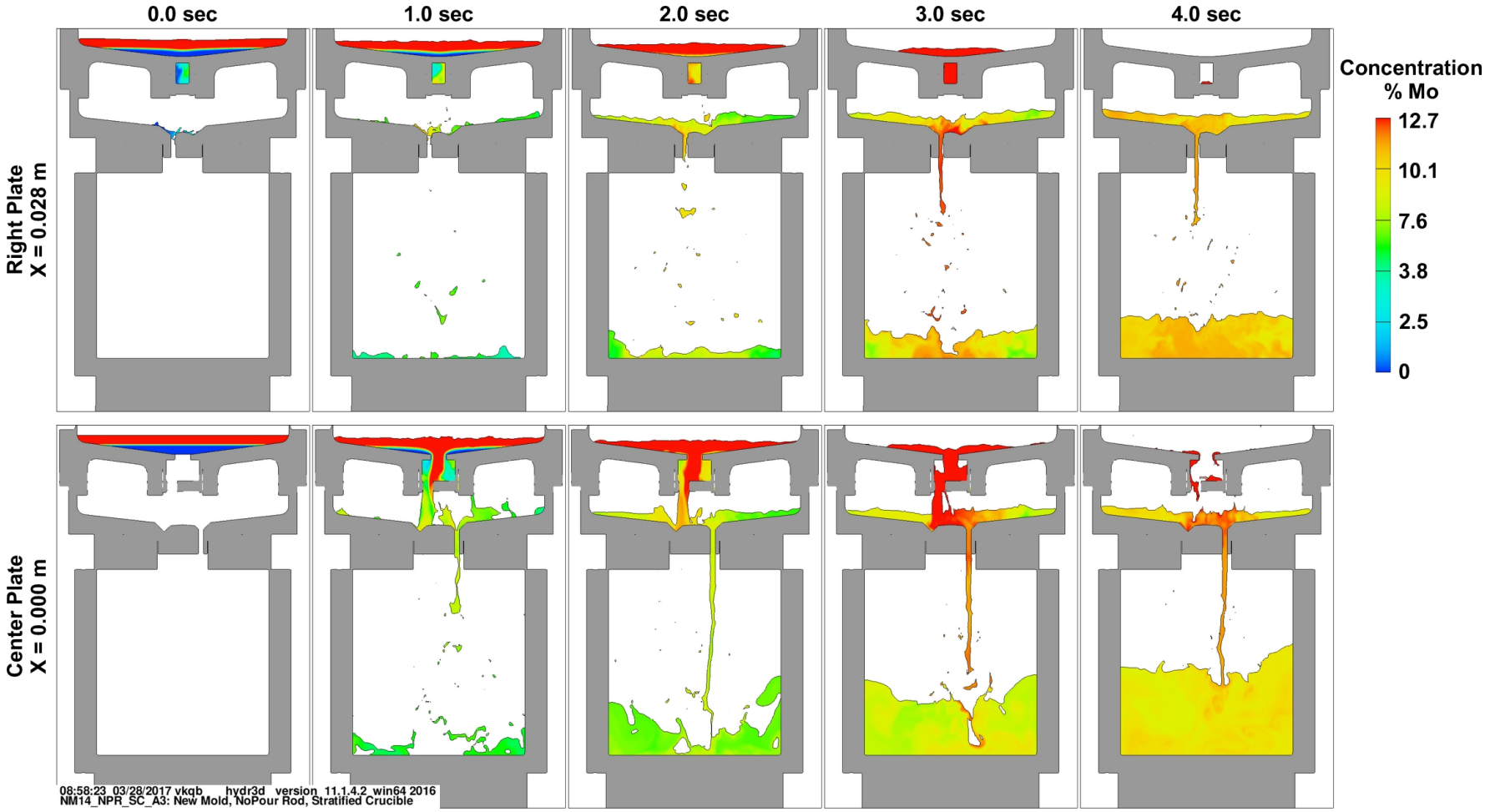

Fig. 23 Concentration of Mo as a function of time for the horizontal mold with the pour rod removed. Top row is through the center of the left plate and the bottom row is through the center plate.

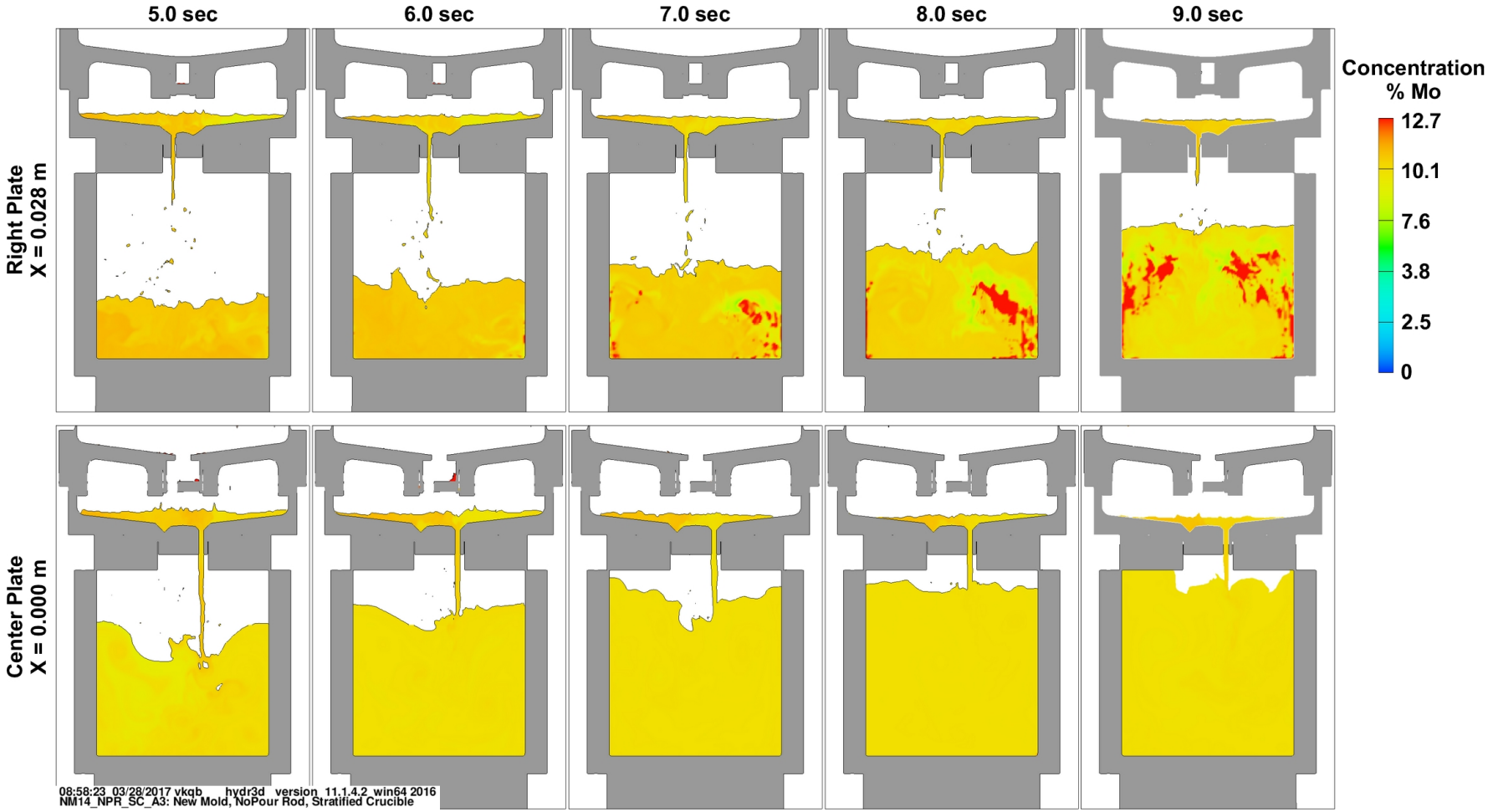

Fig. 23 (cont.) Concentration of Mo as a function of time for the horizontal mold with the pour rod removed. Top row is through the center of the left plate and the bottom row is through the center plate.

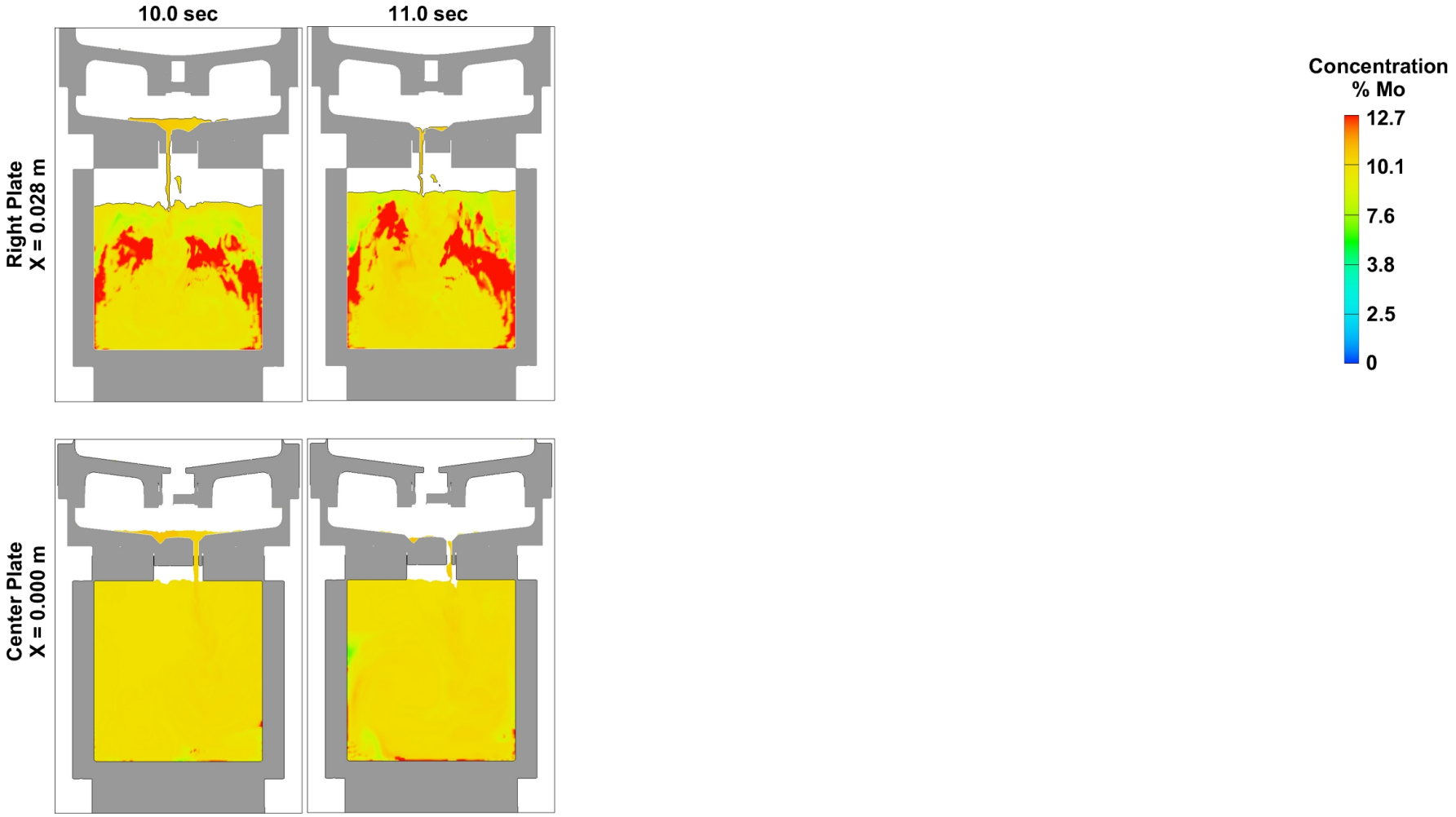

Fig. 23 (cont.) Concentration of Mo as a function of time for the horizontal mold with the pour rod removed. Top row is through the center of the left plate and the bottom row is through the center plate.

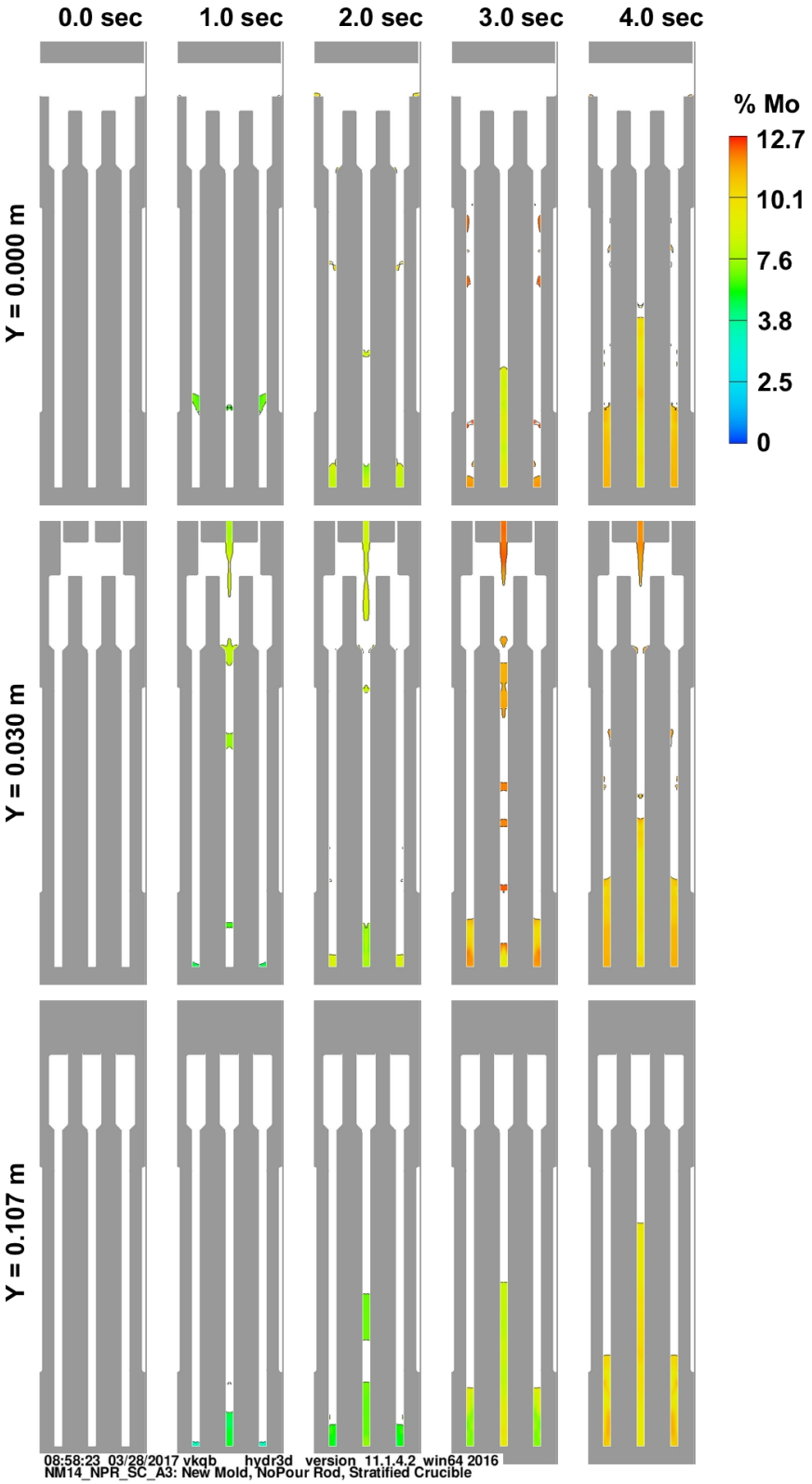

Fig. 24 X-Y cross-section of concentration of Mo as a function of time for the horizontal mold with the pour rod removed. Top row is through the center Y=0, middle row is below the distributor discharge hole Y=0.030m, and bottom row is near edge at Y=0.107m.

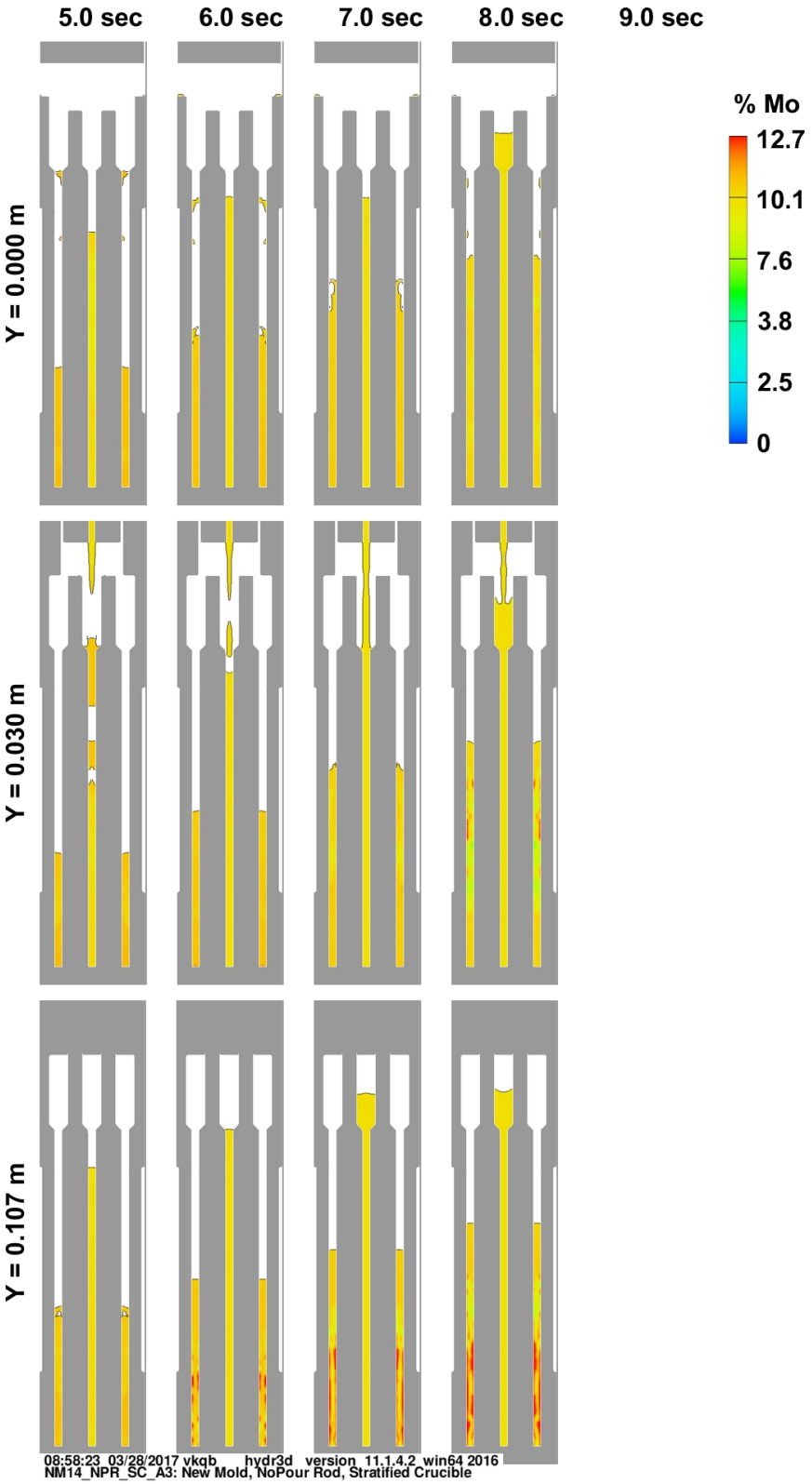

Fig. 24 (cont.) X-Y cross-section of concentration of Mo as a function of time for the horizontal mold with the pour rod removed. Top row is through the center Y=0, middle row is below the distributor discharge hole Y=0.030m, and bottom row is near edge at Y=0.107m.

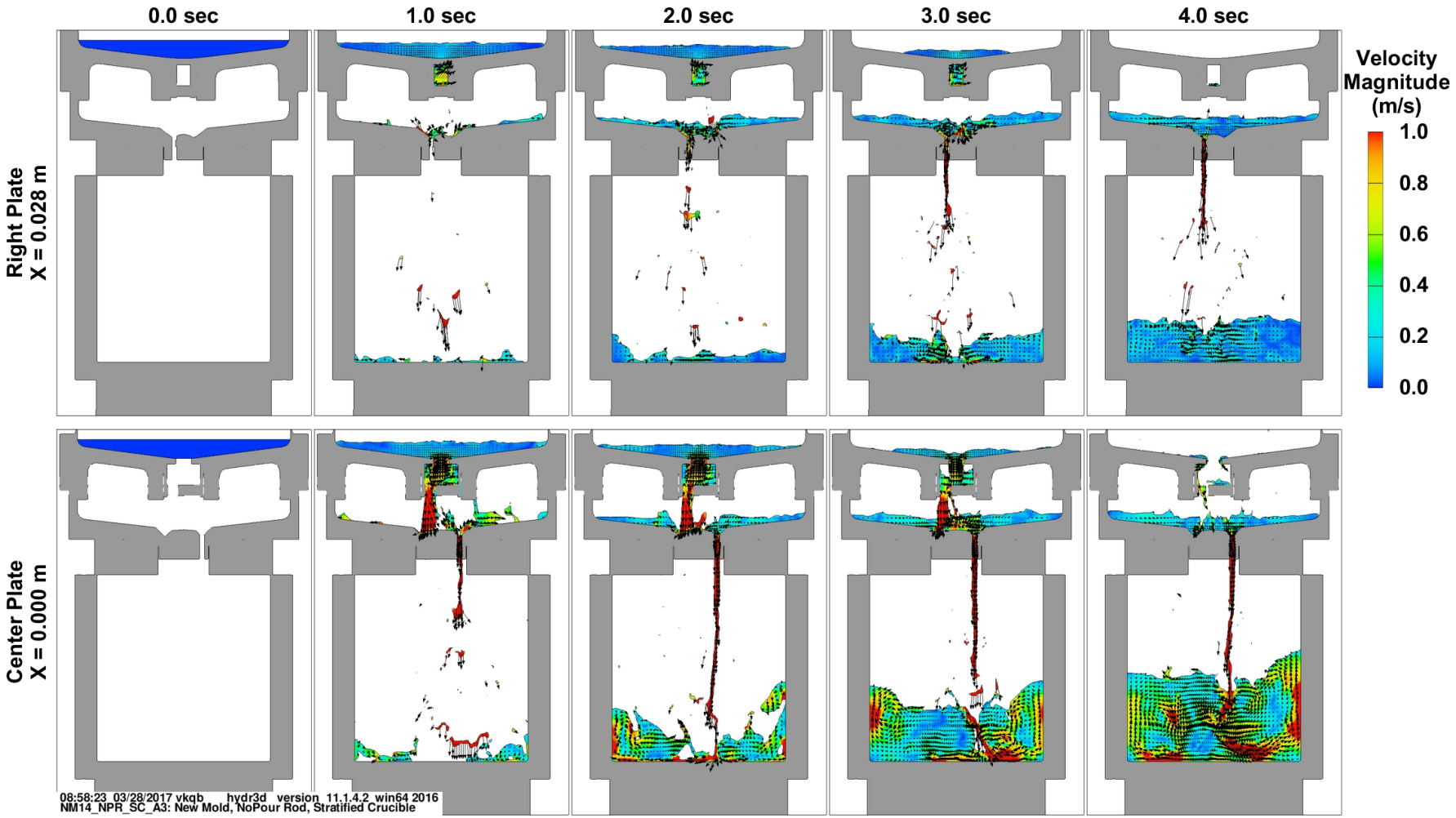

Fig. 25 Velocity magnitude and direction as a function of time for the horizontal mold with the pour rod removed. Top row is through the center of the left plate and the bottom row is through the center plate.

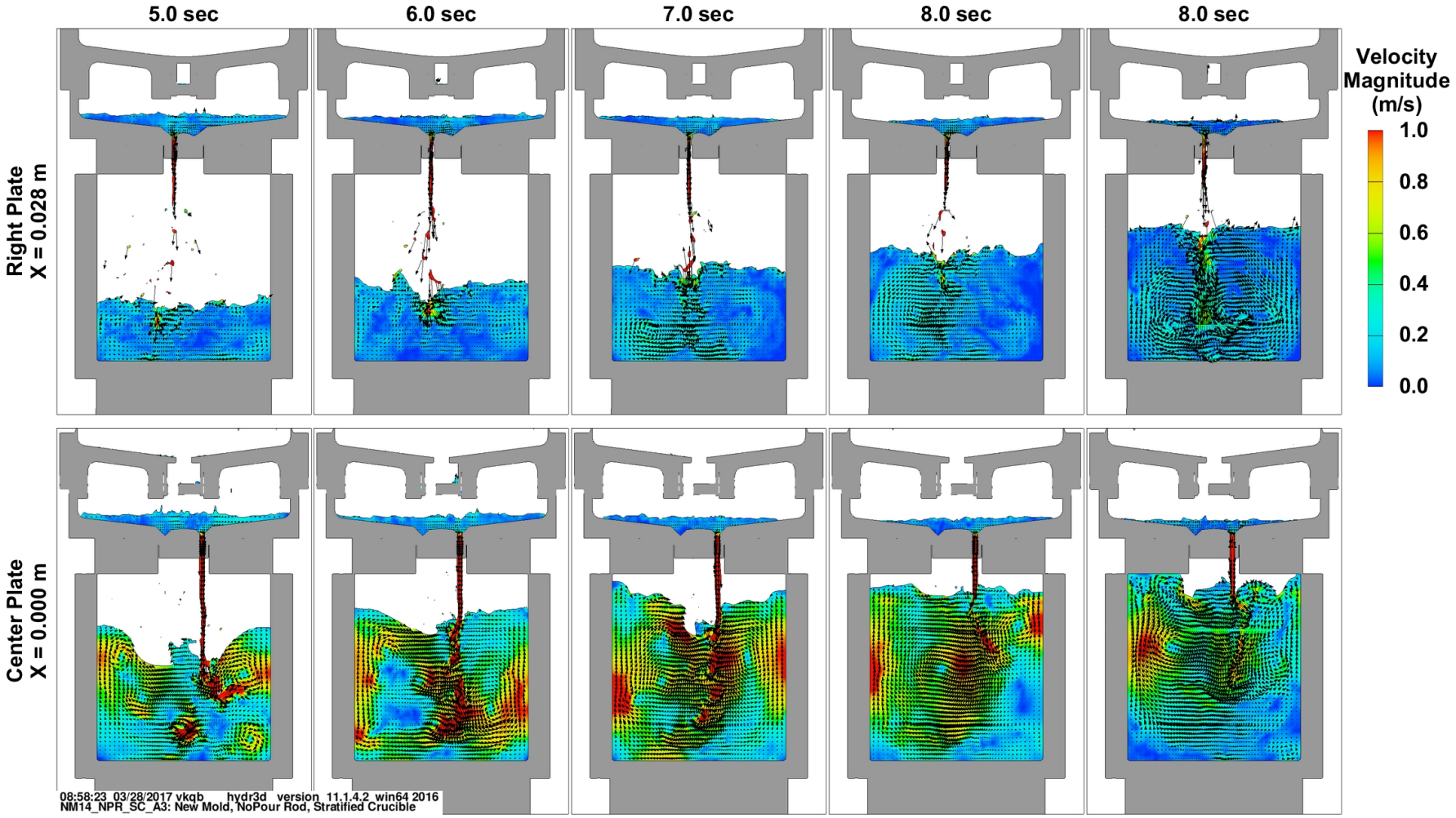

Fig. 25 (cont.) Velocity magnitude and direction as a function of time for the horizontal mold with the pour rod removed. Top row is through the center of the left plate and the bottom row is through the center plate.

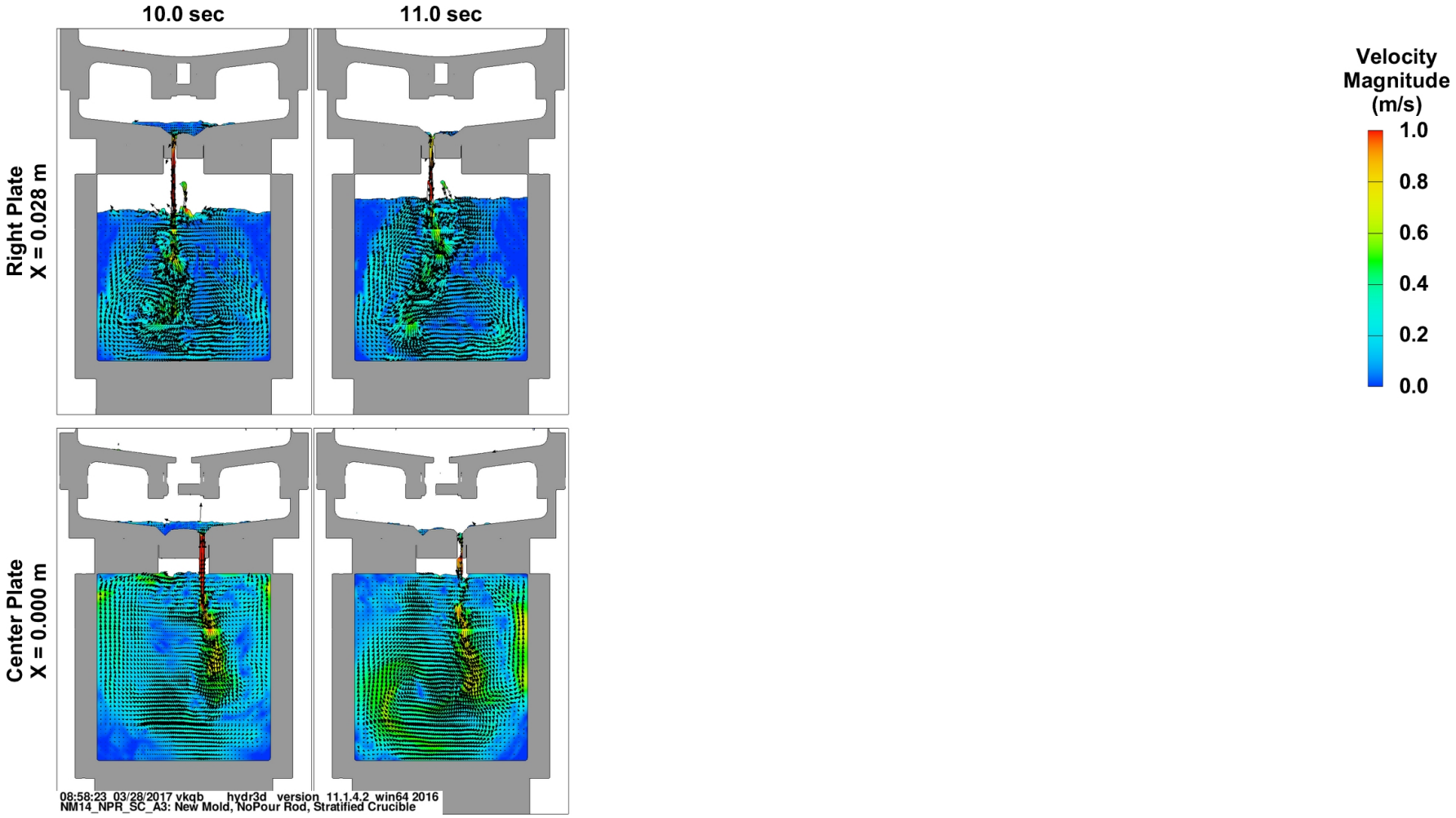

Fig. 25 (cont.) Velocity magnitude and direction as a function of time for the horizontal mold with the pour rod removed. Top row is through the center of the left plate and the bottom row is through the center plate.

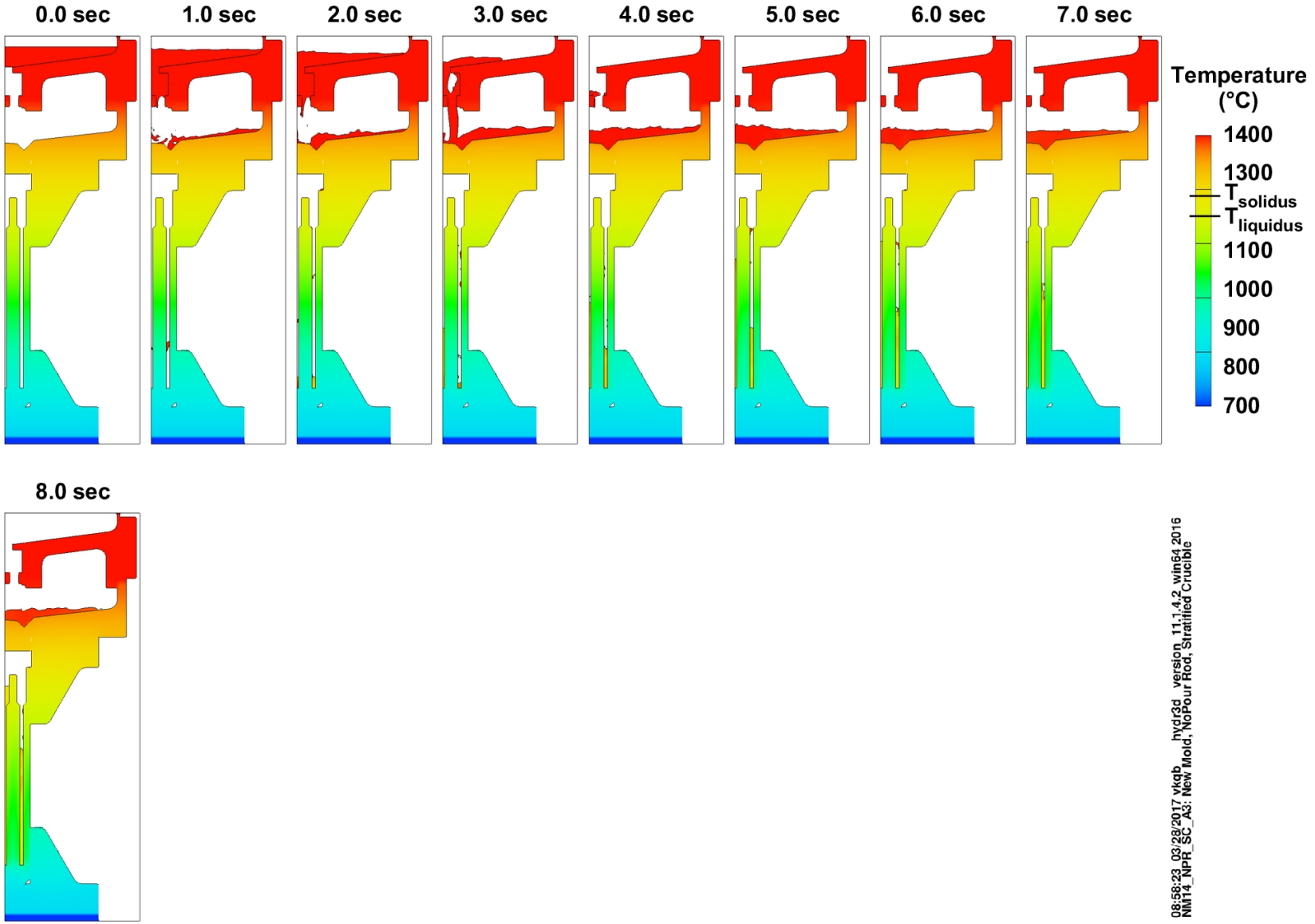

Fig. 26 Temperature of mold and metal as a function of time for the original mold with the pour rod removed. Shown is a X-Z slice along Y=0.

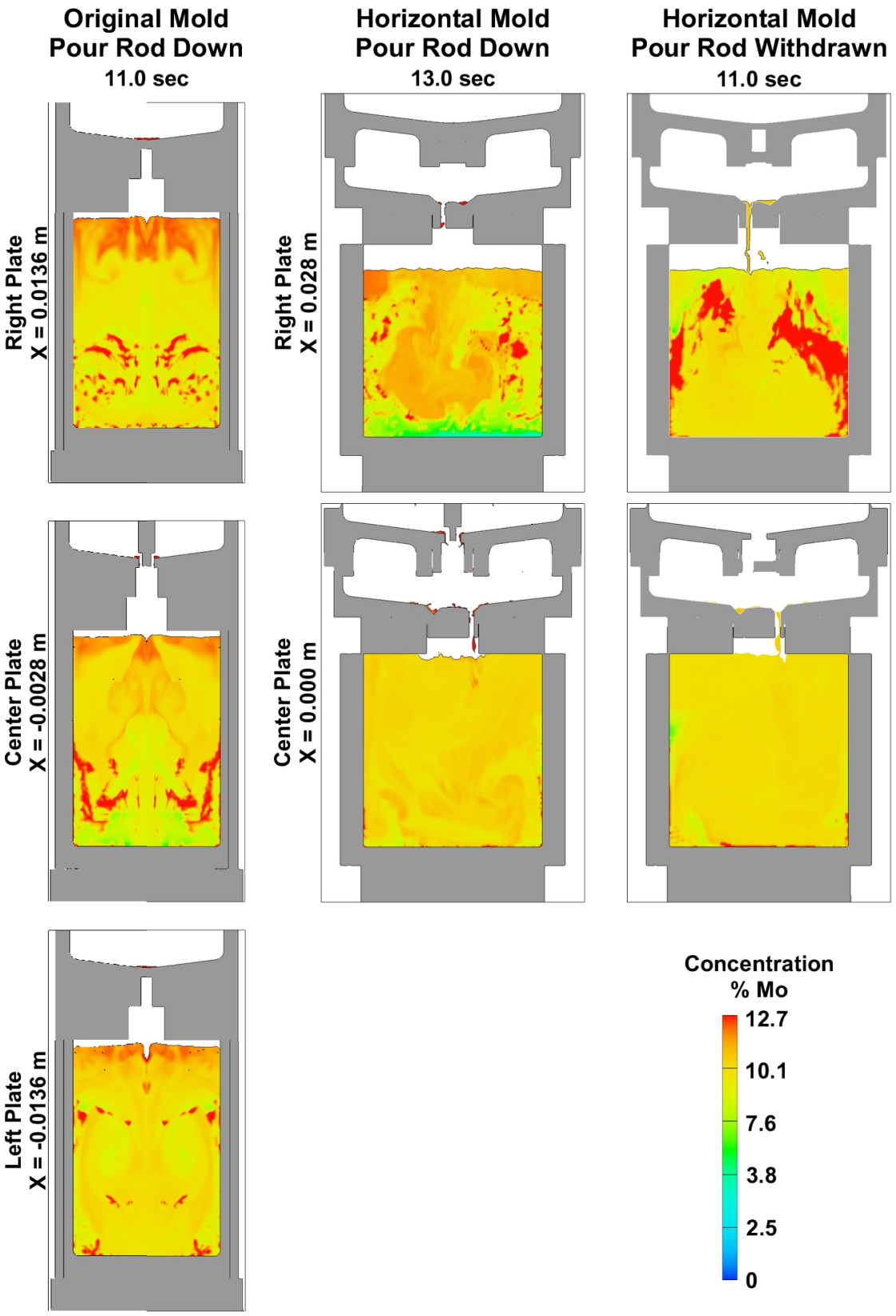

Fig. 27 Comparison of composition distribution at the end of filling for the three different situations considered.

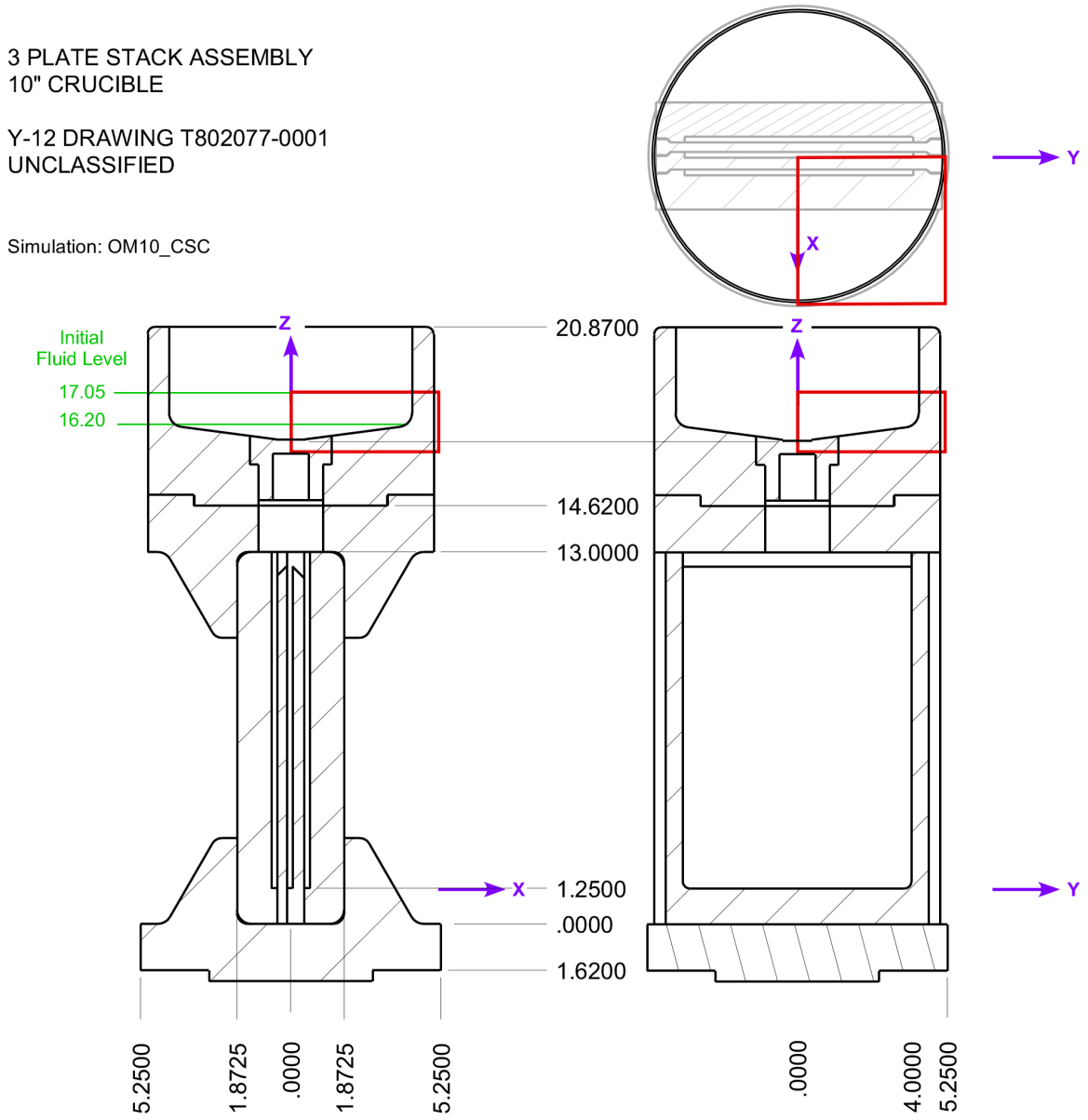

Fig. 28 Simulation setup for the crucible convection simulations in the original Y-12 triple plate mold. Shown is the mold geometry, mesh/simulation boundaries, and initial fluid levels.

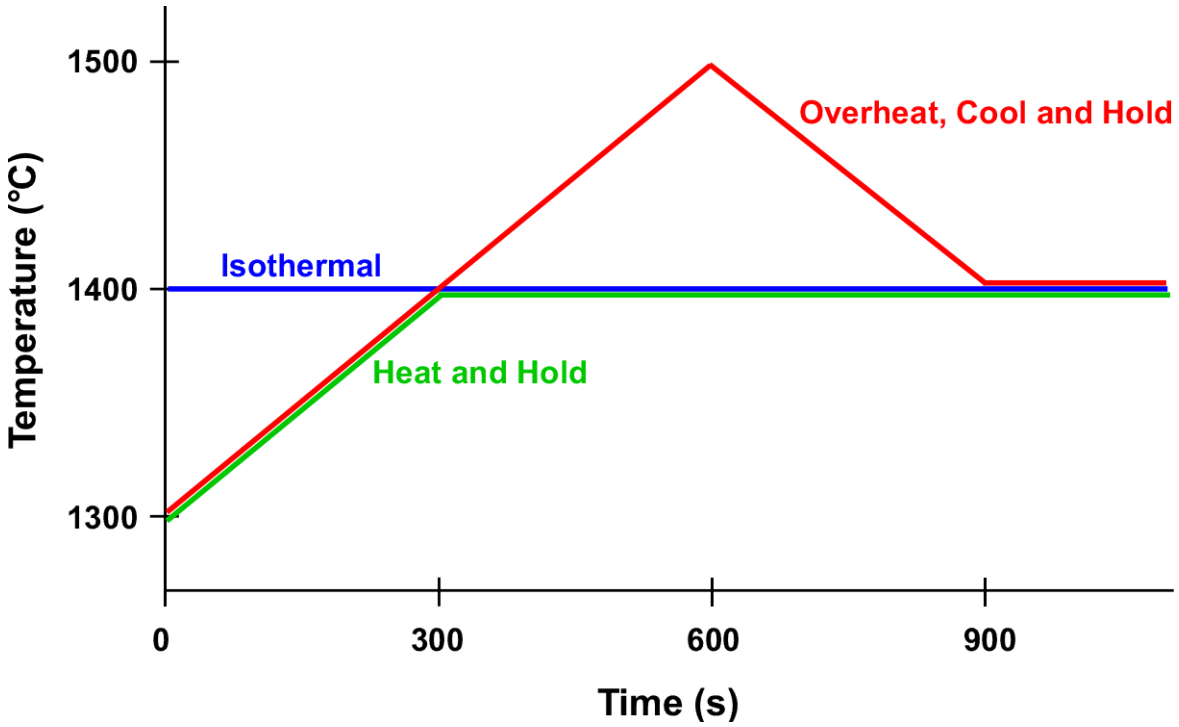

Fig. 29 Imposed boundary condition showing thermal profile of outer surface of crucible as function of time for the crucible convection simulations.

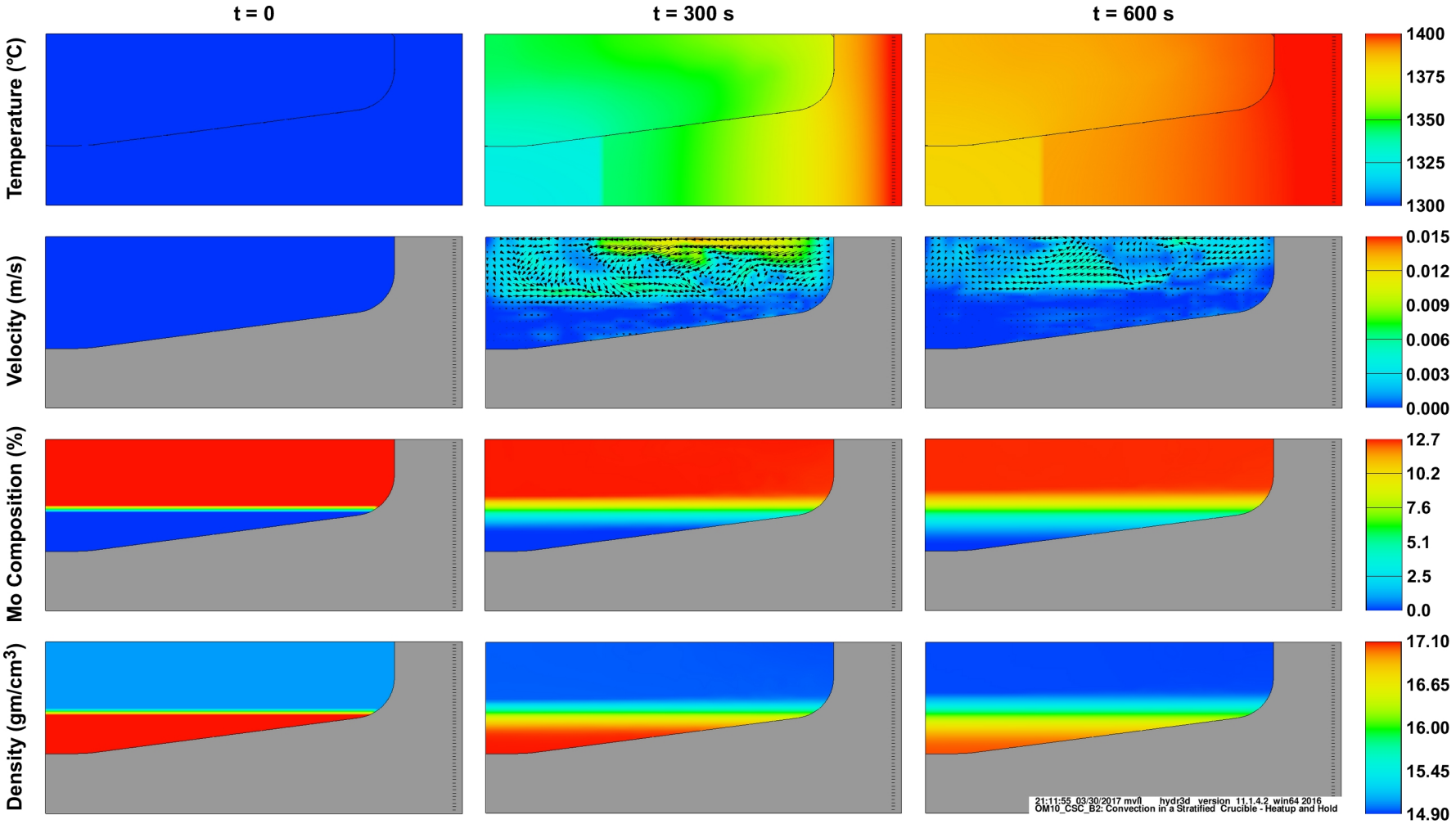

Fig. 30 Simulation results showing temperature, metal velocity, Mo concentration, and density as a function of time for the heat up and hold crucible convection simulation.

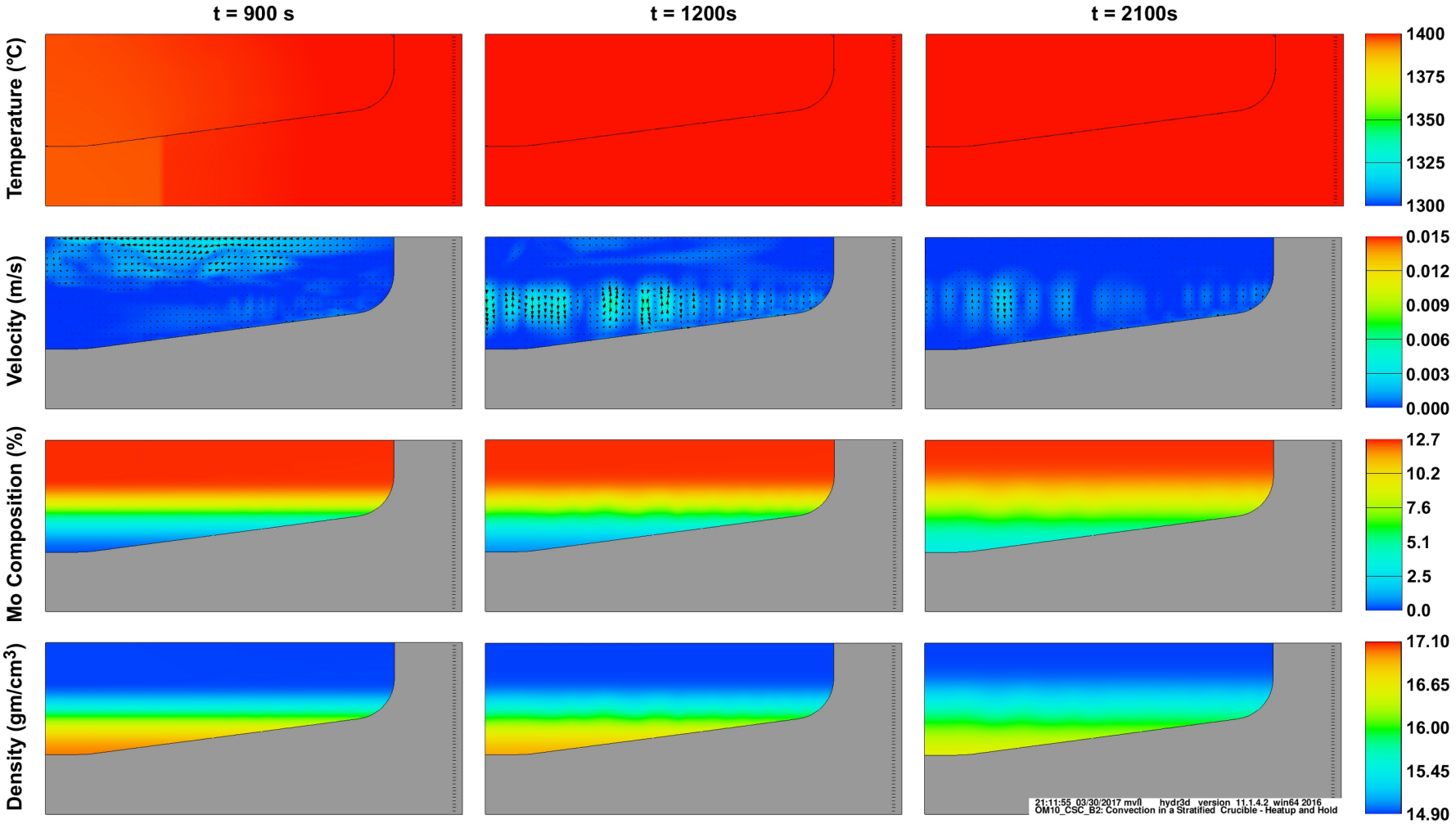

Fig. 30 (cont.) Temperature, metal velocity, Mo concentration, and density as a function of time for the heat up and hold crucible convection simulation.

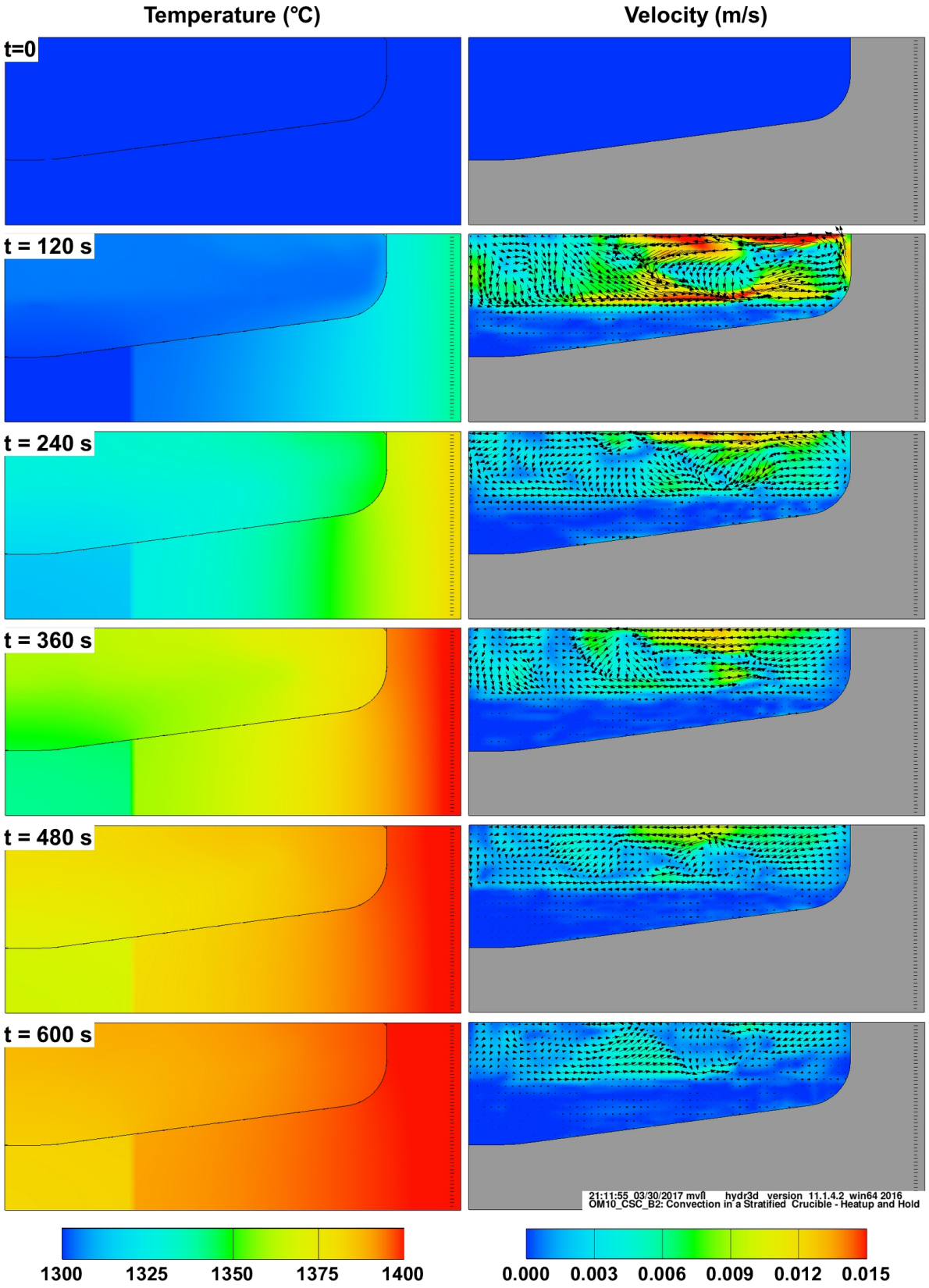

Fig. 31 Temperature and metal velocity as a function of time for the heat up and hold crucible convection simulation.

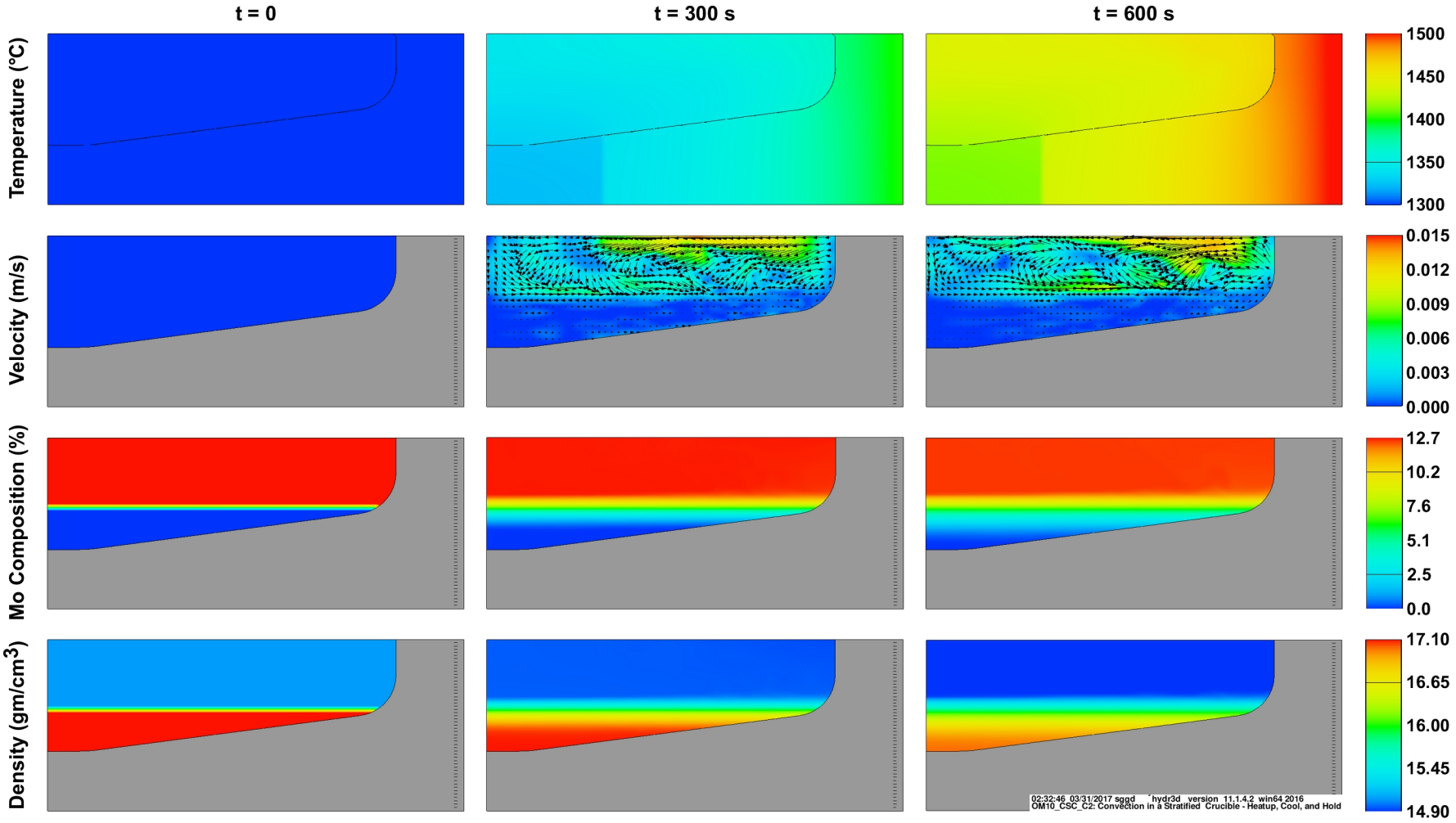

Fig. 32 Temperature, metal velocity, Mo concentration, and density as a function of time for the overheat, cool, and hold crucible convection simulation.

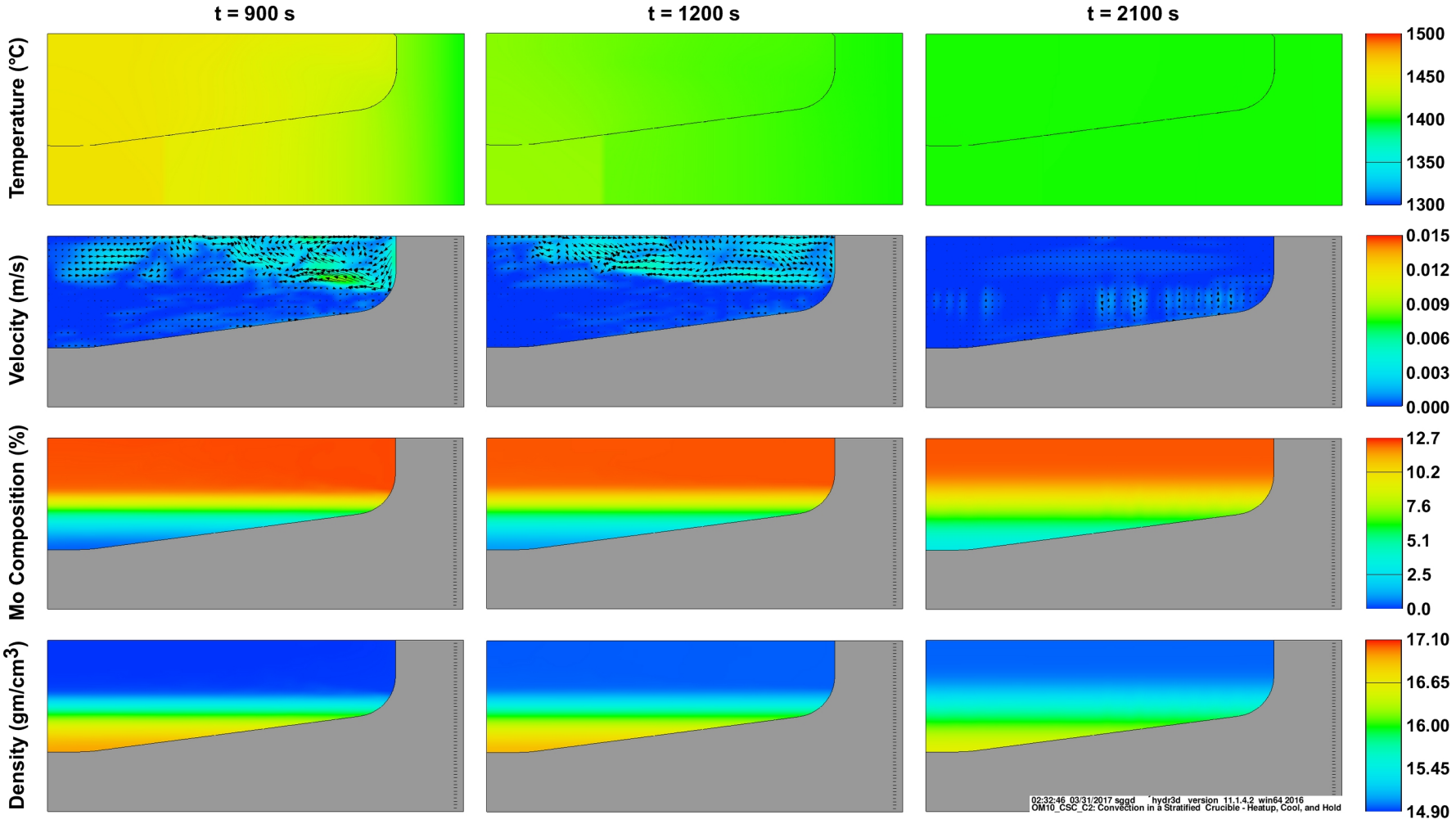

Fig. 32 (cont.) Simulation results showing temperature, metal velocity, Mo concentration, and density as a function of time for the overheat, cool, and hold crucible convection simulation.

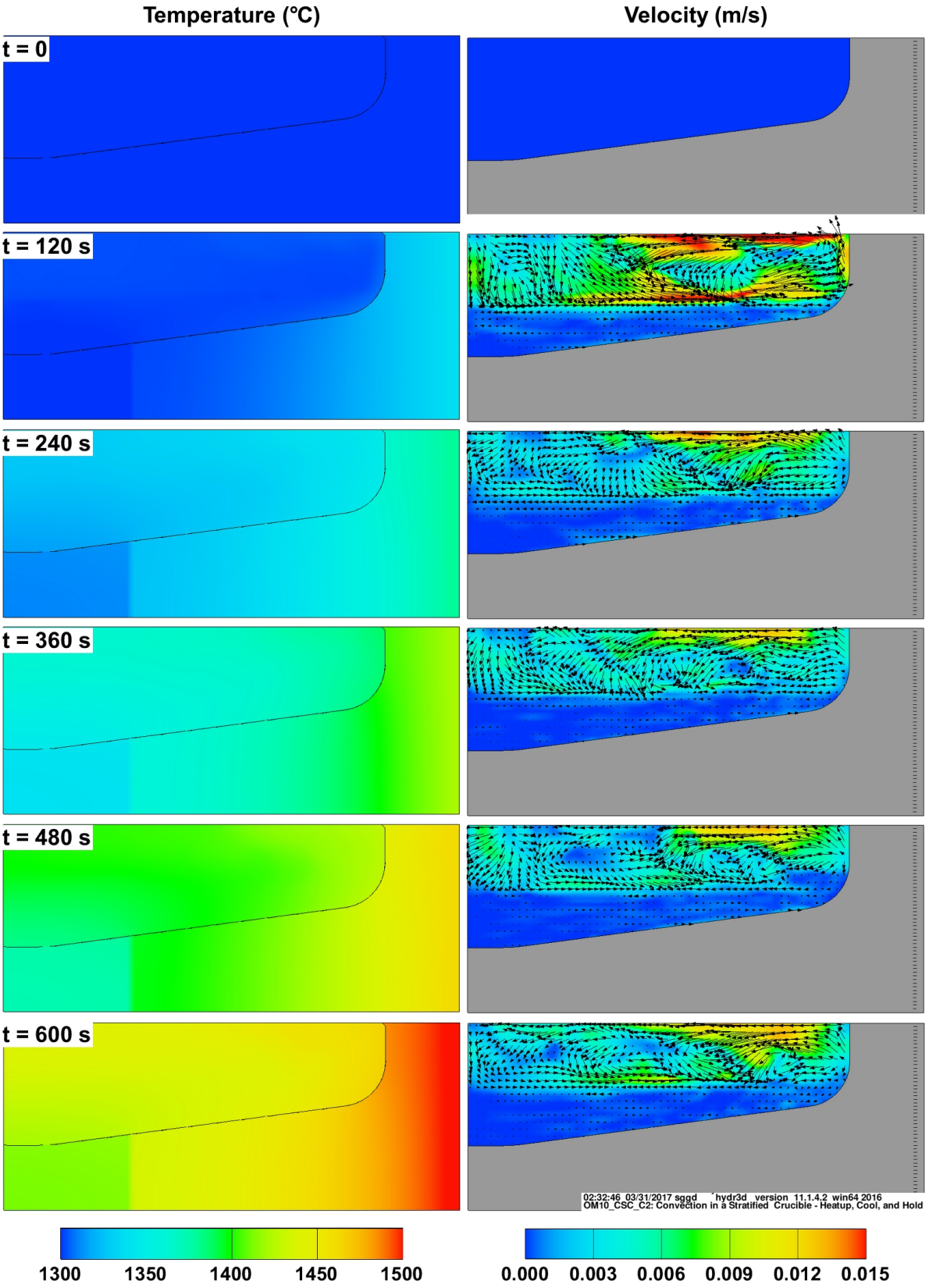

Fig. 33 Temperature and metal velocity as a function of time for the overheat, cool, and hold crucible convection simulation.

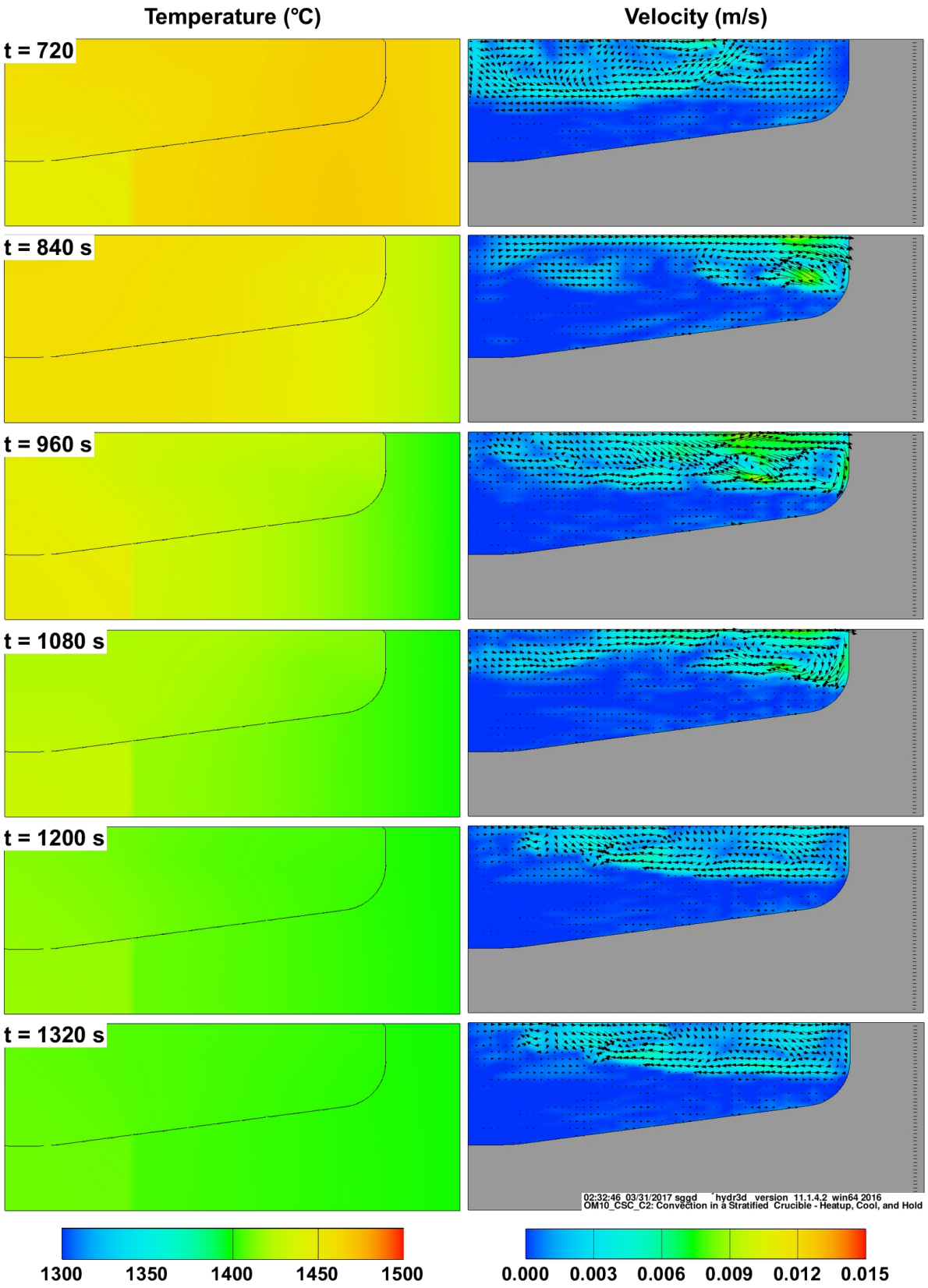

Fig. 33 (cont.) Temperature and metal velocity as a function of time for the overheat, cool, and hold crucible convection simulation.

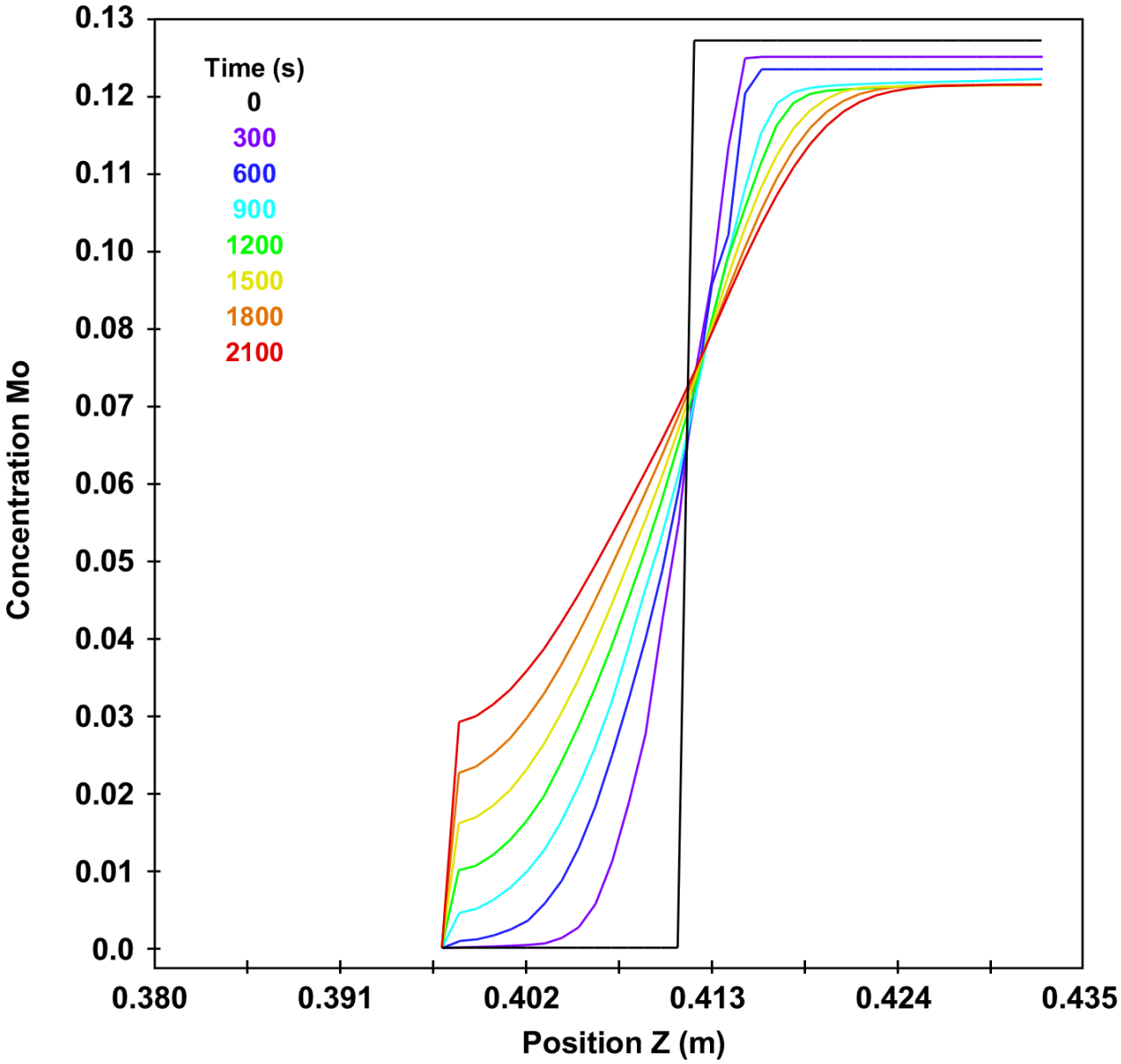

Fig. 34 Mo concentration plotted as function of depth along the Z axis for the overheat, cool and hold crucible convection simulations.

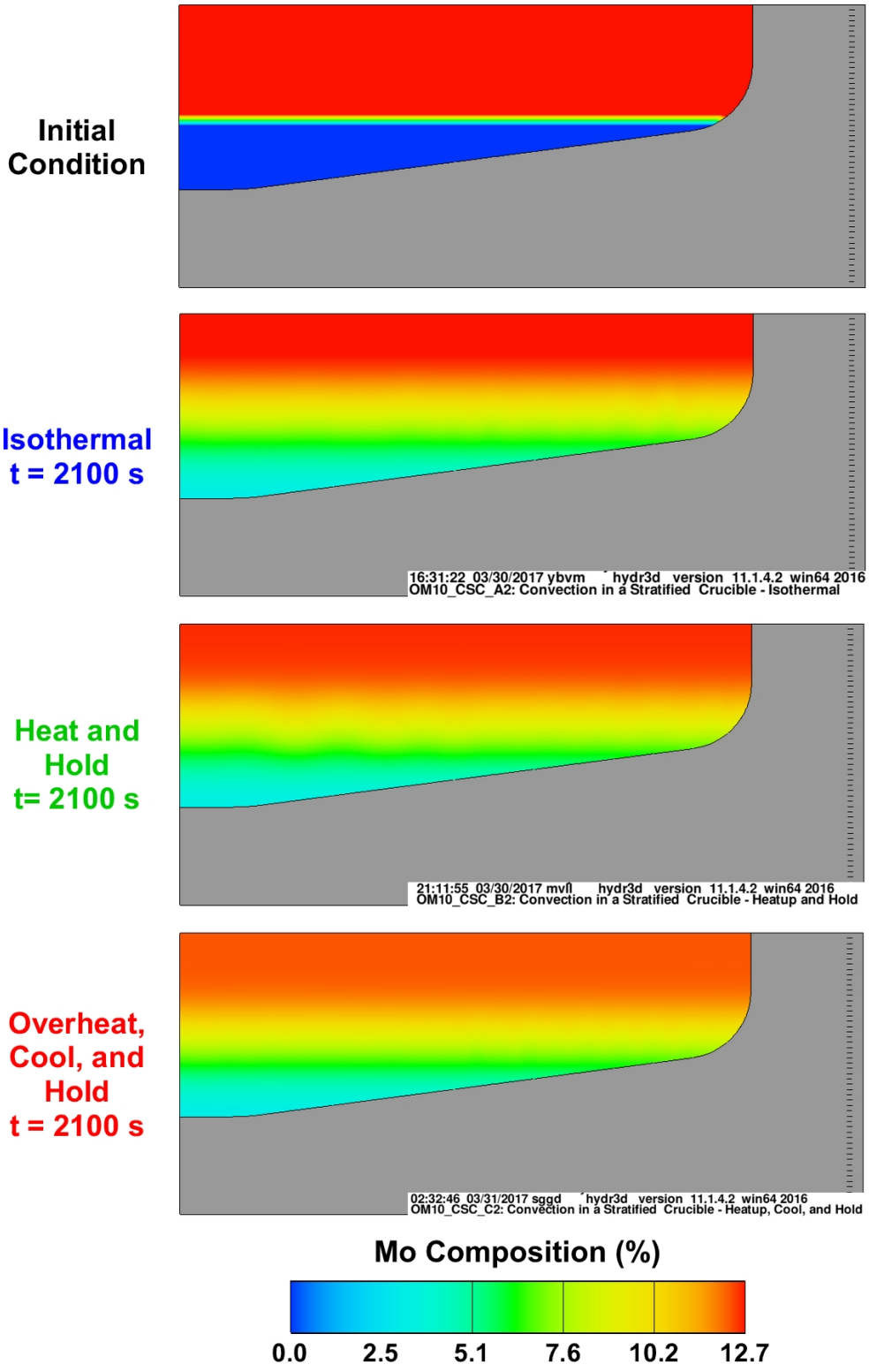

Fig. 35 Comparison of the initial Mo concentration and Mo concentration at 2100 s (35 minutes) for the isothermal; heat and hold; and overheat, cool and hold crucible convection simulations.

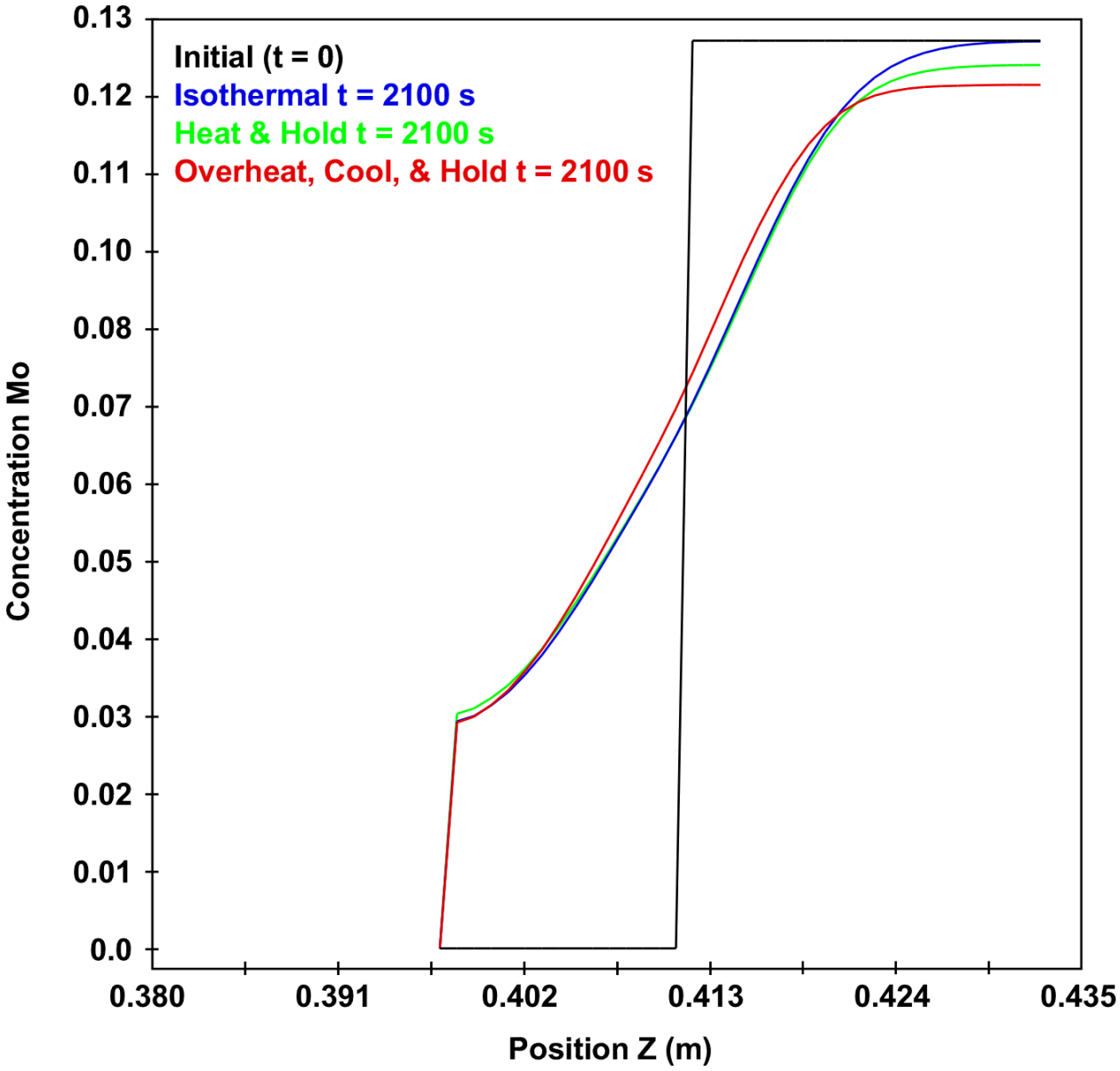

Fig. 36 Comparison of the initial Mo concentration and Mo concentration at 2100 s (35 minutes) for the isothermal; heat and hold; and overheat, cool and hold crucible convection simulations plotted as function of depth alone the Z axis.